Earliest experience of rare but not frequent sounds cause long term changes in the adult auditory cortex

Authors: Muneshwar Mehra[1], Adarsh Mukesh[1] and Sharba Bandyopadhyay[1,2*]

[1] Advanced Technology Development Centre, IIT Kharagpur, [2] Department of Electronics and Electrical Communication Engineering, IIT Kharagpur

[*]Corresponding author

Pages: 27 (+ 44 Supplementary Material), No of Figures: 6 (+ 20 Supplementary +5 Tables)

Author contributions: MM performed all experiments, AM assisted. MM, AM and SB analyzed data. AM did modelling and theoretical derivation. SB supervised the work. SB, MM and AM wrote the manuscript.

Acknowledgements: MM thanks CSIR for Fellowship, AM thanks MHRD for PMRF, SB thanks India Alliance, IIT Kharagpur, MHRD and SRIC for funding. SB gives special thanks to PPC and SDG for support and POK for imbibing interest in the subplate.

Abstract

Early sensory experience during the critical period of development is known to alter sensory cortical response properties and organization. We find that the earliest sound driven activity in the mouse auditory cortex (ACX) can be detected before earcanal opening (ECO). How auditory experience at these ages may influence auditory cortical development is unknown. Particularly, subplate neurons (SPNs), involved in sensory thalamocortical maturation, in the auditory cortex, are also found to be driven by sounds at ages before ECO in mice. We find that SPNs are selective to low probability deviant sounds in auditory streams before ECO, more so than thalamo-recipient, layer 4 (L4) neurons and not after ECO. We hypothesize that SPNs with their deviant selectivity can direct development of L4 responses before ECO. Exposing mice before ECO with a rarely occurring tone in a stream of another tone occurring frequently leads to strengthening of cortical representation of the rare tone, but not the frequent tone in the adult. Control exposure experiments with only a frequently occurring tone and also in other developmental age windows corroborate the importance of low probability sounds in auditory development. With a computational network model of known thalamic inputs to SPNs and L4 we explain the observed developmental plasticity. An information theoretic analysis with sparse coding assumptions also predicts the observations. Thus, salient low probability sounds in the earliest auditory environment causes long term changes in the auditory cortex.

Introduction

Important and salient sensory stimuli occur with low probability, while high probability stimuli, occurring repeatedly, are usually of less importance and are ignored by an organism. Sensory cortical circuitry development is activity dependent and is based on the sensory environment to which an animal is exposed[1,2]. Particularly in the auditory system, altering the natural auditory environment during specific periods (critical period[3–5]) of early development remarkably alters cortical circuitry and organization[6,7]. SPNs, the first born cortical neurons[8,9], play a crucial role in the development of functional cortical circuitry and organization[10–14]. Here, with a new auditory exposure paradigm before the established auditory critical period[2–5] (before ECO) using low probability salient/deviant stimuli in the early auditory environment, we show that the functional auditory cortical (ACX) responses are remarkably altered into adulthood. The alterations are specific to the deviant or rare exposure stimulus. The observed plasticity is an outcome of the unique deviant detection properties we find of SPNs, before ECO, with strong responses to only the rare stimulus. A computational network model derived from our experimental results show how such plasticity occurs. Further, using mutual information maximization and sparse coding principles, we show that the outcome of early exposure with our new paradigm can be predicted theoretically. Hence our results revise the established timelines and concept of auditory critical period and may generalize to other sensory systems.

The development of basic response properties of neurons, in the ACX of the rodent ECO (P12) onwards, like tuning, tuning width, thresholds to tonal sounds or broadband noise and other basic stimuli have been studied[3,15]. In spite of the importance of low probability stimuli[16], developmental profile of response properties to streams or sequences of sounds which are more naturalistic are not known. The changes in response properties of neurons in the ACX, in a lamina specific manner, over the developmental time course, during the critical period have also not been studied. The early transient SP layer is an integral part of the thalamocortical (TC) projection pathway[9–11,17–19], in the auditory or other sensory areas. Although in-vivo sound driven responses in ACX SPNs of ferrets exist[20], they are not fully characterized and not known to exist in mice. SPNs receive collateral inputs from the thalamic axons projecting to layer IV (L4)[8] in the ACX[9,18], but their functional role, if any, in the development of the ACX have not been studied.

Results

Given the importance of low probability stimuli[16] and stimulus specific adaptation in the adult[21,22], single unit responses in L4 and SPNs in A1 and AAF of the developing mice to an oddball stimulus paradigm were first investigated. Single unit responses of the oddball stimulus were obtained from lightly anaesthetized mice (0.5-0.75% isoflurane in oxygen) from postnatal day 12, P12 (after ECO) up to P48 (N=51, male and female). A1 and/or AAF was targeted with custom designed microelectrode arrays (4x4 MEA, 125 µm apart, all 16 of the same length or 8 each staggered by 400 µm or 600 µm, for simultaneous L4 and SPN recording, Fig. S1A), based on vasculature (Fig. S1B)[23–25]. Recording areas and depths were confirmed to be in the primary ACX and from L4 and SP (Figs. S1-3). First, basic responses to broadband noise and tones, at multiple sound levels were obtained (50-100 ms long, gap 2-7s, tones 6-48 kHz in 1/4th or 1/2 oct steps). Next, a series of sound tokens (n = 15 or 10), each 50 ms long (at 4 Hz), of the pattern SSS…SDS…S, with S as Standard and D as Deviant (at 8th/7th position of 15/10 total tokens) were used for the oddball response characterization. S and D could be two distinct tones (6-34 kHz) or a tone and a broadband noise (6-48 kHz with equivalent sound level). To normalize for a neuron's inherent selectivity for a particular S or D, responses were always collected in pairs with the S and D swapped (Fig. S4A). Each SD set of a pair was presented with 10-40 repetitions with a 1-7s silence duration between the end of the previous and start of next stream. To quantify a neuron's selectivity to the deviant we used the common selectivity index

$$CSI = [R_D(f_1)+R_D(f_2)-R_S(f_1)-R_S(f_2)]/[R_D(f_1)+R_D(f_2)+R_S(f_1)+R_S(f_2)] \text{ or}$$

$$[R_D(f)+R_D(N)-R_S(f)-R_S(N)] / [R_D(f)+R_D(N)+R_S(f)+R_S(N)]$$ [16];

where $R_S(.)$ and $R_D(.)$ denote response to S and D respectively. Three cases for $R_S(.)$ were considered: mean response to first S or onset, mean response to S immediately preceding

the deviant or mean response for all the S's; the selectivity values are referred to as CSI(F), CSI(P) and CSI respectively.

Early responses in the auditory cortex show higher deviant selectivity than in the adult

Single unit responses to the SD paradigm with 2 different tones, f_1 and f_2, spaced either 1/4, 1/2 or 1 octave apart were recorded in mice at different ages. Data were simultaneously collected from multiple single units and hence f_1 and f_2 were at various differences from the BF of each of the units. Based on online observations one of the frequencies (f_1 or f_2) was chosen to be at or near the BF of the majority. Figure 1 shows representative responses of 3 single units in L4 and SP during the early developing period after ECO (P12-P15, Fig. 1A-C). Plots of spike dot raster, in response to tones, are shown in Fig. 1A-Ci (top) along with the peri-stimulus time histograms (PSTHs, bottom) for the response to chosen f_1 and f_2 (dark and light grey rectangles in raster). The responses to the SD paradigm (raster plots and PSTHS) for the same units are shown in Fig. 1A-Cii (time scale expanded in Fig. 1A-Ciii). Reliable responses were observed to tones and SD stimuli in the P12-15 group of animals with wider tuning (Methods) in L4 than in SP (0.34 and 0.25 octaves, one sided unpaired t-test, df=101, p<0.010). Simultaneous recordings in L4 and SP (Fig. 1D) showed lower peak response latencies (~5 ms more than first spike latency) for BF tones in SP than in L4 in P12-P13 group (mean 27.38 and 32.27 ms, p<0.0001, df=246 two-sided unpaired *ttest*, Fig. 1E) and in P14-P15 group (mean 27.08 and 30.52 ms, p <0.05, df=78 Fig. 1E).

CSI from the pairs of SD responses (Fig. 1A-Cii) were calculated and the mean CSIs observed as a function of separation of frequencies used (CSI(F), 0.5 octave: p<0.0001, df=48, two-sided unpaired *ttest*; 1 octave: p=0.0031, df=61 Fig. 1F, and CSI, 0.5 octave: p<0.0001, df=48; 1 octave: p<0.0001, df=61 Fig. 1G) for L4 (6 mice, 69 units, 110 cases) were higher than that of SPN (6 mice, 43 units, 65 cases), except at ¼ octave separation for the population of neurons in P12-15 (p<0.099, df=48, Fig. 1F & p<0.2535, df=48 Fig. 1G). CSI(F) is biased to be low due to the large onset response, evident from the lower values of CSI(F) than CSI (Fig. 1F-I). On average, independent of f_1-f_2, SP neurons had lower deviant selectivity than L4 neurons and they reduced from P12 to P15. Further, as age progressed from ECO (P12) to the adult the CSI values and hence deviant selectivity reduced (P12-13$_{L4}$ vs P16-21$_{L4}$: df=60, p=0.0019, two sided unpaired t-test; P12-13$_{L4}$ vs P22-28$_{L4}$: df=98, p<0.0001; P12-13$_{L4}$ vs >P28$_{L4}$: df=119, p<0.0001; P14-15$_{L4}$ vs P14-15$_{SP}$: df=112, p=0.005 Fig. 1H & P12-13$_{L4}$ vs P16-21$_{L4}$: p<0.0001; P12-13$_{L4}$ vs P22-28$_{L4}$: p<0.0001; P12-13$_{L4}$ vs >P28$_{L4}$: p<0.0001; P12-13$_{L4}$ vs P12-13$_{SP}$: df=59, p=0.0011; P14-15$_{L4}$ vs P14-15$_{SP}$: p=0.033 Fig.1I), showing that adults had much weaker selectivity to the deviant than in early ages. The reduction in selectivity to the deviant with age was not due to the distribution of choices of f_1 and f_2 in the different age groups (Fig. S4).

Since deviant selectivity is dependent on f_1-f_2 (Fig. 1F&G) and hence can be confounding we also used an *N-f* pair (a noise token and a single frequency, Fig. 2 and Fig. S5&S6). Since the

noise token is broadband, in this case neurons would show deviant selectivity if there are parallel channels followed by integration based on spectral contrast of sounds[26]. Robust responses were present for the broadband noise token, both, when presented by itself (Fig. S5Bi-Gi, sometimes showing inhibition, Fig. S5Ci) and in the SD paradigm (Fig. 2). Single units responded to noise, both in L4 (Fig. 2A and Fig. S5) and in SP (Fig. 2B and Fig. S6) of A1 not only in the age group P12-P15 but also, expectedly, in L4 neurons for ages above P15. Minimal SPNs were observed beyond P15 (Fig. S1D) and hence SPNs were not targeted beyond P15. In the case of noise and tone as well, the same age dependence of deviant selectivity was observed as with tones. The difference in L4 and SP were similar to that observed with tones for both CSI(F) and CSI. CSI(P) in which R_S(.) is the response rate for the standard token preceding the deviant also showed the same effects (two sided unpaired t-test, P12-13$_{L4}$ vs P22-28$_{L4}$: df=98, p<0.0001; P12-13$_{L4}$ vs >P28$_{L4}$: df=119, p=0.0464 Fig. S7).

In both the SD responses the age dependence of deviant selectivity (P12-13$_{L4}$ vs P16-21$_{L4}$: df=86, p=0.025, two sided unpaired t-test; P12-13$_{L4}$ vs P22-28$_{L4}$: df=152, p<0.0001; P12-13$_{L4}$ vs >P28$_{L4}$: df=118, p<0.0001 Fig. 2C & P12-13$_{L4}$ vs P16-21$_{L4}$: p=0.022; P12-13$_{L4}$ vs P22-28$_{L4}$: p<0.0001; P12-13$_{L4}$ vs >P28$_{L4}$: p<0.0001 Fig. 2D) is found to be correlated with changes in adaptation time constant[27] with age. An exponential decay fit to responses at each successive S token from the onset for every unit, shows that the mean of the time constants increases with age (Fig. S8Ai,B; P12-13$_{L4}$ vs P16-21$_{L4}$: df=74, p=0.027, two sided unpaired t-test; P12-13$_{L4}$ vs P22-28$_{L4}$: df=209, p<0.0001; P12-13$_{L4}$ vs >P28$_{L4}$: df=148, p=0.0026). Similarly the number of S tokens, from the onset, to which neurons respond significantly also increase with age (Wilcoxon ranksum test, P12-P13/P21-P27, P<0.001, (Fig. S8Aii,C), expected from increasing decay time constants. These results also indicate that A1 neurons even early in development do not necessarily only integrate information in parallel frequency channels but also possibly along parallel spectral contrast channels; as responses to deviant tone (high spectral contrast) is observed contrary to the idea that a broadband noise token as S, should cause all frequency channels to adapt, leading to lack of deviant tone response. Response to tones and noise can be passed on to the cortex early in development as parallel channels of information. The above is further corroborated by lower CSI and CSI(F) observed in MGBv computed from *N-f* SD responses (Fig. S9B; A1 P14-15$_{L4}$ vs MGBv P14-15: df=180, p<0.0001, two sided unpaired t-test; A1, P14-15$_{SP}$ vs MGBv P14-15: df=132, p=0.0046; A1 P22-28$_{L4}$ vs MGBv P22-28: df=165, p=0.9755; Fig. S9C A1 P14-15$_{L4}$ vs MGBv P14-15: df=180, p<0.0001, two sided unpaired t-test; A1, P14-15$_{SP}$ vs MGBv P14-15: df=132, p<0.0001; A1 P22-28$_{L4}$ vs MGBv P22-28: df=165, p<0.0001) in two age groups P14-15 (n=2, 27 units, 71 cases) and P24-26 (n=3, 42 units, 79 cases). The higher deviant selectivity in L4 and SP especially in the developing mice (P12-P15) is a cortical phenomenon and is not a reflection of thalamic inputs. The CSI values obtained in the MGBv in P14-15 age group were drastically lower than that observed in L4 (CSI, A1 P14-15$_{L4}$ vs MGBv P14-15: two sided unpaired t-test df=180, p<0.0001) and SPN and lower than L4 at higher ages (P24-26). In both cases, two tones and noise-tone, the CSI values are larger than

182 that obtained with a long stimulus protocol[21] as we use a stream with a single deviant that is
183 repeated.

184 *Mouse ACX neurons have auditory responses before ECO*

185 Low threshold hearing onset coincides with ECO, however high intensity sounds may drive
186 spiking activity in the ACX before ECO. Auditory cortical responses have been shown to exist
187 in ferrets[20] at ages equivalent to P6 in mice[28], however no study reports presence of sound
188 driven activity in the ACX of mice at ages before ECO (P11/12). However, auditory brainstem
189 responses in mice have been shown before ECO[29] and also long term changes in prestin
190 expression have been reported in mice exposed to loud sounds at these early ages[29] (P6-
191 P11). Although the central auditory pathway is functional[29,30] showing spontaneous activity
192 the peripheral auditory system maybe immature. In mice, the external auditory meatus
193 reopens at P7 and the outer ear or pinna is fully mature by P7[31] and middle ear bones lever
194 arm lengths are at 70% of mature values with normal lever ratios by P7[32]. The oval window
195 is also of normal size by P7[32]. Most importantly, mechano-transduction currents from outer
196 hair cells (OHC) and inner HCs (IHC) become maximal in the cochlear base by P2 and at the
197 apex by P5[33,34]. IHCs are fully mature by P5[35] while OHCs are immature with nonlinear
198 capacitance (NC) of OHCs, key to low threshold hearing and high sensitivity of auditory
199 nerve fibers, only starts at P7 and is fully mature at P18. The development of OHC NC is
200 correlated with the expression of the motor protein, prestin, responsible for the OHC NC[35].
201 Thus high intensity sound evoked activity is possible at ages before ECO in mice.

202 To investigate the possibility of auditory responses to high intensity noise and tones in the
203 ACX of mice before ECO[3,36] we performed additional experiments using single unit
204 extracellular recordings, wide-field fluorescence imaging and 2-photon Ca^{2+} imaging in Thy1-
205 GCaMP6f (Jax Labs) at ages P7-11 before ECO (Fig. 3 and Fig. S10-14). Sound evoked long
206 lasting LFP's were present as early as P08 (before ECO, Fig. S10A-B). Single unit activity
207 collected from SP and L4, with 5 repetitions of tones or noise did not show significant
208 responses at P08-10 (Fig. S10C). Sound driven spiking activity in the ACX before ECO, was
209 confirmed first with widefield fluorescence imaging in Thy-1-GCamp6f mice (Fig. 3A and
210 Fig.S11A). Over age, from P07 to P13, progressively larger areas of the cortical surface
211 showed significant responses to multiple tone frequencies (~90 dB SPL, 40 repetitions), with
212 the presence of clear tonotopy in A1 by P13 (Fig. 3A). The presence of significant responses
213 in Ca^{2+} dependent fluorescence could potentially indicate activity in input axons to the ACX
214 and/or spiking responses in ACX in response to sounds as early as P7. We confirm presence
215 of sound driven activity lower in the auditory pathway by performing widefield fluorescence
216 imaging in the inferior colliculus (IC) of Thy1-GCaMP6f (Jax Labs) mice at P9-10 (Fig. 3B).
217 Since 5 repetitions were not sufficient to show significant activity in ACX single units while
218 40 repetitions showed significant sound evoked responses in widefield fluorescence, in both
219 the ACX and the IC, we hypothesize that responses at these early ages have low reliability (%

220 of responding trials, Methods). Moreover, the percentage of responsive cortical surface area
221 and fraction of frequencies that showed significant responses increase with age (Fig 3A, Fig.
222 S11A, Table S3). Both the above indicate gradual maturation of the ACX.

223 To rule out, only input axon activity in the ACX widefield imaging, 2-photon Ca^{2+} imaging of
224 single neurons in L2/3 of the ACX of mice before ECO was also performed with 40
225 repetitions each of noise bursts and different tone frequencies (Methods, Fig. S11B-C). A
226 small fraction of significantly responsive neurons to different tones and broadband noise
227 was found in L2/3 from P07 to P11, before ECO (Table S4-S5). Considering all the neurons
228 that responded with at least 25% reliability (Fig. 3Ci), the population mean df/f in each age
229 was investigated (Fig. 3Cii). Increase in the population mean response strength and
230 decreasing trend in peak latency with age was found (Fig. 3Cii, any frequency tone, Fig. S12,
231 each frequency tone and Fig. S13Ai-ii, noise bursts). The above indicated a gradual
232 maturation of responses up to ECO (P12-13). Also, significant positive correlation is found in
233 response reliability with age (Fig. 3Ciii, Fig. S13Aiii) before ECO, showing gradual response
234 development.

235 Although with 40 repetitions of tone/noise, detecting spurious responses due to high
236 spontaneous activity observed before ECO are unlikely, we used two approaches to rule out
237 such a possibility. In additional 2-photon Ca^{2+} imaging experiments in P9 and P10 mice
238 (before ECO), first we considered >2s baseline before tone presentation. Considering only
239 neurons with >25% reliability of responses (Fig. 3Di) and their population mean df/f (Fig.
240 3Dii), we found that the baseline did not show any such activity as observed following the
241 stimulus onset. Secondly, we also repeated the same imaging experiments with and without
242 sound stimulation. The df/f of the neurons that responded with >25% reliability with sound
243 presentation (Fig. 3Ei, left) was also obtained for the same durations without sound
244 presentation (Fig. 3Ei, right). The population means in the 2 cases (Fig. 3Eii) clearly show the
245 presence of sound driven activity in the ACX L2/3 single neurons before ECO.

246 Two-photon Ca^{2+} imaging of single neurons, simultaneously from L4 and SPNs was beyond
247 our scope. To investigate the nature of spiking activity in L4 and the SP, with larger number
248 of repetitions of tone and noise stimuli (due to the observed low reliability), single unit
249 recordings were done in mice with ear canals closed (n=6, P8-11) with staggered electrodes
250 (Fig. S1A). Unlike with 5 repetitions of stimuli (Fig. S10C), z-scores of spiking responses in
251 50ms time bins (Fig. 3Fi, and Fig S13Bi) show presence of significant sound evoked spiking
252 in SP and L4 neurons before ECO. Population PSTHs of all significantly responding units in SP
253 and L4 (Fig. 3Fii and Fig. S13Bii) show significant sound driven activity before ECO, which get
254 stronger with age.

255

256

SPNs unlike L4 and L2/3 neurons, show deviant selectivity before ECO

As responses to tones and noise exist in the mouse ACX before ECO, we investigated deviant selectivity properties in ACX L2/3, L4 and SPNs. 2-photon Ca^{2+} imaging of the ACX L2/3 single neurons as early as P07 show significant responses to S and D in the *N-f* SD protocol (Fig. S14Ai-ii). Mean response profiles of all significantly responding L2/3 neurons show responses to both the S and D (Fig. S14Aiii-iv). However, distribution of CSI (mean -0.037) values of single neurons based on mean df/f (Fig. S14Av) indicates no preference for the D, in L2/3 single neurons.

Activity of single units during presentation of the SD protocol for f_1-f_2 and *f-N* (30 and 20 reps, 3.3 or 4 Hz repetition rate, Fig. 4Ai) showed peaks in response following the deviant (mainly in SPN) and onset (mainly in L4) as shown in the first 3 columns of Fig. 4A (dot rasters and PSTHs of 3 L4 neurons, dark gray, upper four rows, SD and swap and 3 SPNs, light gray, lower four rows). Population mean PSTHs for all L4 neurons and all SPNs recorded (P8-P12, before ECO) indicate the presence of deviant detection in SP and not L4 (Fig. 4Aii-iii, 3.3 Hz and 4 Hz). Further, based on the spontaneous activity (100 ms preceding the stimulus), z-scores of the example neurons and population of neurons (Fig. S15AB) demonstrate responses (95% CI, one-sided), particularly following the onset and the deviant. In the population mean z-score, the earliest peaks occur in L4 in a 250 ms window with a latency of 50-100 ms from the first token and in SP in a similar window following the deviant. Considering a latency of 100 ms, because of observations in LFPs and by obtaining spike rates in 250 ms windows because of width of significant LFP rms values (50 ms sound and 200 ms gap), CSI(F), CSI and CSI(P) were calculated for L4 and SPN (Fig. 4Bi-iii). There is higher deviant selectivity in SP than in L4 (two sided unpaired t-test, $p<0.01$ for all CSIs). Since in single trials for single neurons the responses were not reliable, we also varied the response window from 50 ms to 300 ms (in steps of 50 ms) and latency from 0 to 350 ms (in steps of 50 ms) and obtained the CSIs for all neurons and we found for what combinations SPNs had significantly higher deviant selectivity than L4 neurons (Fig. S16). Thus in spite of low reliability of responses in the population L4 did not show higher deviant selectivity than SP. Thus neurons in the mouse ACX respond to sounds before ECO with SPNs showing responses to the deviant. Possibly, depending on the strength of SPN to L4 connections, the L4 may or may not have a response. Ten pairs of neurons (between L4 and SP) were found to be connected out of 27 simultaneously recorded L4-SP pairs (Methods) before ECO (Fig. S17). Observed directionality of the connected pairs suggests existence of connections from SPN to L4 (6/12 pairs showed connections from SPN to L4 within spatial distance of 125 microns while 4/15 pairs were found to be connected at distance of >125 microns, $p<0.11$). Directional connectivity as a function of spatial distance clearly suggests columnar organisation of SPN to L4 connections in ACX[19] before ECO (Fig. S17B). Due to the low reliability of responses (Fig. 3Diii-Eiii), to rule out spurious deviant selectivity, we considered 1000 random pairs of windows, in CSI calculations considering two non-overlapping

296 windows 250 ms randomly taken in the standard region before the deviant (Fig. 4Biv) or
297 after the deviant (Fig. 4Bv) where the mean CSIs were not significantly different between L4
298 and SP in >95% of the random pairs. The distributions of mean random-CSIs for SPN and L4
299 also show that the means were not significantly different from 0. Thus SPNs show
300 significantly stronger responses to the deviant than L4 before ECO and lower than L4 after
301 ECO. Such early context dependence of responses in SPNs allow for the possibility of SPNs in
302 sound driven sculpting of TC inputs earlier in development than previously studied[11].

303 *Exposure in a standard deviant acoustic environment before and after ECO show differential*
304 *developmental plasticity for the standard and the deviant frequencies*

305 Broad tonotopic organization in the primary auditory cortex (A1)[23,24] is known to be altered
306 with over-representation of a particular frequency in the adult rats/mice which were
307 exposed to that frequency tone during the critical period (P12 to P15, after ECO)[3,5].
308 However, as observed (Fig. 3-4), spiking and LFP (Fig. 3-4 and Fig. S10-S14) responses in the
309 L2/3, SP and L4 in ACX are present before ECO. Further it is known that the auditory
310 pathway is active before P12 (in rodents), with the TC circuitry maturing[37–39], functional hair
311 cells by P6[40] and SPNs in A1 responds to sounds[20] (in ferrets, at ages developmentally
312 equivalent to mouse P7)[28]. In spite of such activity, exposure of rodents to a single
313 frequency tone from P9-P12, no changes were found in broad tonotopic organization with
314 single unit BF mapping of A1, when the exposed pups were adults[3,5]. SPNs and L4 neurons in
315 the mouse A1 respond to sounds as early as P08-P12 (before ECO, Fig. 3-4 and Fig. S10-12)
316 and SPNs act as deviant detectors with high context dependence (Fig 4 and Fig S13). Such
317 response properties and SPN to L4 connections (Fig. S17)[18] coupled with activity dependent
318 plasticity[1,6] in the early auditory system leads to the hypothesis that exposure to a
319 continuous train of a fixed frequency tone (S) with an embedded low probability (10%) tone
320 (D), before ECO would cause enhanced responses to the D frequency in the adult. Spiking in
321 the SPNs drives L4 spiking[18,19] in a correlated manner, with thalamic spikes in neurons
322 projecting to SPN and L4 would drive strengthening of thalamus to L4 synapse[11]. The above
323 suggests that exclusive responses to the deviant in SPNs would lead to strengthening of the
324 thalamic inputs tuned to the deviant frequency. Mice were exposed (Fig. 5A) to such an SD
325 sound protocol (Methods) from P6-10/11 (S=12 kHz, D=17 kHz or S=20 kHz, D=14 kHz, EX2,
326 Fig. 5A) and single unit recordings in L4 (depth 350-450 μm) in response to pure tones (13
327 frequencies, 6-48 kHz, 1/8th oct apart, 50-90 dB SPL, 10 dB steps) from A1 and AAF were
328 performed in the mice at P28-42. As age controls we did exposures of the SD (S=12 kHz,
329 D=17 kHz) protocol at multiple age groups – P0-5/6 (EX4), P11-15/16 (also, S=14 kHz, D=10
330 kHz, EX1) and P16-21 (EX3). For stimulus control, exposure of mice in age groups P6-10/11
331 (EX6) and P11-15/16 (EX5) were done with only a single frequency (SS protocol, S=12 kHz).
332 Further, a group with normal rearing was considered as control (EX0).

All significant response firing rates from the tuning curves (cartoon tuning curves, Fig. 5B) for each of EX0 to EX6 show that EX3, EX4 and control (EX0) have same median firing rate (ranksum test, 12 sp/s for every case, p_{EX3}=0.8475, p_{EX4}=0.1875 Fig. 5C). All other groups, EX1-2, EX5-6 show increased median firing rates (*ranksum* test, 16-24 sp/s, $p_{EX1,2,5,6}<10^{-6}$, Fig. 5C) compared to EX0. The cumulative distributions (cdfs) of mean firing rates at the respective reference frequencies considered in the different exposure groups (green: S, red: D and blue: SS, Fig. 5D) are within the boundaries (thick gray lines) of EX0 cdfs (except at very low rates in EX3-4). Since any particular frequency out of 13 frequencies could be a reference we considered each of the frequencies in EX0 as a reference frequency (mean with STD, thin gray lines, Fig. 5D) to find the limits of the cdfs in the control. The minimum and the maximum from the 13 cdfs of control are considered as the boundaries. With our limited resolution mapping, we did not find any apparent over representation of any particular frequency in BF maps showing broad tonotopy (A1 and AAF) on the cortical surface (Fig. S18A) in any of the exposure cases (EX1-2 and EX5-6), unlike other studies with EX5 group[3,5] (Fig. S18B). Other than lower spatial resolution of single unit sampling, it may also be due to parameters of exposure (sound frequency, duration and repetition rate).

From the tuning curves, population mean response rates to the relevant reference frequency (RF) were plotted as a function of BF (re RF in octaves, Fig. 5B). For S/D exposures (EX1-4) we obtained two plots, with S as RF and D as RF (green and red respectively), for SS exposures (EX5-6), S was the RF (blue) and for the control C (gray) each of the 13 frequencies were considered as RFs separately. The maximum rate in the profile (as a function of BF re RF) of the 13 reference frequencies (EX0 case) is considered as the upper boundary of observed rates at RF in control (Fig. S19 and Fig. 5E), minimum being '0'. When considering normalized firing rates (with rate at BF as 100%) the population mean responses to reference frequencies (for EX1-2 and EX5-6) were largely within the maximum boundary suggesting no frequency specific change in normalized rates compared to control (Fig. S19). The population mean rate as a function of BF re RF for EX2&5 and EX1&6 (Fig. 5Ei and ii) show differential effects on response strength at BF to the S and D for SD exposure before ECO and after ECO. After ECO in the critical period of P11-15, the S frequency responses (with S as BF) are strengthened in comparison to that of D, while before ECO the opposite effect is observed. No such changes are observed in exposure before P6 and after P15 (Fig. S20 bar plots, two sided unpaired t-test, P11-15 standard vs deviant: df=107, p=0.009; P6-10 standard vs deviant: df=120, p=0.002). In comparison when SS exposure is done after ECO there is a strengthening of responses to S and not after ECO. Only in the case of SS for P11-15 exposure there is increase of S responses of neurons with S as BF beyond the boundary of control (gray dashed line, Fig. S20) and that for D before ECO SD exposure. Comparisons (significant or not) with the population of 13 control rate profiles are marked on respective bars (gray '*' or NS, Fig. S20). When considering each set of exposure frequencies, for the merged groups of SD exposure with different sets S and D frequencies, the response to D is greater than that of S before ECO (p<0.01 20/14 kHz and p<0.07 12/17 kHz) and that of D is

less than that of S after ECO ($p<0.01$ 14/10 kHz and $p<0.01$ 12/17 kHz). Further, when normalizing the response rates by the mean response at BF of other frequencies (>1/2 octave away from the exposed frequencies) we find that in the SD exposure the response to D of neurons with D as BF is significantly higher before ECO and is significantly lower after ECO (Fig. 5E, barplots, unpaired t-test, P11-15 standard vs deviant: $p<0.05$, df=107; P6-10 standard vs deviant: $p<0.05$, df=120). Response to S in SD exposure before ECO is lower than 1 with $p<0.051$ and no effect is seen in S after ECO. Response to S at S as BF is not significantly different from 1 in the SS exposure before or after ECO. Thus there is a differential long term plasticity of responses to the low probability sound frequency depending on the period of development during which animals are exposed in the SD environment. It coincides with the differential deviant selectivity before and after ECO observed in the ACX L4 and SPNs involved early in development, in setting up the ACX circuitry.

Model binary network with observed deviant selectivity of SPNs and L4 shows stronger representation of deviant frequency before ECO and standard frequency after ECO

To explain the observed exposure dependent developmental plasticity based on L4 and SPN deviant selectivity we use a binary network model (Supplementary Material, Fig. 6A) of early developing TC circuitry of the ACX[18] similar to that considered in the visual cortex[11]. Thalamic inputs selective for either of two inputs, S or D (green and red, Fig. 6A) are considered to make synapses on an SPN, sending collateral inputs to a L4 neuron[8]. The SP and L4 neurons are modelled as integrate and fire neurons with absolute and relative refractory[11]. The SPN neuron makes a synapse onto the L4 neuron as known[9] (Fig. S17). All synapses are considered depressing in nature[41,42](Fig. 6B) such that L4 and SPN responses to oddball paradigm show similar adaptation observed early in development (Fig. 1-2, Fig. S8). Also, all synapses except the thalamic inputs to SPN are plastic changing their strengths with an asymmetric Hebbian spike timing dependent plasticity (STDP) rule (Fig. 6C). We consider the model with two different starting points, one representing the period before ECO and another after ECO (Fig. 6D & Ei-ii). In the earlier developmental period (before ECO), the SP CSI was 0.41 and that of L4 was -0.02 and in the later developmental time period SP CSI was -0.17 and that of L4 was 0.4 (Fig. 6D), mimicking our observations (Figs. 1,2&4). The differences in the initial point of the network (Supplementary Material) in the two cases are supported by other data[18] and our observations of larger time constants later in development (Fig. S8) and increased thalamic synaptic weights on L4 due to normal development, lower SPN to L4 connectivity (Fig. S17B) and reduced SPN rates through higher thresholds. We use the same exposure protocols SD and SS for the two periods to show the nature of how the thalamic inputs to L4 develop (Fig. 6E).

During early development with higher deviant selectivity in SP than in L4, with an SD exposure, the D thalamic input to L4 strengthens faster than that of the S, which will lead to

strengthening of responses to the D stimulus in the adult (Fig. 5E). Whereas in the same period with an SS exposure the S thalamic input does not show strengthening at a fast rate (as D, above) leading to normal representation of the S input (Fig. 5E, bar plot P6-11) equivalent to S in the SD case. On the other hand later in development with L4 showing higher deviant selectivity than SP, but higher time constants of response decay with more responses to the S frequency now, shows that in the SD protocol the S thalamic input synapse strengthens faster with the D input weakening as the SP has lower drive for D than before. Further, with the only S stimulus also the S inputs, expectedly strengthens leading to normal responses to S as observed (Fig. 5E, barplot). Thus higher correlated activity between the L4 and thalamus introduced by SP during the D stimulus because of the high SP deviant selectivity in the SD exposure, causes increased responses to the low probability D stimulus in the adult. The lack of such activity and lowering of deviant selectivity in SP and more responses to S in the later part of development the SD exposure now shows the opposite effect.

Sparse coding and information maximization principles imply strengthening of response to low probability stimuli

While a network model mechanistically addresses the observations, we theoretically address the observations of early exposure to a low probability stimulus leading to strengthening of its responses and its weakening in later exposure case. Our observations and model results are contrary to the usual ideas of long term plasticity - a repeated presentation of a stimulus in the critical period leads to strengthening of the representation of that particular stimulus in the long term[1,3,5,7]. Auditory cortical spiking activity is known to be sparse and sparse coding principles theoretically explain a number of known receptive field types in the auditory pathway[43–45]. Assuming minimal activity based coding in single neurons underlying sparse representation in populations and that such representation is one of the goals of the developing auditory system while maximizing information about the stimulus in the responses we use an objective function (Eqn. 1) as the desired optimization performed by activity driven plasticity.

$CI_k = I(R_k, T) - \rho(r_o + xa_k)$ ... (1a)

$CI_{total} = \sum_{k=1}^{N} CI_k = \sum_{k=1}^{N} I(R_k, T) - \rho\left(Nr_o + x\sum_{k=1}^{N} a_k\right)$ ... (1b)

In Eq. 1, $I(R_k,T)$ is the mutual information (*MI*) between the stimulus (a random variable T which is either S or D, with probabilities (1-x) and x, where x is small and is considered as the probability of the deviant stimulus) and the response rate in the kth token is R_k, ρ is a constant, N is the total number of stimulus tokens. CI_k is considered as the constrained information function at the kth token. The mean ensemble response rates are assumed to be r_0 and $(r_0 + a_k)$ for S and D at the kth stimulus respectively, and assumed to have a Gaussian distribution both having variance σ^2. The mathematical proof of the optimization is provided in the supplementary material. However, the basis is as follows. The mutual

information would increase as the separation between the two rates (a_k) increases. However since sparse activity requires minimal activity by single neurons to code the two stimuli, to minimize the summed activity, a must be positive and small. So the response to the deviant needs to be larger than that of the standard. However, the relative weightage of *MI* and the summed activity (ρ) can allow a to be increasing or decreasing and still cause CI_k to be increasing.

We show that the condition for which CI_{total} keeps increasing by considering $\Delta CI = CI_n - CI_m$ ($n>m$) with the assumption that the sequence $\{a_k\}$ is monotonic is

$$\Delta CI = CI_n - CI_m = x\left[\frac{{a_n}^2 - {a_m}^2}{2\sigma^2} + \Lambda(a_n) - \Lambda(a_m) - \rho\{a_n - a_m\}\right]$$

$$= x(a_n - a_m)\left[\frac{a_n + a_m}{2\sigma^2} + \frac{\Lambda(a_n) - \Lambda(a_m)}{a_n - a_m} - \rho\right] \ldots (2)$$

From the last expression in Eq. 2, under 2 different ranges of ρ, ΔCI is increasing with a increasing or a decreasing respectively. The theoretical analysis suggests that before and after ECO the relative importance of coding or discrimination and minimal activity is changed. Based on the above, sparseness in later stages (after ECO), when spike rates are higher, needs to be weighted more than earlier stages (before ECO) to explain the differential effect observed before and after ECO in the response to the low probability stimulus.

Discussion

Auditory critical period has long been studied using a single tone presentation throughout the critical period of P12-P15, starting with low threshold hearing coinciding with ECO[15,46]. The frequency over-representation observed with such exposures have been shown to be absent in exposure periods other than the 'critical period'. Multiple studies have also shown possible mechanisms of closure of such a critical period[4,47–49], however, the starting of critical period in spite of those studies, remain unclear. In our results we show that responses in the mouse ACX exist before ECO as in another study[20] in equivalent ages in the ferret. Further, we find that a key element in the development of thalamocortical circuitry, the SPNs, have unique response properties, showing high selectivity to deviant stimuli. Since spiking in SPNs drive spiking in the thalamo-recipient L4 neurons, developmentally, the stimulus statistics itself is able to guide thalamocortical potentiation, through a pre-attentive mechanism. The results of exposure experiments show that relative to a repeatedly occurring standard frequency, before ECO, representation of a low probability deviant stimulus is strengthened more. Thus low probability salient stimuli before ECO at ages equivalent to human gestational week 25[28] cause long term plasticity. It potentially explains observations in humans of maternal voice recognition in infants[50,51]. The results

484 also suggest that prenatal sensory environment, can influence cortical development and
485 may also generalize to other sensory systems given the unique response properties of the
486 SPNs. Although our results are derived based on tones as stimuli, the possibility of coding of
487 auditory objects by the neurons in the ACX can also be addressed through similar
488 experiments. For example, specific response selectivity to species specific vocalizations in
489 mice and other species[52,53] could also be explained based on the low probability salient
490 occurrence of such sounds during early development. Corresponding experiments for other
491 sensory systems can lead to better understanding of cortical development.

492 Our model results, with two inputs explain the observations and an extension to a whole
493 network can also produce similar results. The model currently does not include inhibition,
494 an element crucial in development, as synaptic plasticity rules of inputs/outputs of
495 inhibitory neurons at such ages are not available. It is likely that it plays a crucial role as the
496 maturation of inhibition is controlled by SPNs[11]. Also effect of inhibitory switch, occurring
497 before ECO, on the activity driven plasticity observed before ECO, needs to be investigated.
498 The closure of critical period, around P16 also coincides with the observed near absence of
499 SPNs in mice from P15. Thus mechanisms implicated in critical period closure like inhibition,
500 adenosine, cholinergic inputs[4,47–49], could also be tied to SPNs since SPNs guide
501 development of subcortical projections. Finally, exposures with selective inhibition of SPN
502 activity during relevant periods of development are required to establish the SPN driven
503 cortical development further.

504 **Methods**

505 All animal experiments were approved by Institutional Animal Ethics Committee
506 (IAEC) of Indian Institute of Technology Kharagpur. Detailed methods are provided in the
507 Supplementary Materials. C57BL6/J strain mice (National Institute of Nutrition, Hyderabad,
508 India or Jax Labs) across different developmental time windows or in young adults (P29-P48)
509 were deeply anesthetized for surgery (2-2.5% isoflurane) and prepared by making a
510 craniotomy (3-4 mm diameter, based on stereotaxic co-ordinates and landmarks) for in-vivo
511 electrophysiological recordings from A1/AAF or MGB, with 16 channel electrodes
512 (Microprobes for Lifesciences) under isoflurane (0.5-1%) in a sound chamber (IAC Acoustics).
513 LFP and spiking responses to sounds (played through TDT free-field speakers ES1,
514 attenuated by PA5 and generated with TDT RX6) were obtained with a unity gain headstage
515 and preamps (Plexon Inc) and stored using National Instruments DAQ card. Sound
516 generation, data acquisition and online/offline analysis were done with custom written
517 MATLAB routines. Anatomical labelling and confirmation of recordings from A1/AAF and
518 from L4 or SP was done using multiple approaches (lipophilic tracer injections in recording
519 site, nissil sections and IHC). Exposure in specific auditory environments of mouse litters for
520 the different time windows were done in another sound chamber (IAC Acoustics)
521 maintaining a 8hr-16hr light dark cycle.

522 **Figure Legends**

523 Figure 1. Deviant selectivity of SP and L4 reduces with age in A1 with tone tokens. A-C) Spike
524 dot rasters and PSTHs of 3 neurons (2 in L4 and 1 in SP identified in title) in the developing
525 A1; i: pure tone rasters followed by PSTHs of chosen SD and frequencies, dark and light gray
526 bars in rasters; ii: pair of dot rasters and PSTHs to oddball presentations (SD and swap); iii:
527 time expanded PSTH at onset and deviant in ii. D) Dot rasters of response to tones of
528 example SP and L4 recorded simultaneously. E) Latencies of L4 and SP neurons recorded
529 simultaneously in P12-13 and P14-15 age groups showing lowering of latencies with age and
530 SPNs having lower latency than L4 neurons. F-G) Bar plots of mean deviant selectivity
531 measured by CSI(F) and CSI respectively for different f_1-f_2 values for L4 (dark) and SP (light).
532 H-I) Overall mean deviant selectivity for tone stimuli measured by CSI(F) and CSI respectively
533 as a function of age.

534 Figure 2. Deviant selectivity of SP and L4 reduces with age in A1 with tone and noise tokens.
535 A-B) Pairs of PSTHs to oddball presentations (SD and swap) for 6 representative L4 neurons
536 (A) of different ages (identified in the titles) and that of 3 SPNs (B). C-D) Overall mean
537 deviant selectivity for noise and tone tokens measured by CSI(F) and CSI respectively as a
538 function of age.

539 Figure 3. Neurons in the mouse ACX and IC respond to sounds before ECO. A) Wide field
540 fluorescence imaging based significant response ($p<0.05$, paired ttest, 40 repetitions)
541 regions (white contours) in 3 different ages before ECO and P13, after ECO. Smoothed df/f
542 traces with SEMs of selected regions (square) responding to selected frequencies (color) are
543 shown to the right of each image. The black bar represents the stimulus duration. B) As in A,
544 widefield fluorescence responses before ECO in the IC at P9 and P10. C) i) Mean df/f (40
545 repetitions) of L2/3 neurons (each row) in response to a single frequency tone (before and
546 after, P12-13, ECO). White line shows stimulus onset. ii) Population mean df/f of the age
547 groups (color) of neurons shown in Fig. Ci. iii) Box plot showing response reliability of all
548 L2/3 neurons imaged at the different ages. Straight line shows linear fit between %
549 reliability and age with the p value of correlation between them. D) i-ii) Extended 2-photon
550 Ca^{2+} imaging data showing mean df/f (40 repetitions) of single neurons (each row) and
551 population mean df/f (below) at two ages before ECO, showing long (>2s) spontaneous
552 window. E) Single neuron mean df/f and population mean df/f of the same age groups in
553 response to sound (i) and the same neurons without sound stimulation (ii), with 40
554 repetitions in each case. F) i) z-scores of single unit responses to tones at different age
555 groups before ECO in L4 and SP. z-score was computed in each 50 ms bin for each case (each
556 row is 1 unit in response to 1 frequency tone, 50 ms long, 10-30 repetitions). Top set are
557 units from L4 bottom set are for SPNs. The white vertical line represents stimulus onset. ii)
558 Population mean PSTHs of all the recorded units across different age groups which had a z-

score>1 in at least 1 time bin, with respective p-values (paired t-test). The black lines represent the stimulus onset.

Figure 4. SPNs unlike L4 neurons show deviant selectivity before ECO. A) i) Dot rasters and PSTHs of 3 L4 neurons (upper 4 rows, SD and Swap) and 3 SP neurons (lower 4 rows, SD and Swap) are shown in the first 3 columns (Insets: Raster for deviant responses and peaks). ii) Mean population PSTHs of all L4 and SP neurons (upper and lower two plots respectively) to SD (30 reps, 3.3 Hz) and its swap. iii) Same as Aii, for responses to SD (20 reps, 4Hz). B) i-iii) Population (3.3 and 4 Hz combined) histograms of CSI(F), CSI and CSI(P) for SP and L4 (light and dark gray bars respectively) show significantly higher deviant selectivity in SP. iv-v) Similar histograms with mean CSI calculated for each of 1000 random pair of SD response windows selections for S response and D response either before deviant (iv) or after deviant (v).

Figure 5. Exposure to an SD stimulus environment before ECO causes long term plasticity of responses to the D sound and not after ECO. A) Different exposure paradigms (EX0-6) by age and exposure stimulus are represented. B) Cartoon of different tuning curves and construction of profile of response to RF as a function of BF re RF. C) Boxplots for all significant rate responses in all tuning curves collected in the different EX groups. D) CDF plots of response rate distributions of different RFs considered in the different cases. Thin gray line shows mean an STD of CDFs of 13 such CDFs of control data with each of the 13 frequencies considered as RF. Thick gray lines show boundaries of the control CDFs. E) Profile of population mean response rates for 4 exposure cases (EX2&5, S,D and SS in i and EX1&6, S,D and SS in ii), and maximum boundary of 13 response profiles of control data shown in thick gray. Inset bar plot summarizes normalized (by mean response at BF to other frequencies >1/2 octave away from RF) population mean response to RF for neurons with BF at RF of all 6 EX cases (2 bars each, red and green for SD exposure cases and 1 blue for SS).

Figure 6. A binary network model of developing ACX with SP and TC inputs can explain observations of early exposure driven plasticity. A) Cartoon of network of SP and L4 neurons with 2 TC inputs to both SPN and L4, one selective for S and one for D. SPN projects to L4 (gray synapse). B) All synapses were depressing in nature with the example EPSP profile shown. C) The asymmetric STDP learning rule followed by all synapses on the L4 neuron is shown. LTD window was longer and modifications occurred over -80 to 40 ms of post–pre spike times. D) Sample PSTHs in earliest part of development (representing before ECO) shows high deviant selectivity in SP and low in L4 in the model neurons. E) Temporal evolution of the relevant synaptic strengths in the two exposure periods (i: Before ECO and ii: After ECO) for simulations of exposure with SD or SS protocol.

References

1. Schreiner, C. E. & Polley, D. B. Auditory map plasticity: Diversity in causes and consequences. *Current Opinion in Neurobiology* vol. 24 143–156 (2014).

2. Hensch, T. K. Critical period plasticity in local cortical circuits. *Nature Reviews Neuroscience* (2005) doi:10.1038/nrn1787.

3. de Villers-Sidani, E., Chang, E. F., Bao, S. & Merzenich, M. M. Critical Period Window for Spectral Tuning Defined in the Primary Auditory Cortex (A1) in the Rat. *J. Neurosci.* (2007) doi:10.1523/JNEUROSCI.3227-06.2007.

4. Takesian, A. E., Bogart, L. J., Lichtman, J. W. & Hensch, T. K. Inhibitory circuit gating of auditory critical-period plasticity. *Nat. Neurosci.* (2018) doi:10.1038/s41593-017-0064-2.

5. Barkat, T. R., Polley, D. B. & Hensch, T. K. A critical period for auditory thalamocortical connectivity. *Nat. Neurosci.* (2011) doi:10.1038/nn.2882.

6. Zhou, X. & Merzenich, M. M. Enduring effects of early structured noise exposure on temporal modulation in the primary auditory cortex. *Proc. Natl. Acad. Sci. U. S. A.* (2008) doi:10.1073/pnas.0800009105.

7. Zhang, L. I., Bao, S. & Merzenich, M. M. Persistent and specific influences of early acoustic environments on primary auditory cortex. *Nat. Neurosci.* **4**, 1123–1130 (2001).

8. Luhmann, H. J., Kirischuk, S. & Kilb, W. The Superior Function of the Subplate in Early Neocortical Development. *Front. Neuroanat.* **12**, (2018).

9. Kanold, P. O. & Luhmann, H. J. The Subplate and Early Cortical Circuits. *Annu. Rev. Neurosci.* (2010) doi:10.1146/annurev-neuro-060909-153244.

10. Kanold, P. O., Kara, P., Reid, R. C. & Shatz, C. J. Role of subplate neurons in functional maturation of visual cortical columns. *Science (80-.).* (2003) doi:10.1126/science.1084152.

11. Kanold, P. O. & Shatz, C. J. Subplate Neurons Regulate Maturation of Cortical Inhibition and Outcome of Ocular Dominance Plasticity. *Neuron* (2006) doi:10.1016/j.neuron.2006.07.008.

12. Ghosh, A. & Shatz, C. J. Involvement of subplate neurons in the formation of ocular dominance columns. *Science (80-.).* (1992) doi:10.1126/science.1542795.

13. Ghosh, A., Antonini, A., McConnell, S. K. & Shatz, C. J. Requirement for subplate neurons in the formation of thalamocortical connections. *Nature* (1990) doi:10.1038/347179a0.

14. McConnell, S. K., Ghosh, A. & Shatz, C. J. Subplate neurons pioneer the first axon pathway from the cerebral cortex. *Science (80-.).* (1989)

633 doi:10.1126/science.2475909.

634 15. Chang, E. F., Bao, S., Imaizumi, K., Schreiner, C. E. & Merzenich, M. M. Development
635 of spectral and temporal response selectivity in the auditory cortex. *Proc. Natl. Acad.*
636 *Sci. U. S. A.* (2005) doi:10.1073/pnas.0508239102.

637 16. Ulanovsky, N., Las, L. & Nelken, I. Processing of low-probability sounds by cortical
638 neurons. *Nat. Neurosci.* (2003) doi:10.1038/nn1032.

639 17. Ghosh, A. & Shatz, C. J. A role for subplate neurons in the patterning of connections
640 from thalamus to neocortex. *Development* (1993).

641 18. Zhao, C., Kao, J. P. Y. & Kanold, P. O. Functional Excitatory Microcircuits in Neonatal
642 Cortex Connect Thalamus and Layer 4. *J. Neurosci.* (2009) doi:10.1037/pha0000116.

643 19. Viswanathan, S., Bandyopadhyay, S., Kao, J. P. Y. & Kanold, P. O. Changing
644 Microcircuits in the Subplate of the Developing Cortex. *J. Neurosci.* **32**, 1589–1601
645 (2012).

646 20. Wess, J. M., Isaiah, A., Watkins, P. V & Kanold, P. O. Subplate neurons are the first
647 cortical neurons to respond to sensory stimuli. *Proc. Natl. Acad. Sci.* (2017)
648 doi:10.1073/pnas.1710793114.

649 21. Pérez-González, D. & Malmierca, M. S. Adaptation in the auditory system: an
650 overview. *Front. Integr. Neurosci.* (2014) doi:10.3389/fnint.2014.00019.

651 22. Nieto-Diego, J. & Malmierca, M. S. Topographic Distribution of Stimulus-Specific
652 Adaptation across Auditory Cortical Fields in the Anesthetized Rat. *PLoS Biol.* (2016)
653 doi:10.1371/journal.pbio.1002397.

654 23. Bandyopadhyay, S., Shamma, S. A. & Kanold, P. O. Dichotomy of functional
655 organization in the mouse auditory cortex. *Nat. Neurosci.* (2010)
656 doi:10.1038/nn.2490.

657 24. Issa, J. B. *et al.* Multiscale Optical Ca2+Imaging of Tonal Organization in Mouse
658 Auditory Cortex. *Neuron* (2014) doi:10.1016/j.neuron.2014.07.009.

659 25. Sawatari, H. *et al.* Identification and characterization of an insular auditory field in
660 mice. *Eur. J. Neurosci.* (2011) doi:10.1111/j.1460-9568.2011.07926.x.

661 26. Barbour, D. L. & Wang, X. Contrast tuning in auditory cortex. *Science (80-.).* (2003)
662 doi:10.1126/science.1080425.

663 27. Mill, R., Coath, M., Wennekers, T. & Denham, S. L. Abstract stimulus-specific
664 adaptation models. *Neural Computation* (2011) doi:10.1162/NECO_a_00077.

665 28. Clancy, B., Darlington, R. B. & Finlay, B. L. Translating developmental time across
666 mammalian species. *Neuroscience* (2001) doi:10.1016/S0306-4522(01)00171-3.

667 29. Chang, A. *et al.* Specific Influences of Early Acoustic Environments on Cochlear Hair
668 Cells in Postnatal Mice. *Neural Plast.* (2018) doi:10.1155/2018/5616930.

669 30. Babola, T. A. *et al.* Homeostatic Control of Spontaneous Activity in the Developing
670 Auditory System. *Neuron* (2018) doi:10.1016/j.neuron.2018.07.004.

671 31. Anthwal, N. & Thompson, H. The development of the mammalian outer and middle
672 ear. *J. Anat.* (2016) doi:10.1111/joa.12344.

673 32. Huangfu, M. & Saunders, J. C. Auditory development in the mouse: Structural
674 maturation of the middle ear. *J. Morphol.* (1983) doi:10.1002/jmor.1051760302.

675 33. Kim, K. X. & Fettiplace, R. Developmental changes in the cochlear hair cell
676 mechanotransducer channel and their regulation by transmembrane channel-like
677 proteins. *J. Gen. Physiol.* (2013) doi:10.1085/jgp.201210913.

678 34. Lelli, A., Asai, Y., Forge, A., Holt, J. R. & Géléoc, G. S. G. Tonotopic gradient in the
679 developmental acquisition of sensory transduction in outer hair cells of the mouse
680 cochlea. *J. Neurophysiol.* (2009) doi:10.1152/jn.00136.2009.

681 35. Abe, T. *et al.* Developmental expression of the outer hair cell motor prestin in the
682 mouse. *J. Membr. Biol.* (2007) doi:10.1007/s00232-007-9004-5.

683 36. Polley, D. B., Thompson, J. H. & Guo, W. Brief hearing loss disrupts binaural
684 integration during two early critical periods of auditory cortex development. *Nat.*
685 *Commun.* (2013) doi:10.1038/ncomms3547.

686 37. Ruebsamen, R. & Lippe, W. The development of cochlear function. in *Development of*
687 *the auditory system* (eds. Rubel, E., Poppe, A. & Fay, R.) 193–270 (Springer, 1997).

688 38. Shnerson, A. & Pujol, A. Development: anatomy, electrophysiology, and behavior. in
689 *The auditory psychobiology of the mouse* (ed. Willot, J.) 395–425 (Charles C. Thomas,
690 1983).

691 39. Pujol, R., Lavigne-Rebillard, M. & Lenoir, M. Development of sensory and neural
692 structures in the mammalian cochlea. in *Development of the auditory system* (eds.
693 Rubel, E., Popper, A. & Fay, R.) 146–192 (Spinger, 1997).

694 40. Tritsch, N. X. *et al.* Calcium action potentials in hair cells pattern auditory neuron
695 activity before hearing onset. *Nat. Neurosci.* (2010) doi:10.1038/nn.2604.

696 41. Mill, R., Coath, M., Wennekers, T. & Denham, S. L. A neurocomputational model of
697 stimulus-specific adaptation to oddball and markov sequences. *PLoS Comput. Biol.*
698 (2011) doi:10.1371/journal.pcbi.1002117.

699 42. Yarden, T. S. & Nelken, I. Stimulus-specific adaptation in a recurrent network model
700 of primary auditory cortex. *PLoS Comput. Biol.* (2017)
701 doi:10.1371/journal.pcbi.1005437.

702 43. Hromádka, T., DeWeese, M. R. & Zador, A. M. Sparse representation of sounds in the
703 unanesthetized auditory cortex. *PLoS Biol.* (2008) doi:10.1371/journal.pbio.0060016.

704 44. Lewicki, M. S. Efficient coding of natural sounds. *Nat. Neurosci.* (2002)
705 doi:10.1038/nn831.

706 45. Smith, E. C. & Lewicki, M. S. Efficient auditory coding. *Nature* (2006)
707 doi:10.1038/nature04485.

708 46. Sun, Y. J. *et al.* Fine-tuning of pre-balanced excitation and inhibition during auditory
709 cortical development. *Nature* **465**, 927–931 (2010).

710 47. Blundon, J. A. *et al.* Restoring auditory cortex plasticity in adult mice by restricting
711 thalamic adenosine signaling. *Science (80-.).* (2017) doi:10.1126/science.aaf4612.

712 48. Vickers, E. D. *et al.* Parvalbumin-Interneuron Output Synapses Show Spike-Timing-
713 Dependent Plasticity that Contributes to Auditory Map Remodeling. *Neuron* (2018)
714 doi:10.1016/j.neuron.2018.07.018.

715 49. Courtney E. Yaeger, Dario Ringach, J. T. T. Neuromodulatory control of localized
716 dendritic spiking in critical period cortex. *Nature* **567**, 100–104 (2019).

717 50. Mehler, J. *et al.* A precursor of language acquisition in young infants. *Cognition* (1988)
718 doi:10.1016/0010-0277(88)90035-2.

719 51. Voegtline, K. M., Costigan, K. A., Pater, H. A. & DiPietro, J. A. Near-term fetal response
720 to maternal spoken voice. *Infant Behav. Dev.* (2013)
721 doi:10.1016/j.infbeh.2013.05.002.

722 52. Portfors, C. V., Roberts, P. D. & Jonson, K. Over-representation of species-specific
723 vocalizations in the awake mouse inferior colliculus. *Neuroscience* (2009)
724 doi:10.1016/j.neuroscience.2009.04.056.

725 53. Wang, X. & Kadia, S. C. Differential Representation of Species-Specific Primate
726 Vocalizations in the Auditory Cortices of Marmoset and Cat. *J. Neurophysiol.* (2001)
727 doi:10.1152/jn.2001.86.5.2616.

728 54. Paxinos, G. & Franklin, K. B. J. *Paxinos and Franklin's the Mouse Brain in Stereotaxic*
729 *Coordinates*. *São Paulo, Academic Press* (2012). doi:10.1364/OE.20.020998.

730 55. Torii, M. & Levitt, P. Dissociation of corticothalamic and thalamocortical axon
731 targeting by an EphA7-mediated mechanism. *Neuron* (2005)
732 doi:10.1016/j.neuron.2005.09.021.

733 56. Osheroff, H. & Hatten, M. E. Gene expression profiling of preplate neurons destined
734 for the subplate: Genes involved in transcription, axon extension, neurotransmitter
735 regulation, steroid hormone signaling, and neuronal survival. *Cereb. Cortex* (2009)
736 doi:10.1093/cercor/bhp034.

737 57. Hoerder-Suabedissen, A. *et al.* Novel markers reveal subpopulations of subplate
738 neurons in the murine cerebral cortex. *Cereb. Cortex* (2009)
739 doi:10.1093/cercor/bhn195.

740 58. Gee, J. M. *et al.* Imaging Activity in Neurons and Glia with a Polr2a-Based and Cre-
741 Dependent GCaMP5G-IRES-tdTomato Reporter Mouse. *Neuron* (2014)
742 doi:10.1016/j.neuron.2014.07.024.

Figures

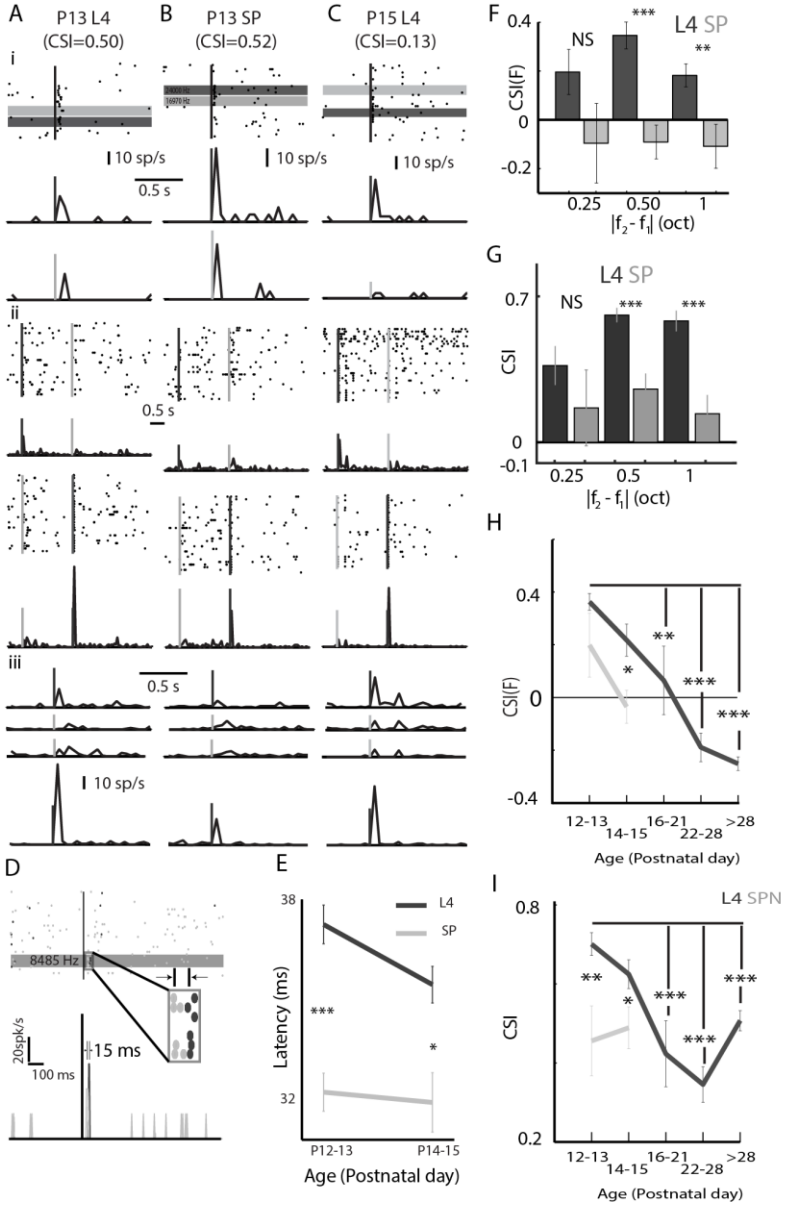

Figure 1. Deviant selectivity of SP and L4 reduces with age in A1 with tone tokens. A-C) Spike dot rasters and PSTHs of 3 neurons (2 in L4 and 1 in SP identified in title) in the developing A1; i: pure tone rasters followed by PSTHs of chosen SD and frequencies, dark and light gray bars in rasters; ii: pair of dot rasters and PSTHs to oddball presentations (SD and swap); iii: time expanded PSTH at onset and deviant in ii. D) Dot rasters of response to tones of example SP and L4 recorded simultaneously. E) Latencies of L4 and SP neurons recorded simultaneously in P12-13 and P14-15 age groups showing lowering of latencies with age and SPNs having lower latency than L4 neurons. F-G) Bar plots of mean deviant selectivity measured by CSI(F) and CSI respectively for different f_1-f_2 values for L4 (dark) and SP (light). H-I) Overall mean deviant selectivity for tone stimuli measured by CSI(F) and CSI respectively as a function of age.

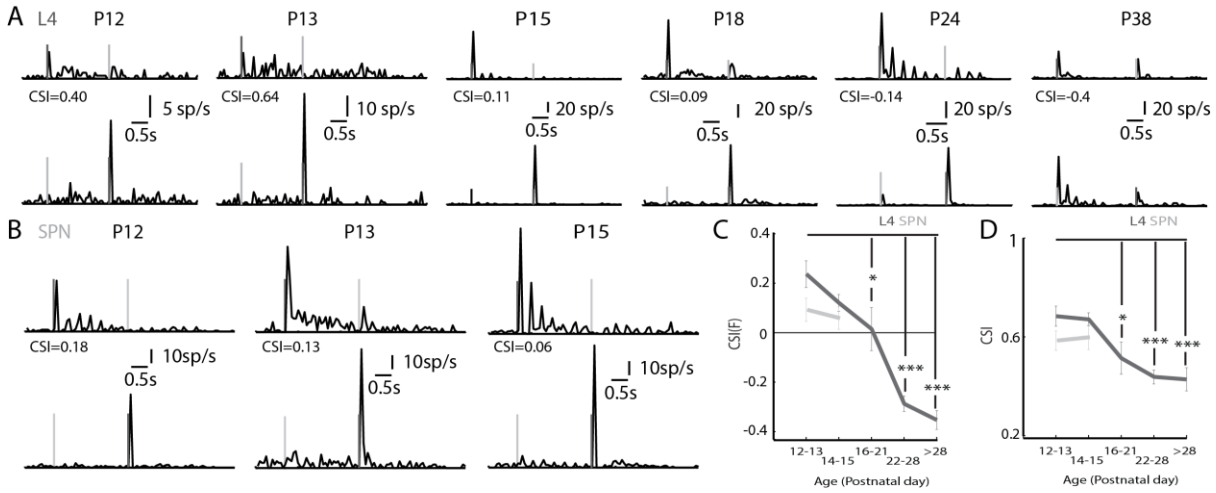

Figure 2. Deviant selectivity of SP and L4 reduces with age in A1 with tone and noise tokens. A-B) Pairs of PSTHs to oddball presentations (SD and swap) for 6 representative L4 neurons (A) of different ages (identified in the titles) and that of 3 SPNs (B). C-D) Overall mean deviant selectivity for noise and tone tokens measured by CSI(F) and CSI respectively as a function of age.

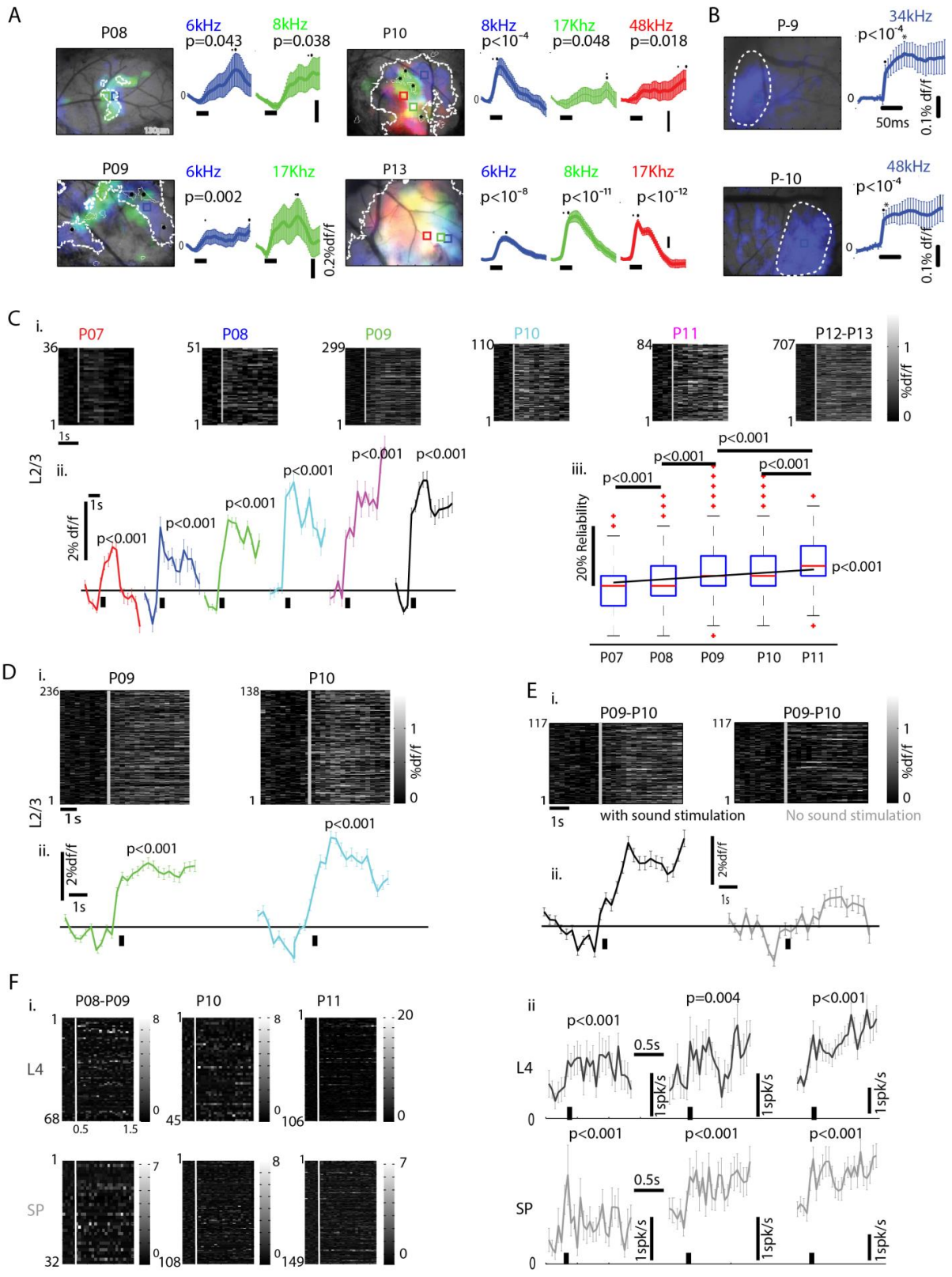

Figure 3. Neurons in the mouse ACX and IC respond to sounds before ECO. A) Wide field fluorescence imaging based significant response (p<0.05, paired ttest, 40 repetitions) regions (white contours) in 3 different ages before ECO and P13, after ECO. Smoothed df/f

traces with SEMs of selected regions (square) responding to selected frequencies (color) are shown to the right of each image. The black bar represents the stimulus duration. B) As in A, widefield fluorescence responses before ECO in the IC at P9 and P10. C) i) Mean df/f (40 repetitions) of L2/3 neurons (each row) in response to a single frequency tone (before and after, P12-13, ECO). White line shows stimulus onset. ii) Population mean df/f of the age groups (color) of neurons shown in Fig. Ci. iii) Box plot showing response reliability of all L2/3 neurons imaged at the different ages. Straight line shows linear fit between % reliability and age with the p value of correlation between them. D) i-ii) Extended 2-photon Ca^{2+} imaging data showing mean df/f (40 repetitions) of single neurons (each row) and population mean df/f (below) at two ages before ECO, showing long (>2s) spontaneous window. E) Single neuron mean df/f and population mean df/f of the same age groups in response to sound (i) and the same neurons without sound stimulation (ii), with 40 repetitions in each case. F) i) z-scores of single unit responses to tones at different age groups before ECO in L4 and SP. z-score was computed in each 50 ms bin for each case (each row is 1 unit in response to 1 frequency tone, 50 ms long, 10-30 repetitions). Top set are units from L4 bottom set are for SPNs. The white vertical line represents stimulus onset. ii) Population mean PSTHs of all the recorded units across different age groups which had a z-score>1 in at least 1 time bin, with respective p-values (paired t-test). The black lines represent the stimulus onset.

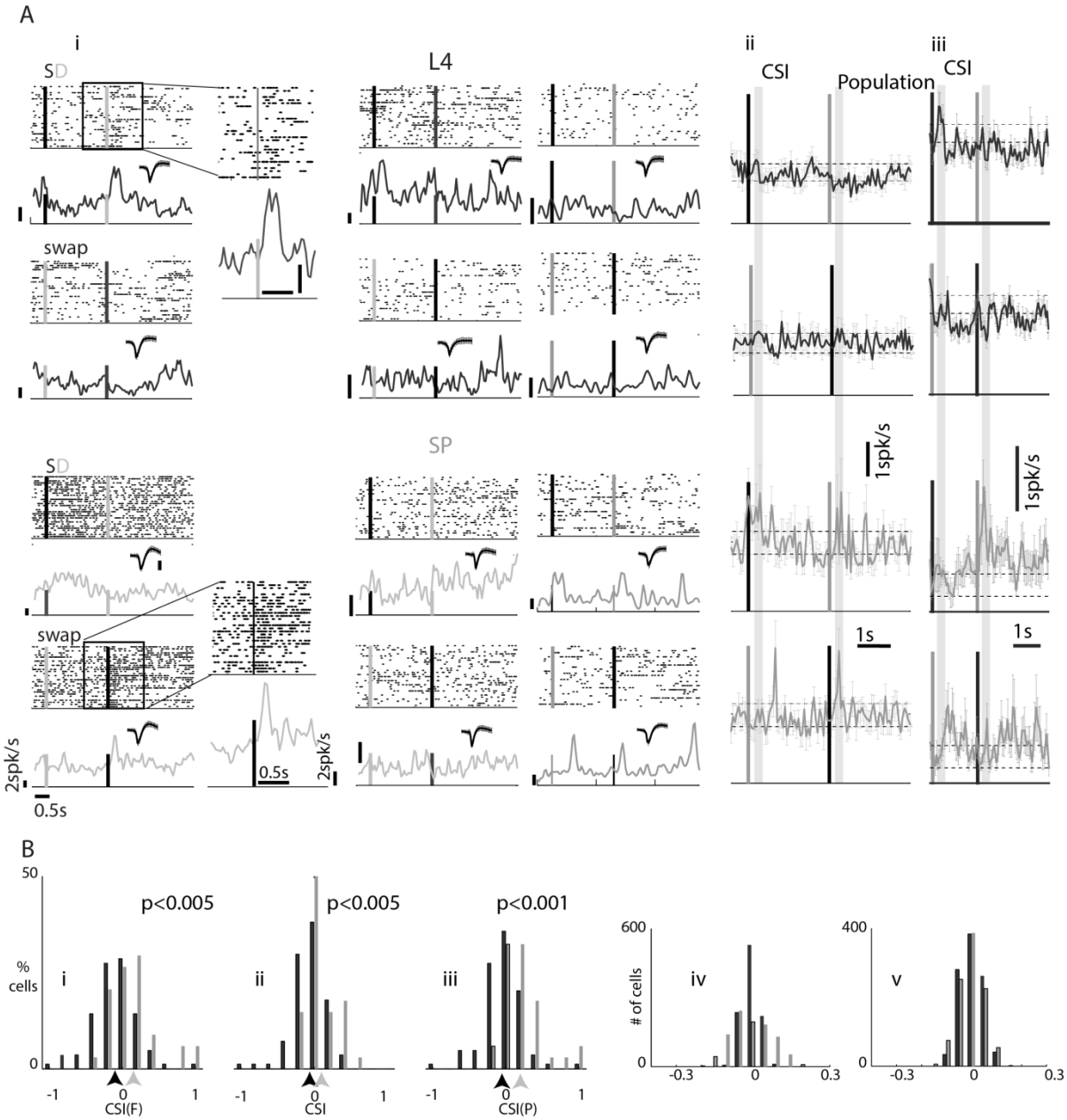

Figure 4. SPNs unlike L4 neurons show deviant selectivity before ECO. A) i) Dot rasters and PSTHs of 3 L4 neurons (upper 4 rows, SD and Swap) and 3 SP neurons (lower 4 rows, SD and Swap) are shown in the first 3 columns (Insets: Raster for deviant responses and peaks). ii) Mean population PSTHs of all L4 and SP neurons (upper and lower two plots respectively) to SD (30 reps, 3.3 Hz) and its swap. iii) Same as Aii, for responses to SD (20 reps, 4Hz). B) i-iii) Population (3.3 and 4 Hz combined) histograms of CSI(F), CSI and CSI(P) for SP and L4 (light and dark gray bars respectively) show significantly higher deviant selectivity in SP. iv-v) Similar histograms with mean CSI calculated for each of 1000 random pair of SD response windows selections for S response and D response either before deviant (iv) or after deviant (v).

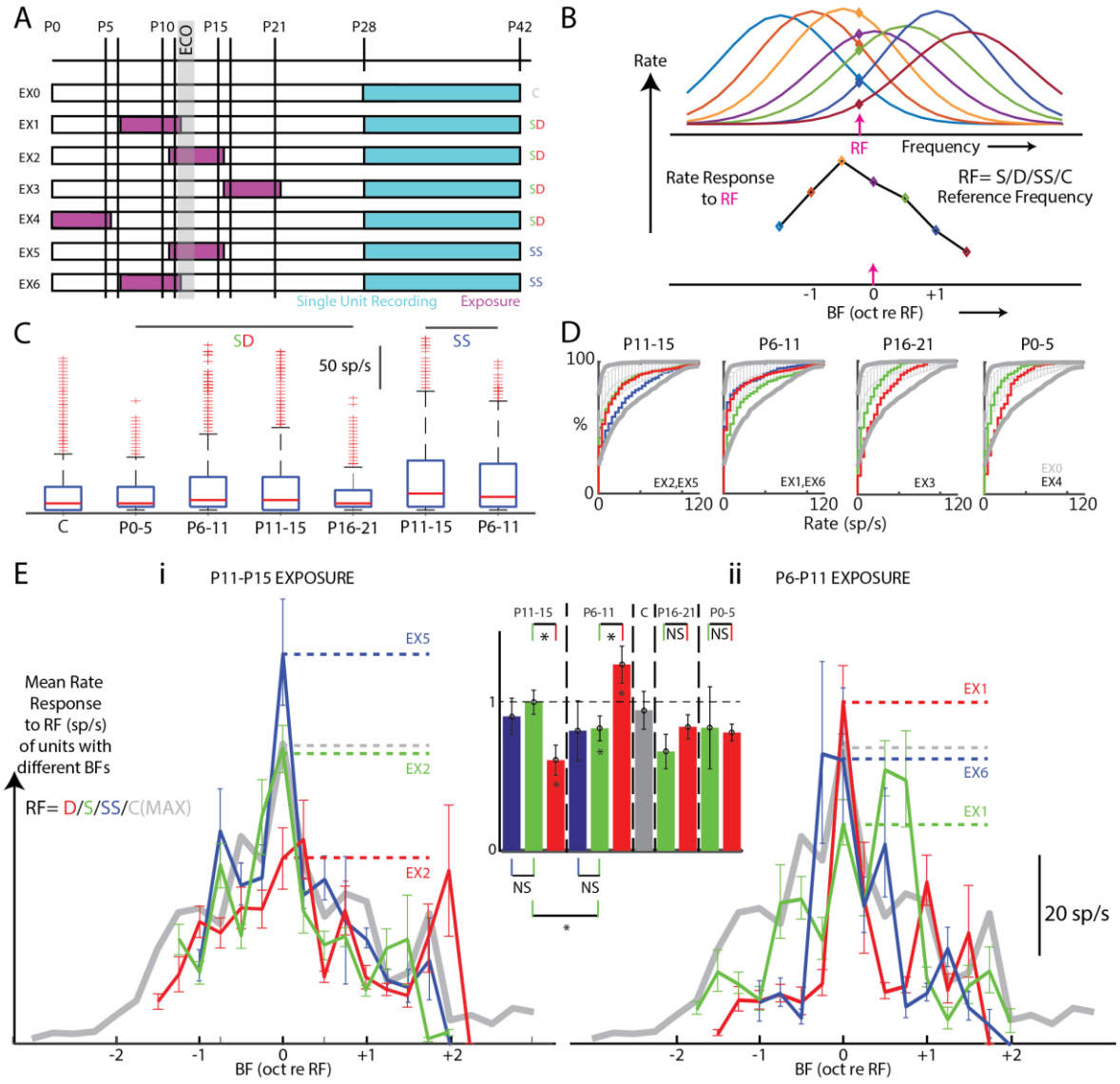

Figure 5. Exposure to an SD stimulus environment before ECO causes long term plasticity of responses to the D sound and not after ECO. A) Different exposure paradigms (EX0-6) by age and exposure stimulus are represented. B) Cartoon of different tuning curves and construction of profile of response to RF as a function of BF re RF. C) Boxplots for all significant rate responses in all tuning curves collected in the different EX groups. D) CDF plots of response rate distributions of different RFs considered in the different cases. Thin gray line shows mean an STD of CDFs of 13 such CDFs of control data with each of the 13 frequencies considered as RF. Thick gray lines show boundaries of the control CDFs. E) Profile of population mean response rates for 4 exposure cases (EX2&5, S,D and SS in i and EX1&6, S,D and SS in ii), and maximum boundary of 13 response profiles of control data shown in thick gray. Inset bar plot summarizes normalized (by mean response at BF to other frequencies >1/2 octave away from RF) population mean response to RF for neurons with BF at RF of all 6 EX cases (2 bars each, red and green for SD exposure cases and 1 blue for SS).

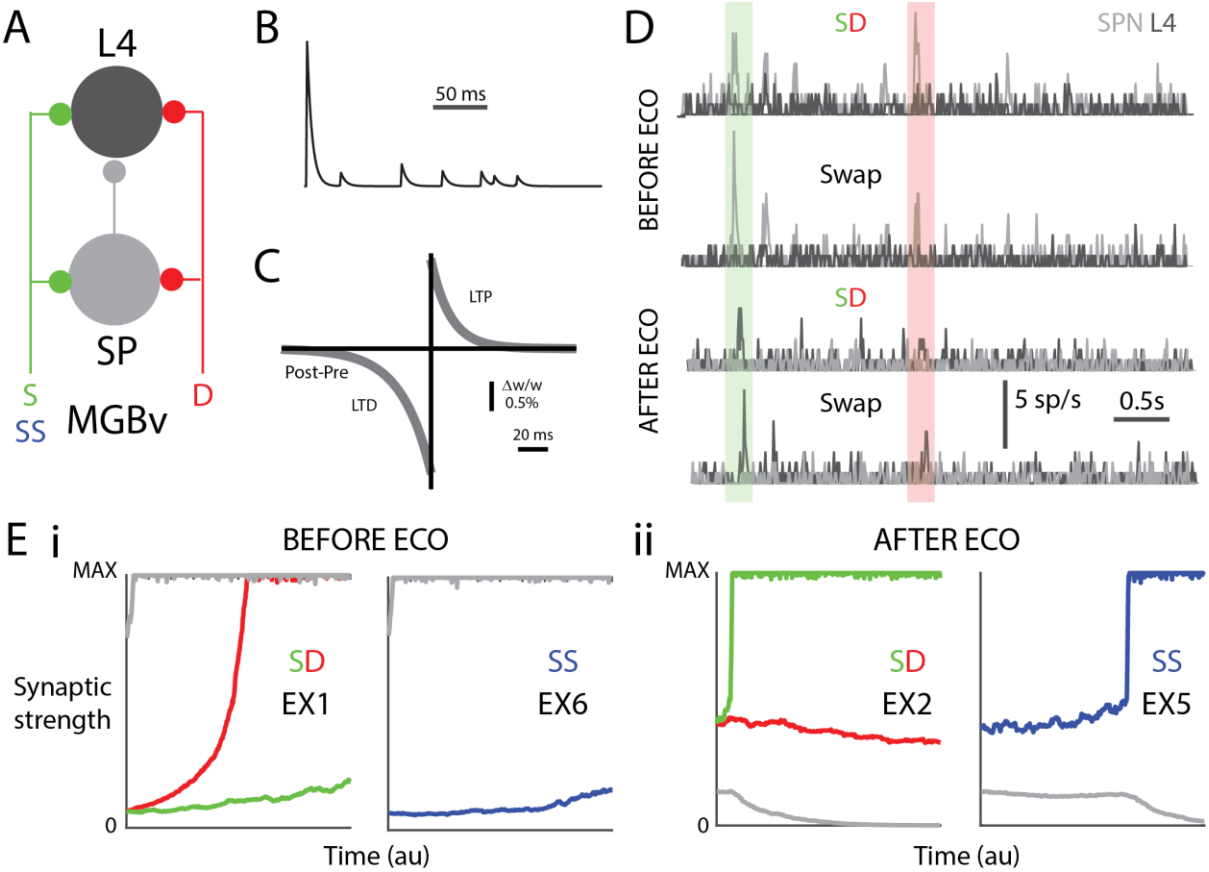

Figure 6. A binary network model of developing ACX with SP and TC inputs can explain observations of early exposure driven plasticity. A) Cartoon of network of SP and L4 neurons with 2 TC inputs to both SPN and L4, one selective for S and one for D. SPN projects to L4 (gray synapse). B) All synapses were depressing in nature with the example EPSP profile shown. C) The asymmetric STDP learning rule followed by all synapses on the L4 neuron is shown. LTD window was longer and modifications occurred over -80 to 40 ms of post–pre spike times. D) Sample PSTHs in earliest part of development (representing before ECO) shows high deviant selectivity in SP and low in L4 in the model neurons. E) Temporal evolution of the relevant synaptic strengths in the two exposure periods (i: Before ECO and ii: After ECO) for simulations of exposure with SD or SS protocol.

832 **Supplementary Material**

833 **Detailed Materials and Methods**

834 **Subjects**

835 All animal experiments were approved by Institutional Animal Ethics Committee
836 (IAEC) of Indian Institute of Technology Kharagpur.

837 In-vivo electrophysiological recordings were performed on C57BL6/J strain mice
838 (National Institute of Nutrition, Hyderabad, India or Jax Labs) across different
839 developmental time windows in two different contexts, tone-tone (f_1-f_2) pairs (P12-P13, n=3
840 mice, 28 L4 units, 9 SPN units, 47 L4 cases, 14 SPN cases, ; P14-P15, n=3 mice , 41 L4 units,
841 34 SPN units, 63 L4 cases, 51 SPN cases; P16-P21, n=3 mice, 11 units, 15 cases; P22-P28,
842 n=4 mice, 24 units, 53 cases; >P28, n=3 mice, 26 units, 74 cases) and Noise-tone (N-f) pairs
843 (P12-P13, n=10 mice, 45 L4 units, 54 SPN units, 57 L4 cases, 101 SPN cases ; P14-P15, n=8
844 mice, 66 L4 units, 59 SPN units, 115 L4 cases, 67 SPN cases; P16-21, n=4 mice, 20 units, 31
845 cases; P22-P28, n=6 mice, 38 units, 97 cases ; >P28, 7 mice, 44 units, 63 cases). For
846 experiments in mice before ECO single unit or LFP responses with 5 stimulus repetitions for
847 tone and noise we recorded in 9 mice (38 units: P08=1; P09, n=2; P10, n=2; P11, n=3; P12,
848 n=1). In an additional 8mice, single unit responses to tones, noise (10-30 repetitions) and SD
849 paradigm with 30 repetitions were obtained. Over all before ECO n=15animals were
850 included to have responses (P08, n=2; P09, n=4; P10, n=4; P11, n=4; P12, n=1)) out of 38
851 animals tried. For recording L2/3 responses, 2-photon Ca^{+2} imaging was performed on Thy1-
852 Gcamp6f (n=12, P07=2; P08=1; P09=3; P10=3; P11=1; P12=1; P13=1) mice. In a subset of the
853 above animals (n=9, P07=1; P08=1; P09=3; P10=3; P13=1) wide field fluorescence imaging
854 was performed.

855 **Anatomical labelling**

856 In order to guide in-vivo electrophysiology and identify SP layer based on
857 morphology and cytoarchitecture of neurons, Nissl staining was performed at different age
858 groups. Mice of ages P6 (n=2 mice), P13 (n=2 mice), P16 (n=2 mice) and P18 (n=2 mice) were
859 initially perfused and the brains were harvested. Since ear canal opening is after P11 and as
860 the cortical size stabilizes by P21, the above ages were chosen initially for the
861 characterization. Nissl stains were performed after obtaining coronal sections of the
862 auditory regions based on mouse atlas[54]. For further confirmation, immunohistochemistry
863 was performed on brain slices across different developmental time points (P06-P07, n=2
864 mice; P08-P11, n=3 mice, P12-13, n=5mice; P14-P16, n=2mice; P17-P19, n=2 mice; P20-28,
865 N=3 mice; >P28, n=2 mice) with known markers of SP which are Complexin 3 (Cplx3);
866 Synaptic Systems (122302) and Connective Tissue Derived Growth Factor (CTGF); Santa Cruz
867 (sc-14939). Paraformaldehyde (PFA) fixed brain tissue was embedded in a 3% agarose
868 block. Brain embedded block was fixed on a vibrotome (Leica) sectioning platform. 50

869 micron thin sections of auditory slices were cut, blocked and permeabilized in a buffer
870 containing, 1% BSA, 0.3% Triton X and 10% Normal Donkey Serum (for CTGF) or 10% Normal
871 Goat Serum (for Cplx3). Sections were incubated in primary antibodies (Cplx3: 1:500 and
872 CTGF: 1:500) overnight and followed by washing with 1X PBS five times. Thereafter, sections
873 were incubated for two hours in Secondary antibodies (Cplx3: anti rabbit 594, Invitrogen
874 and CTGF: anti goat 488, Invitrogen) diluted in buffer, 1% BSA, 3% serum and 0.3% triton X
875 at room temperature. Sections were rinsed, mounted and imaged under epifluorescence
876 microscopy. Depth of SP in different regions and at different developmental time scales
877 was determined from these initial studies and was used as a guide for performing
878 electrophysiology recordings. Further confirmation about recordings from input layer (Layer
879 IV) was also obtained from SCNN1-td-tomato (cross of SCNN1-cre and floxed-td-tomato: JAX
880 mice) mice, which have SCNN1 expressing neurons (specific to Layer IV) labelled, allowing
881 confirmation of recordings in Layer IV. Sections were imaged using epi-fluorescence
882 microscopy (Xcite illumination, Bruker) and analysed for cytoarchitecture using custom
883 written codes in MATLAB.

884 **In-vivo extracellular single unit recordings**

885 Initially animals were anaesthetised with deep anaesthesia (5% Isoflurane) inside the
886 induction chamber. Initial Induction aids in maintaining anaesthesia level in animals even
887 after bringing down the anaesthesia levels (1.5-2%) during surgery. Core body temperature
888 was maintained constantly at 37°C with a heating pad, throughout the experiment. A central
889 incision was made and the left temporal portion of the skull was exposed. Exposed left
890 temporalis was cleaned with application of alcohol. Thereafter, tissue clearance was done
891 by rubbing the skull with 3% of Hydrogen peroxide. A 5mm diameter region was marked on
892 the left hemisphere. Skull was firmly fixed after keeping the mark at the centre of a head
893 plate. Craniotomy was performed over the estimated auditory cortical area. After
894 performing craniotomy, experimental animal was shifted immediately to a sound proof
895 chamber (IAC Acoustics). The depth of anaesthesia was monitored constantly throughout
896 the experiment with paw pinches. During recording sessions anaesthesia was brought down
897 to a concentration of 0.5-1%, in order to get robust responses from primary auditory cortex.

898 Extracellular recordings were performed from the left auditory cortex using tungsten
899 Micro Electrodes Array (MEA) of impedance 3-5 Mega ohms (MicroProbes, USA). A 4X4
900 custom designed metal MEA with inter electrode spacing of 125 microns was lowered into
901 the auditory cortex using a micromanipulator (MP-285, Sutter Instrument Company,
902 Novato, CA). We also performed recording using arrays separated by 400 or 600 microns in
903 length to record across laminae simultaneously (for example, Layer IV and SP, Fig. S1).
904 Signals were acquired after passing through a unity gain headstage (Plexon, HST16o25)
905 followed by PBX3 (Plexon) preamp with gain of X1000, to obtain wideband signal (used to
906 extract LFP, 0.7 Hz to 6 kHz) and spike signals (150 Hz to 8 kHz) in parallel and acquired

907 through National Instruments Data Acquisition Card (NI-PCI-6259) at 20 KHz sampling rate,
908 controlled through custom written MATLAB (Mathworks, Natick, USA) routines. Further, all
909 online/offline analysis was performed using custom written MATLAB routines. To obtain
910 laminar profile of responses from primary auditory cortex (A1), multiple depths were
911 covered by advancing the electrodes in depth at 100-150 micron steps.

912 Since the size and location of A1 over development varies, it is important to confirm
913 location of recording to be A1. For A1 recordings additional physiological information based
914 on tuning – existence of broad tonotopy, across electrodes in the recording array, latency of
915 responses, selectivity to tone stimuli was used to confirm recordings in primary auditory
916 areas (A1 and Anterior Auditory Field (AAF)). Based on location of electrode tracks and
917 comparison with mouse brain atlas[54] and landmarks (location relative to rhinal vein, size of
918 hippocampus in coronal slices) also provides additional confirmation of recording location.
919 In many experiments after recording a DiI crystal[55], a lipophilic tracer, was inserted into the
920 cortex at the recording location. After allowing passive travel of the tracer for 20-30 days at
921 35°C , brain slices are cut to look for labelled fibres and cell bodies in the ventral division of
922 the MGB (lemniscal structure projecting to A1) allowing confirmation of recordings in A1 Fig.
923 S1C). We further confirmed recordings from electrode location in primary regions
924 subsequently, from broad tonotopy observed (Fig. S1B). The recording depths targeted for
925 L4 and SPN were based on known depths of L4 and SPNs in ACX[19]; also, in a separate groups
926 of mice (P12-P13, n=5; P14-P16, n=3) depth of SPNs was determined to be above 900 µm
927 based on two methods. First by cell morphology in Nissl stains of coronal slices (Fig. S1D)
928 and second by immunostaining coronal slices containing A1 with antibodies of SPN
929 markers[56,57], *Complexin3* and *CTGF* (Fig. S2), at different ages (Fig. S2C) and depth range of
930 L4 from expression of *SCNN1* (B6.Cg-Tg(Scnn1a-cre)3Aibs/J mouse, Jax Labs, 09613 crossed
931 with CAG-tdTomato mouse Jax Labs, 07909), a L4 specific marker[19]. In a subset of mice in
932 which electrophysiological recordings were performed we confirmed electrode recording
933 site to be in SP layer from electrode tracks along with immunostaining as above (Fig. S3A)
934 and electrodes to be in L4 by performing recordings in the *SCNN1-cre*-td-Tomato (P14 and
935 P18) mice (Fig. S3). Depths of other layers (L2/3 and L5/6) were determined based on the
936 above results.

937 **Acute craniotomy for widefield imaging and 2-photon Ca^{2+} imaging**

938 A standard surgical procedure was performed as mentioned above in in-vivo
939 electrophysiology recordings. Animals were initially anaesthetised under isoflurane
940 (induction at 5% isoflurane followed by 2% isoflurane). After removing the skin and tissue
941 above the skull, a metallic head plate was implanted above the estimated auditory cortical
942 area. Craniotomy of around 3mm diameter was performed over left auditory area. Smaller
943 size craniotomy was preferred, as it gave us the advantage to minimize brain motion.
944 Thereafter, craniotomy was filled with 1.5% low melting-point Agarose and immediately a

945 5mm coverslip was imbedded over the craniotomy. Animals were then transferred to the 2-
946 photon imaging setup and the level of anaesthesia was reduced down to 0.1-0.2% isoflurane
947 during the recordings.

948 **Auditory stimulation for in-vivo electrophysiology**

949 Stimulus was presented inside sound proof chamber, 10 cm away from the right ear
950 (contralateral) of the mouse, with TDT electrostatic speakers (ES1) driven by TDT drivers ED1
951 after attenuation by TDT attenuators (PA5) generated through TDT RX6 using custom made
952 software written in MATLAB. The acoustic calibrations, performed with microphone 4939
953 (Brüel & Kjær, Denmark), of the ES1 speakers (TDT) in the sound chamber, showed a typical
954 flat (+/- 7 dB) calibration curve from 4-60 kHz.

955 **Auditory stimulation for imaging**

956 Stimulus was presented through electrostatic speaker (ES1) placed 2cm away from
957 the right ear of the mouse pups Stimulus was generated through custom written software in
958 MATLAB (Mathworks), passed through TDT RZ6 multifunctional processor. Acoustic
959 calibrations were performed using microphone 4939 (Brüel & Kjær, Denmark) and showed a
960 typical flat (+/- 7 dB) calibration curve from 4-60 kHz. Auditory stimuli consisted of
961 broadband noise (6-48 kHz, 40 repetitions), tones (40 repetitions of respective frequencies),
962 and series of sound token representing SD paradigm (30 repetitions). Only for one of the
963 animals (P12, after ear canal opening) 5 repetitions of each tonal frequency were delivered.
964 Each of the stimuli was interleaved with a gap of 5s. The loudest intensities of sounds at 80-
965 90 dB SPL were presented to ear, in order to allow mechanotransduction at younger ages
966 (before ear canal opening).

967 Single units spike times were obtained from the acquired spike channel data using
968 threshold crossing and spike sorting with custom written software in MATLAB.

969 **Wide Field Imaging**

970 For wide field calcium imaging, imaging signals were acquired using a 14-bit
971 CoolSNAP HQ2 CCD camera (Photometrics). Images of surface vasculature were acquired
972 using blue LED illumination (470 nm), and wide field GCaMP6f signals were recorded at ~30
973 Hz using blue illumination (470 nm)[58]. Fluorescence signals were acquired at 4x binning of
974 1040x1392 pixels, using a 4X objective (Olympus). Based on the auditory landmarks (Medial
975 cerebral artery (MCA) and rhinal vein position) and the responses to different frequencies,
976 the region of interest and the focal plane of the image (150-300 µm) were moved to desired
977 coordinates for performing 2-photon imaging.

978

979

980 **Two-Photon Calcium Imaging**

981 Two photon calcium imaging was performed using a commercially available 2-
982 photon microscopy system (Prairie View Technologies). The microscopy was controlled by
983 Prairie View software (Prairie View Technologies). For imaging, excitation beam of
984 wavelength 860nm generated from Insight laser (Spectra Physics, USA) was directed over
985 the exposed brain volume. The laser was delivered through 20X/0.8 NA water immersion
986 objective (2mm WD, Olympus). The laser power was adjusted from 50mW to 80mW
987 depending upon the condition of the specimen. Frames in region of interests (~150 µm x
988 200 µm with 1.16 µm pixel size) were imaged at ~4-6 Hz (160-250ms frame period, 1.2-4 µs
989 dwell time) with the stimulus presented at usually the 6th (to the 10th) frame in a sequence
990 of 20-30 frames per stimulus.

991 **Exposure protocol**

992 For another set of experiment, animal litters were exposed to sound sequences inside a
993 soundproof chamber with maintained 8-hr light and 16hr dark cycle, continuously for 5 days
994 in 4 age groups (P0-P5/6, P6-P10/11, P11-P15/16 and P16-P21).

995

996 Table S1

Age of exposure	Protocol	Litter	Animals	Units	Tuning curves
Control	No exposure	2	3+3	400	815
P6-P11	SD (12kHz-17kHz) SD (20kHz-14kHz)	1+1	5+3	256 197	504 525
P11-P16	SD (12kHz-17kHz) SD (14kHz-10kHz)	1+1	2+3	367 233	700 553
P16-P21	SD (12kHz-17kHz)	1+1	2+2	130	255
P0-P5	SD (12kHz-17kHz)	1+1	2+2	183	370
P11-P16	SS (only 12kHz)	1	3	327	642
P6-P11	SS (only 12kHz)	1	3	194	487

997

998 The litters were kept along with the breeders in a cage. Each exposure stimulus was
999 synthesised online and presented through electrostatic speaker, kept 5cm above the cage,
1000 using custom written codes on MATLAB. All the age groups were presented with sequence
1001 of stimuli having 50 ms sound tokens with a 250 ms inter-token gap at 90 dB SPL. The
1002 sequence (SD) had token of two frequencies, a standard (S) having an arrival probability of
1003 90% and a deviant (D) arriving with 10% probability. For only standard exposure (SS), there

1004 was no D frequency. After sound exposure animals were returned immediately to home
1005 cages in animal house and reared up in normal environment until experiments were
1006 performed. During recording sessions, mapping of primary auditory cortex was performed.
1007 Tone pips (50 ms, 5 ms up down ramps, 6-48 kHz, 0.25 octaves difference at 10-50 dB above
1008 threshold, 10 dB increments, 5 repetitions of each frequency-Intensity combination) was
1009 presented to the right ear. Extracellular responses were recorded from thalamo-recipient
1010 layer (Deep Layer III and layer IV) at depth 350-500 microns. Frequency responses area
1011 (FRA) was constructed of each unit for minimum of three sound levels played. Single units
1012 from A1 having response peak latency within 9 ms to 31 ms were included in the analysis.
1013 This window was selected on the basis of population mean and variance of response peak
1014 latencies obtained across all sound levels.

1015

1016 **Data Analysis**

1017

1018 *Identification of Subplate Layer*

1019

1020 SP Layer from nissl staining was based on compartmentalization drawn by cell sparse zone
1021 above and the horizontally oriented cytoarchitecture of the SP layer. Based on above
1022 features manual points (perpendicular to lamina) using MATLAB on slice images were
1023 selected to define depth and width of the SP layer. Similar analysis was performed too on
1024 the immunolabelled brain slice images.

1025

1026 *Rate Calculation*

1027 Neuronal firing rate was computed by calculating mean response within stimulus duration
1028 or token. Only single units that responded (compared to spontaneous activity 400ms
1029 preceding stimulus, 2-tailed t-test, $p<0.05$) to at least one of the stimuli (sound token (*f* or
1030 *N*) as standard or deviant) used were considered for analysis.

1031

1032 *Latency Analysis (Fig. 1D)*

1033 For each neuron, tuning parameters (Best Frequency (BF), Latency and Tuning width) were
1034 defined using custom written codes in MATLAB. Best frequency for a neuron is the
1035 frequency which elicits maximum response within stimulus duration (50 ms) to a given
1036 frequency at given sound level. Latency to stimulus onset was defined as the time bin (5 ms
1037 resolution) at which peak response was observed for a BF.

1038 Tuning width was computed using the Full width Half Maximum (FWHM). Only single peak
1039 tuning curves were considered for tuning width analysis. A continuous stretch of
1040 frequencies crossing the threshold (half of the maximum amplitude) was considered as the
1041 tuning width of a neuron.

1042

Adaptation Time Constants (Fig. S8)

A time course analysis was performed to fit the response rates for a SSS…..SDS….SS stimuli. Across all age groups and cortical layers, we employed exponential fitting to only those responsive units which have significant responses for tone as standards. To compute exponential decay time constants, the average spike rate in each token before the deviant was fitted with a first degree exponential curve, based on least square error method. Fitting was performed using the 'fit' function in MATLAB.

LFP Analysis (Fig. 3A, Fig. S10)

For LFP analysis, baseline shifting was performed to have mean of baseline 200 ms preceding the stimulus at 0. To obtain LFP, acquired wideband signals were notch filtered (50Hz, Butterworth 8th order, to remove AC supply line noise) and then bandpass filtered (between 1 Hz and 300 Hz, Butterworth 2nd order). LFPs were smoothed further using a Gaussian window, SD 150 ms. Due to the unreliability of responses as observed in the spiking data before ECO, for our population analysis we considered all the LFP recorded for all presented frequencies in order to quantify the response magnitude in terms of population mean amplitude and mean RMS value (across 50ms bin). LFP responses crossing the threshold of 200 mV throughout the recorded time window were excluded from population analysis.

Connectivity between pairs (Fig. S17)

Cross-correlation between pairs of PSTHs (nrep= 20-30 repetitions of SD stimulus and swap, bin size = 2ms) was used to detect connections between simultaneously recorded pairs of neurons (SP-L4 pairs). Bootstrap analysis was done to get variability in the cross-correlograms (MATLAB xcorr function, up to lag of 20 ms) by randomly resampling (same number of repeats from the existing 20-30 repeats) with replacement, 100 times. Thus a mean and SD (dark line with errorbar (Fig. S17A) of the correlograms were obtained. To compare with spurious cross correlations, all repeats from both neurons were mixed to give (2*nrep spike trains) and randomly nrep of them were assigned to each of the neurons and from these PSTHs cross-correlograms were obtained with mean and SD by repeating the process 100 times (gray lie with errorbar, Fig. S17A). Non-overlap of errobars were considered to be significant connections between the pair of neurons. We used 1.65-SD for data in P12 and above groups and 1-SD in before ECO group due to large difference in firing rates of single units in the two cases.

1083 Table S2

Interelectrode distance		Connected pairs /Total pairs SP ⟶ L4	Connected pairs /Total pairs L4 ⟶ SP
125	Before ECO P12-P13	6/12 27/102	4/12 22/102
200-300	Before ECO P12-P13	3/12 16/78	3/12 16/78
350-400	Before ECO P12-P13	0/2 5/10	0/2 4/10
>400	Before ECO P12-P13	1/1 2/10	1/1 4/10

1084

1085 **Imaging Analysis**

1086 Wide Field imaging analysis was performed using custom codes written in MATLAB
1087 (Mathworks). For analysis of the wide field data raw images collected were binned at 4x and
1088 then smoothed with a moving window of 4x4. Further analysis was done on the smoothed
1089 images. In order to find the significant pixels, a one-sided t-test across all the iterations was
1090 performed between the 5 frames immediately preceding the stimulus onset and a moving
1091 window of 5 frames after the stimulus onset in all 130 µm by 130 µm square areas. Only
1092 those pixels which gave a p-value less than 0.05 on at least one window after the stimulus
1093 onset were considered for further analysis. The mean change in df/f with time traces was
1094 constructed for pixels showing significant positive responses. These traces were further
1095 smoothed with a moving average window of 5 frames and a one-sided t-test was performed
1096 again to find the first significant post-stimulus frame and the frame with the most significant
1097 response. Some of these traces which showed the maximum response are shown in the
1098 main text (Fig.3A) and supplementary figure (Fig. S11C).

1099

1100

1101

1102

1103

1104

1105

1106

1107 Table S3

Sl.no.	Age	Tonal stimuli played (~90db SPL, in kHz)	Significant responsive frequencies and respective % responding areas	Fraction of frequencies played showed responses (%)
1.	P-7	8.5,12,17,24,48	8.5kHz: 2.86%	20.00%
2.	P-8	6,8.5,12,17,24,34, 48	6kHz: 0.56%; 8.5kHz: 3.67%	28.57%
3.	P-9	6,8.5,12,17,24,34, 48	6kHz: 26.9%; 17kHz: 3.44%; 24kHz: 0.56%; 48kHz: 1.31%	57.14%
4.	P-10	6,8.5,12,17,24,34, 48	8.5kHz: 37.12%; 12kHz: 4.38%; 17kHz: 0.5%; 48kHz: 19.93%	57.14%
5.	P-13	6,8.5,12,17,24,34, 48	6kHz: 43.8%; 8.5kHz: 79.8%; 12kHz: 13.54%; 17kHz: 70.8% 24kHz: 22.9%	71.42%

1108

1109 2-photon imaging analysis was performed using custom codes written in MATLAB
1110 (Mathworks). Imaging sequences were aligned by performing X-Y drift correction. Cells
1111 were selected manually by selecting the centre point of the cell on the motion corrected
1112 mean image. ROI (5 µm radius) were drawn based on the cell centres. Raw Fluorescence
1113 signal over time (F) of the selected ROIs across all frames were extracted. For each trial,
1114 relative fluorescence was computed by using $\Delta F/F_0 = (F - F_0)/ F_0)$, where F_0 corresponds to
1115 baseline fluorescence. Baseline fluorescence amplitude was estimated by computing mean
1116 of fluorescence values over 5 frames before the stimulus onset. Neurons on stimulation to
1117 tones and noise were considered to be significantly responsive as follows. One-sided paired
1118 ttest's were performed between mean df/f over 3 of the successive frames before the
1119 stimulus and each one of 4 windows, of 3 successive frames after stimulus onset (up to the
1120 6th frame, ~1.2-1.5s). If any of the 4 moving windows showed a significant increase in mean
1121 df/f (40 repetitions) over baseline, the neuron was considered responsive.

1122 Table S4

Sl.no.	Age	Fraction of cases (all neurons in response to different frequency tone) that showed significant responses.
1.	P-7	5.78%
2.	P-8	4.13%
3.	P-9	5.91%
4.	P-10	3.08%
5.	P-11	2.31%
6.	P12-P13	8.23%

1123

1124 Table S5

Sl.no.	Age	Fraction of cases (all neurons in response to broadband noise) that showed significant responses.
1.	P-7	5.35%
2.	P-8	10.25%
3.	P-9	8.11%

1125

1126 For significant responses in single trials to compute reliability, a trial was deemed responsive
1127 if the mean df/f of 4 frames (~1s) after the stimulus after stimulus onset was greater than
1128 1*STD (STD obtained from 40 repetitions) of the mean of the 4 baseline frames preceding
1129 the stimulus. Given the unreliability of the responses before ear canal opening, for the
1130 population traces (Fig. 3B), only those neurons were considered in the pool which evoked
1131 significant responses to >25% of the trials (>25% reliability). Reliability was computed as the
1132 proportion of trials that showed significant responses (above).

1133 In case of the SD paradigm, each SD set of a pair (SD and swap) was collected with 30
1134 repetitions. Cells in the pair of datasets (SD and swap) were matched for further analysis, as
1135 the imaging for each SD dataset lasted long (> 5 mins), there could be drifts between two
1136 datasets. Thus the matching was based on correlations (MATLAB function corr2) between
1137 different relative x-y translations (+/- 5.8 µm or 5 pixels) between the two x-y drift corrected
1138 (see above) mean images acquired in each SD set of a pair. The relative x-y translation that
1139 gave the maximum correlation was used to then consider same cells in both datasets if the

cell centers were within 5.8 µm. Only cells that matched in the 2 datasets were considered further. Many neurons did not show significant responses (d-prime<1, between pre stimulus frames df/f values and post stimulus, S onset or post D) in the average df/f of all 30 repetitions. However, as responses had low reliability, significant responses (d-prime>1) were observed in stretches of 10 repetitions of the stimuli (moving average was performed of 10 repetitions to check for significant responses). Response window of 6 frames after standard and deviant token onset and the baseline window of 3 frames before stimulus onset were considered for drawing significance. Pairs of neurons which intermittently responded to standards or deviants in at least 3 moving repetition windows (of 10 repetitions) were considered for population analysis. Mean df/f traces could become negative and hence the mean df/f of each trial was shifted by adding the minimum df/f over all frames before calculating CSI from 2-photon Ca^{2+} imaging data. CSI was calculated from mean translated (as above) df/f of 6 frames following S onset and eight frames after D for each set in a pair. CSI is calculated as done with mean rates, replacing rate by df/f. Since other than the onset token and deviant token there were no responses in single units at early ages these mean values likely do not include effects of other S's.

Details of Binary Network Model of L4 and SP with TC Inputs

We built a binary neural network consisting to two separate thalamic input units for standard and deviant. The thalamic units project to a sub-plate neuron and further to a cortical neuron. The sub-plate neuron also projects to the cortical neuron. A similar model was used to demonstrate ocular dominance in the visual cortex[11,9]. The spike rate of the two thalamic inputs are given by,

$$f_{std}(r) = \begin{cases} 8 & when\ a\ standard\ token\ comes \\ 0.15 & when\ a\ deviant\ token\ comes \\ 0.1 & spontaneous\ rate \end{cases}$$

$$f_{dev}(r) = \begin{cases} 0.15 & when\ a\ standard\ token\ comes \\ 8 & when\ a\ deviant\ token\ comes \\ 0.1 & spontaneous\ rate \end{cases}$$

The synaptic weight of the thalamo-subplate projections were kept constant at a value of 0.2. The projections received by the cortical neuron was kept plastic and learning was implemented following the below plasticity rule.

$$\frac{\Delta w}{w} = \begin{cases} Amp_{strength} * e^{-\frac{\Delta t}{\tau_{strength}}} & potentiation \\ -Amp_{weak} * e^{-\frac{\Delta t}{\tau_{weak}}} & depression \end{cases}$$

Where $\Delta t = |t_{post\ synaptic} - t_{pre\ synptic}|$

$Amp_{strength} = 0.015$ $\quad \tau_{strength} = 13\ ms$

$Amp_{weak} = 0.021$ $\quad \tau_{weak} = 20\ ms$

We performed simulations for two regimes, one for the early development phase and one for the later. For the early phase, we kept the synaptic weight of the sub-plate projections at a value of 0.22 and that of the thalamo-cortical projections at a smaller value of 0.02. This was done to mimic the early stages of cortical development where the thalamic projections are unable to drive the cortical activity alone and are aided by the sub-plate for driving the cortical activity[1,2,20].

In the later phase, both these weights were kept at an intermediate value of 0.04 and 0.12 respectively. This reflects the intermediate stage of development where the thalamo-cotical projections are strengthening and the sub-plate-cortical connections are weakening[2,20].

All the synapses were kept depressing throughout the simulation with the following equations governing their dynamics[41],

$$\frac{dx_r}{dt} = -M.\frac{x_r}{\tau_{re}} + \frac{x_i}{\tau_{ir}} \qquad \frac{dx_e}{dt} = +M.\frac{x_r}{\tau_{re}} - \frac{x_e}{\tau_{ei}} \qquad \frac{dx_e}{dt} = \frac{x_e}{\tau_{ei}} - \frac{x_i}{\tau_{ir}}$$

Where M=1 whenever a spike occurs.

For thalamus, $\tau_{re} = 0.9\ ms$ $\tau_{ei} = 10\ ms$ $\tau_{ir} = 4200\ ms\ (early)\ \&\ 100ms\ (later)$

For sub-plate, $\tau_{re} = 0.9\ ms$ $\tau_{ei} = 27\ ms$ $\tau_{ir} = 4200\ ms\ (early)\ \&\ 100ms\ (later)$

The value of τ_{ir} was chosen in accordance with our electrophysiology data which shows a decrease in adaptation in later ages.

The sub-plate and the cortical neuron were modelled on the principles of integrate and fire neuron[1]. The membrane potential can be written as follows,

$$V_{sp}(t) = g_{std}(t-1) * w_{s1}(t-1) * x_{r_{std}}(t-1) + g_{dev}(t-1) * w_{s2}(t-1) * x_{r_{dev}}(t-1)$$
$$V_{l4}(t) = g_{std}(t-1) * w_{l1}(t-1) * x_{r_{std}}(t-1) + g_{dev}(t-1) * w_{l2}(t-1) * x_{r_{dev}}(t-1) + g_{sp}(t-1) * w_{sp}(t-1) * x_{r_{sp}}(t-1)$$

Where g(t) is the conductance and can be written as,

$$g(t) = spk_trn * k(t)$$

$k(t)$ is the convolution kernel

$$k(t) = e^{-(t-t_{spk})/\tau_{syn}}$$
$$\tau_{syn} = 10\ ms$$

The threshold of Layer IV neuron was kept constant at 0.1 for both the regimes, while that of the subplate neuron was kept at 0.05 for the early regime and 0.15 for the late regime.

The refractory period dynamics after each spike was modelled with a separate exponential given by[1],

$$V_{\Delta}(t) = \beta * e^{-(t-t_{spk})/\tau_{refr}}$$
$$\tau_{refr} = 2\ ms$$
$$\beta = 5$$

The voltage drops by the above value after every spike. The refractory period lasts for 20ms after the spike. A leak of 10% was also incorporated[1].

The model gets a drive from the thalamic activity, modeled by uncorrelated Poisson spikes in the two thalamic units. The stimulus train consists of standard and deviant tokens occurring with a probability of 0.9 and 0.1 respectively in the standard-deviant protocol and consisted of only standard tokens in case of only standard protocol. Each token is 50ms long separated by a 250ms inter-token-interval with a sampling rate of 1000/sec.

Theoretical Analysis for Optimization based on Mutual Information Maximization and Sparseness

We consider the same stimulus train that we used in the exposure experiments.
We assume the probability of deviant to be x and that of standard to be 1-x

$$p(t_{std}) = 1 - x \qquad p(t_{dev}) = x$$

The responses for each of the two tokens are normally distributed

$$p(r|t_{std}) = \frac{1}{\sigma\sqrt{2\pi}} \exp\left(-\left(\frac{(r-r_o)^2}{2\sigma^2}\right)\right) \; or \; g_s \quad p(r|t_{dev}) = \frac{1}{\sigma\sqrt{2\pi}} \exp\left(-\left(\frac{\left(r-(r_o+a_k)\right)^2}{2\sigma^2}\right)\right) or \; g_d$$

We consider the variance σ^2 and mean response for the standard token $r_o$to be constant. The mean response for the deviant token varies with each successive token and its difference from the mean standard response takes values a_k for every kth token. We assume all the tokes to be independent and without any history dependence (no adaptation). Thus,

$$p(r) = xg_d + (1-x)g_s$$

We wish to know the trend of $f(k)$ with successive tokens that will enhance the discriminability between the standard and the deviant token. To do that, we use mutual information as a measure of discriminability paired with a sparse coding constraint and try to maximize it.
Our constrained information for the kth token is,

$$CI_k = I(R_k, T) - \rho(r_o + xa_k)$$

Where $I(R_k, T)$ denotes the mutual information between the response at the kth token and the stimulus. ρ is the langrage multiplier which is constraining the mean response at the kth token. The langragian has been constructed to minimize the mean response at the kth token (sparse representation).
We need to find the value of ρ which will maximize the mutual information between the entire stimulus train and the total response along with maintaining a sparse representation

throughout the stimulus period. We can write the total constrained information as the sum of the constrained information of independent individual tokens,

$$CI_{total} = \sum_{k=1}^{N} CI_k = \sum_{k=1}^{N} I(R_k, T) - \rho\left(Nr_o + x\sum_{k=1}^{N} a_k\right)$$

Where N is the total number of tokens.

For any token, $I(R_k, T)$ can be written as,

$$\begin{aligned}
I(R,T) &= \int_0^{r_{max}} \left[\sum_T \left\{p(r,t)\ \ln\left(\frac{p(r,t)}{p(r)p(t)}\right)\right\}\right] dr \\
&= \int_0^{r_{max}} \left[\sum_T \left\{p(r|t)\ p(t) \ln\left(\frac{p(r|t)p(t)}{p(r)p(t)}\right)\right\}\right] dr \\
&= \int_0^{r_{max}} \left[\sum_T \left\{p(r|t)\ p(t) \ln\left(\frac{p(r|t)}{p(r)}\right)\right\}\right] dr \\
&= \int_0^{r_{max}} \left[p(r|t_{dev})\ p(t_{dev}) \ln\left(\frac{p(r|t_{dev})}{p(r)}\right) + \ p(r|t_{std})\ p(t_{std}) \ln\left(\frac{p(r|t_{std})}{p(r)}\right)\right] dr \\
&= \int_0^{r_{max}} \left[\ xg_d \ln\left(\frac{g_d}{xg_d + (1-x)g_s}\right) + \ (1-x)g_s \ln\left(\frac{g_s}{xg_d + (1-x)g_s}\right)\right] dr \\
&= \int_0^{r_{max}} [\ xg_d \ln g_d + \ (1-x)g_s \ln g_s - (xg_d + (1-x)g_s)\ \ln(xg_d + (1-x)g_s)]\ dr \\
&= -\tfrac{1}{2}\ \ln(2\pi e\sigma^2) - \textstyle\int_0^{r_{max}} [\ (xg_d + (1-x)g_s)\ \ln(xg_d + (1-x)g_s)]\ dr \\
&= -\tfrac{1}{2}\ \ln(2\pi e\sigma^2) - \textstyle\int_0^{r_{max}} \left[(xg_d + (1-x)g_s)\ \ln\{g_s(xA(r) + (1-x))\}\right] dr \qquad \textit{where } A(r) = \tfrac{g_d}{g_s} \\
&= -\frac{1}{2}\ \ln(2\pi e\sigma^2) - x\int_0^{r_{max}} [g_d \ln g_s]\ dr - (1-x)\int_0^{r_{max}} [g_s \ln g_s]\ dr - \int_0^{r_{max}} \left[(xg_d + (1-x)g_s)\ \ln(xA(r) + (1-x))\right] dr \\
&= -\frac{1}{2}\ \ln(2\pi e\sigma^2) + \frac{x}{2}\ln(2\pi e\sigma^2) + \frac{xa^2}{2\sigma^2} + \frac{1-x}{2}\ln(2\pi e\sigma^2) - \int_0^{r_{max}} \left[(xg_d + (1-x)g_s)\ \ln(xA(r) + (1-x))\right] dr \\
&= \frac{xa^2}{2\sigma^2} - \int_0^{r_{max}} \left[(xg_d + (1-x)g_s)\ \ln(xA(r) + (1-x))\right] dr \\
&= \frac{xa^2}{2\sigma^2} - \int_0^{r_{max}} \left[(xg_d + (1-x)g_s)\ \ln\left\{(1-x)\left(\frac{xA(r)}{1-x} + 1\right)\right\}\right] dr \\
&= \frac{xa^2}{2\sigma^2} - \ln(1-x)\int_0^{r_{max}} [xg_d + (1-x)g_s]\ dr - \int_0^{r_{max}} \left[(xg_d + (1-x)g_s) \ln\left(\frac{xA(r)}{1-x} + 1\right)\right] dr \\
&= \frac{xa^2}{2\sigma^2} - \ln(1-x) - \int_0^{r_{max}} \left[(xg_d + (1-x)g_s) \ln\left(\frac{xA(r)}{1-x} + 1\right)\right] dr
\end{aligned}$$

We wish to use the Taylor expansion of ln in the above expression. To do that we need,

$$\frac{xA(r)}{1-x} < 1$$
$$x < \frac{1}{1 + A(r)}$$

We see that $A(r)$ is the ratio of two normal distributions and it can be reduced to,

$$A(r) = exp\left(\frac{a(2r - 2r_o - a)}{2\sigma^2}\right)$$

Since x is a constant and is only dependent on the stimulus, we set a limit for x that will make this expression valid for all the possible rates,

$$x < \frac{1}{1 + exp\left(\frac{a(2r - 2r_o - a)}{2\sigma^2}\right)}$$

If we assume that on the 1st token (when the discrimination has not yet started), the mean rate for standard and deviant is the same (a=0), we see that,

$$x < \frac{1}{2}$$

Thus we proceed further with an assumption that the probability of the arrival of the deviant is less than 50% and the results that we discuss later will hold true only on this assmption.

We now perform the Taylor series expansion,

$$\frac{xa^2}{2\sigma^2} - \ln(1-x) - \int_0^{r_{max}} \left[(xg_d + (1-x)g_s) \sum_{i=1}^{\infty} \left\{ \frac{-1^{i+1}}{n} \left(\frac{xA(r)}{1-x} \right)^i \right\} \right] dr$$

$$= \frac{xa^2}{2\sigma^2} - \ln(1-x) - x \sum_{i=1}^{\infty} \left[\frac{-1^{i+1}x^i}{i(1-x)^i} \int_0^{r_{max}} \{g_d\{A(r)\}^i\}\, dr \right] - (1-x) \sum_{i=1}^{\infty} \left[\frac{-1^{i+1}x^i}{i(1-x)^i} \int_0^{r_{max}} \{g_s\{A(r)\}^i\}\, dr \right]$$

$$= \frac{xa^2}{2\sigma^2} - \ln(1-x) - x \sum_{i=1}^{\infty} \left[\frac{-1^{i+1}x^i}{i(1-x)^i} \frac{1}{\sigma\sqrt{2\pi}} \int_0^{r_{max}} \left\{ exp\left(-\frac{\left(r - (r_o + a)\right)^2 + i\left(a^2 - 2a(r - r_o)\right)}{2\sigma^2} \right) \right\} dr \right]$$
$$- (1-x) \sum_{i=1}^{\infty} \left[\frac{-1^{i+1}x^i}{i(1-x)^i} \frac{1}{\sigma\sqrt{2\pi}} \int_0^{r_{max}} \left\{ exp\left(-\frac{(r - r_o)^2 + i\left(a^2 - 2a(r - r_o)\right)}{2\sigma^2} \right) \right\} dr \right]$$

$$= \frac{xa^2}{2\sigma^2} - \ln(1-x) - x \sum_{i=1}^{\infty} \left[\frac{-1^{i+1}x^i}{i(1-x)^i} \frac{1}{\sigma\sqrt{2\pi}} \int_0^{r_{max}} \left\{ exp\left(-\frac{\left((r - r_o)^2 + a^2 - 2(r - r_o)a + ia^2 - 2ia(r - r_o)\right)}{2\sigma^2} \right) \right\} dr \right] -$$
$$(1-x) \sum_{i=1}^{\infty} \left[\frac{-1^{i+1}x^i}{i(1-x)^i} \frac{1}{\sigma\sqrt{2\pi}} \int_0^{r_{max}} \left\{ exp\left(-\frac{(r - r_o)^2 + ia^2 - 2ia(r - r_o)}{2\sigma^2} \right) \right\} dr \right]$$

$$= \frac{xa^2}{2\sigma^2} - \ln(1-x) - x \sum_{i=1}^{\infty} \left[\frac{-1^{i+1}x^i}{i(1-x)^i} \frac{1}{\sigma\sqrt{2\pi}} exp\left(-\frac{(i+1)a^2}{2\sigma^2} \right) \int_0^{r_{max}} \left\{ exp\left(-\frac{\left((r - r_o)^2 - 2(r - r_o)a - 2ia(r - r_o)\right)}{2\sigma^2} \right) \right\} dr \right]$$
$$- (1-x) \sum_{i=1}^{\infty} \left[\frac{-1^{i+1}x^i}{i(1-x)^i} \frac{1}{\sigma\sqrt{2\pi}} exp\left(-\frac{ia^2}{2\sigma^2} \right) \int_0^{r_{max}} \left\{ exp\left(-\frac{(r - r_o)^2 - 2ia(r - r_o)}{2\sigma^2} \right) \right\} dr \right]$$

$$= \frac{xa^2}{2\sigma^2} - \ln(1-x) - x \sum_{i=1}^{\infty} \left[\frac{-1^{i+1}x^i}{i(1-x)^i} \frac{1}{\sigma\sqrt{2\pi}} exp\left(-\frac{(i+1)a^2}{2\sigma^2} \right) \int_0^{r_{max}} \left\{ exp\left(-\frac{(r^2 + {r_o}^2 - 2rr_o - 2ra + 2r_oa - 2iar + 2iar_o)}{2\sigma^2} \right) \right\} dr \right]$$
$$- (1-x) \sum_{i=1}^{\infty} \left[\frac{-1^{i+1}x^i}{i(1-x)^i} \frac{1}{\sigma\sqrt{2\pi}} exp\left(-\frac{ia^2}{2\sigma^2} \right) \int_0^{r_{max}} \left\{ exp\left(-\frac{r^2 + {r_o}^2 - 2rr_o - 2iar + 2iar_o}{2\sigma^2} \right) \right\} dr \right]$$

$$= \frac{xa^2}{2\sigma^2} - \ln(1-x) - x \sum_{i=1}^{\infty} \left[\frac{-1^{i+1}x^i}{i(1-x)^i} \frac{1}{\sigma\sqrt{2\pi}} exp\left(-\frac{(i+1)a^2 + {r_o}^2 + 2r_oa + 2iar_o}{2\sigma^2} \right) \int_0^{r_{max}} \left\{ exp\left(-\frac{(r^2 - 2(r_o + a + ia)r)}{2\sigma^2} \right) \right\} dr \right]$$
$$- (1-x) \sum_{i=1}^{\infty} \left[\frac{-1^{i+1}x^i}{i(1-x)^i} \frac{1}{\sigma\sqrt{2\pi}} exp\left(-\frac{ia^2 + {r_o}^2 + 2iar_o}{2\sigma^2} \right) \int_0^{r_{max}} \left\{ exp\left(-\frac{r^2 - 2(r_o + ia)r}{2\sigma^2} \right) \right\} dr \right]$$

$$= \frac{xa^2}{2\sigma^2} - \ln(1-x)$$
$$- x \sum_{i=1}^{\infty} \left[\frac{-1^{i+1}x^i}{i(1-x)^i} \frac{1}{\sigma\sqrt{2\pi}} exp\left(-\frac{(i+1)a^2 + {r_o}^2 + 2r_oa + 2iar_o - (r_o + a + ia)^2}{2\sigma^2} \right) \int_0^{r_{max}} \left\{ exp\left(-\frac{\left(r - (r_o + a + ia)\right)^2}{2\sigma^2} \right) \right\} dr \right]$$
$$- (1-x) \sum_{i=1}^{\infty} \left[\frac{-1^{i+1}x^i}{i(1-x)^i} \frac{1}{\sigma\sqrt{2\pi}} exp\left(-\frac{ia^2 + {r_o}^2 + 2iar_o - (r_o + ia)^2}{2\sigma^2} \right) \int_0^{r_{max}} \left\{ exp\left(-\frac{\left(r - (r_o + ia)\right)^2}{2\sigma^2} \right) \right\} dr \right]$$

$$= \frac{xa^2}{2\sigma^2} - \ln(1-x) - x \sum_{i=1}^{\infty} \left[\frac{-1^{i+1}x^i}{i(1-x)^i} exp\left(-\frac{(i+1)a^2 + {r_o}^2 + 2r_oa + 2iar_o - (r_o + a + ia)^2}{2\sigma^2} \right) \right]$$
$$- (1-x) \sum_{i=1}^{\infty} \left[\frac{-1^{i+1}x^i}{i(1-x)^i} exp\left(-\frac{ia^2 + {r_o}^2 + 2iar_o - (r_o + ia)^2}{2\sigma^2} \right) \right]$$

$$= \frac{xa^2}{2\sigma^2} - \ln(1-x) - x \sum_{i=1}^{\infty} \left[\frac{-1^{i+1}x^i}{i(1-x)^i} exp\left(\frac{ia^2(i+1)}{2\sigma^2} \right) \right] - (1-x) \sum_{i=1}^{\infty} \left[\frac{-1^{i+1}x^i}{i(1-x)^i} exp\left(\frac{ia^2(i-1)}{2\sigma^2} \right) \right]$$

$$= \frac{xa^2}{2\sigma^2} - \ln(1-x) - \sum_{i=1}^{\infty} \left[\frac{-1^{i+1}x^{i+1}}{i(1-x)^i} exp\left(\frac{ia^2(i+1)}{2\sigma^2} \right) + \frac{-1^{i+1}x^i}{i(1-x)^{i-1}} exp\left(\frac{ia^2(i-1)}{2\sigma^2} \right) \right]$$

$$= \frac{xa^2}{2\sigma^2} - \ln(1-x) - x + x \sum_{i=1}^{\infty} \left[\frac{-1^i}{i(i+1)} \frac{x^i}{(1-x)^i} exp\left(\frac{i(i+1)a^2}{2\sigma^2} \right) \right]$$

$$= \frac{xa^2}{2\sigma^2} - \ln(1-x) - x + x\Lambda(a)$$

Where $\Lambda(a) = \sum_{i=1}^{\infty} \left[\frac{-1^i}{i(i+1)} \frac{x^i}{(1-x)^i} exp\left(\frac{i(i+1)a^2}{2\sigma^2} \right) \right]$

On a careful examination, we see that the above expression will always be positive.
We find the change in constrained information between two tokens m&n (m<n)

$$\Delta CI = CI_n - CI_m = \{MI_n - MI_m\} - \rho x\{a_n - a_m\}$$
$$= x\left[\frac{{a_n}^2 - {a_m}^2}{2\sigma^2} + \Lambda(a_n) - \Lambda(a_m) - \rho\{a_n - a_m\}\right]$$
$$= x(a_n - a_m)\left[\frac{a_n + a_m}{2\sigma^2} + \frac{\Lambda(a_n) - \Lambda(a_m)}{a_n - a_m} - \rho\right]$$

We want the above expression to be greater than or equal to zero. Thus, we get two cases,

Case 1: $a_n > a_m$

We need,

$$\frac{a_n + a_m}{2\sigma^2} + \frac{\Lambda(a_n) - \Lambda(a_m)}{a_n - a_m} > \rho$$
$$\frac{a_n + a_m}{2\sigma^2} + \frac{\sum_{i=1}^{\infty}\left[\frac{-1^i}{i(i+1)}\frac{x^i}{(1-x)^i}\left\{exp\left(\frac{i(i+1){a_n}^2}{2\sigma^2}\right) - exp\left(\frac{i(i+1){a_m}^2}{2\sigma^2}\right)\right\}\right]}{a_n - a_m} \geq \rho$$

We see that as a increases, the 2nd term in the above expression increases with the exponential of the square of the increase in a. The 2nd term over all will be much larger than 1. If we assume a monotonic behavior in a, the least value of $\Lambda(a_n) - \Lambda(a_m)$ will be between the first two tokens. Thus we can say that,

$$\rho \leq \frac{a_2 + a_1}{2\sigma^2} + \frac{\sum_{i=1}^{\infty}\left[\frac{-1^i}{i(i+1)}\frac{x^i}{(1-x)^i}\left\{exp\left(\frac{i(i+1){a_2}^2}{2\sigma^2}\right) - exp\left(\frac{i(i+1){a_1}^2}{2\sigma^2}\right)\right\}\right]}{a_2 - a_1}$$

The above expression sets a limit on the value of ρ or in other words the weightage of sparseness which will keep the mutual information increasing.
This case corresponds to the early age results, where the responses for deviant was greater than that of standard (a>0).

Case 2: $a_n < a_m$
We need,

$$\frac{a_n + a_m}{2\sigma^2} + \frac{\Lambda(a_n) - \Lambda(a_m)}{a_n - a_m} \leq \rho$$
$$\frac{a_n + a_m}{2\sigma^2} + \frac{\sum_{i=1}^{\infty}\left[\frac{-1^i}{i(i+1)}\frac{x^i}{(1-x)^i}\left\{exp\left(\frac{i(i+1){a_n}^2}{2\sigma^2}\right) - exp\left(\frac{i(i+1){a_m}^2}{2\sigma^2}\right)\right\}\right]}{a_n - a_m} \leq \rho$$

We see that as a decreases, the 2nd term in the above expression decreases with the exponential of the square of the increase in a. The 2nd term over all will be much less than -1. If we assume a monotonic behavior in a, the largest value of $\Lambda(a_n) - \Lambda(a_m)$ will be between the first two tokens. Thus we can say that,

$$\rho \geq \frac{a_2 + a_1}{2\sigma^2} + \frac{\sum_{i=1}^{\infty}\left[\frac{-1^i}{i(i+1)}\frac{x^i}{(1-x)^i}\left\{exp\left(\frac{i(i+1){a_2}^2}{2\sigma^2}\right) - exp\left(\frac{i(i+1){a_1}^2}{2\sigma^2}\right)\right\}\right]}{a_2 - a_1}$$

The above expression sets a limit on the value of ρ or in other words the weightage of sparseness which will keep the mutual information increasing.
This case corresponds to the later age results, where the responses for standard was less than that of deviant (a<0).

Supplementary Figure Legends

Figure S1. A) Schematic of types of 4x4 electrode arrays used – either all electrodes were of same lengths (i) or they had alternate short and long electrodes (ii) either 600 μm apart or 400 μm apart. B) Sample locations of recordings of single units mapped onto the cortical surface showing broad clearer tonotopy in P29 than in P15. C) Representative confirmation of recording in A1 in lower age groups P12, P13, P18 with DiI injections in the recording site with labelling in MGBv (inset). D) Thickness of SP as a percentage of cortical thickness and depth of L4 and SP over age determined from cell morphology with Nissl stains.

Figure S2. SP depth and thickness determined with immunohistochemistry (IHC) by labelling SPNs with antibodies of SPN markers Complexin-3 (A) and CTGF (B).

Figure S3. Slices were cut from brains (fixed) in which single unit recordings were performed in the ACX (representative examples at 3 ages, in A) and IHC was performed. Electrode tracks show recordings performed in SPN and in case of dual recordings (second electrode type, Fig. S1A) in SCNN1-td-tomato mouse show electrodes in L4 and SPN simultaneously (B).

Figure S4. Top and bottom row show bar plots of mean CSI(F) and mean CSI for neurons in L4 at different f_1 and f_2 separations.

Figure S5. A) Schematic of SD tokens and its swap, which is the stimulus presentation protocol. B-G) Data from six representative L4 units at different ages (P12-P38, same as in Fig. 2), given in titles with respective CSI(F), are shown as dot rasters and PSTHs in response to the 4 stimulus sets (i-iv) – noise at multiple sound levels, pure tones at different frequencies, *f-N* SD stimulus and its swap. The chosen frequency and sound level of noise used in the SD stimuli are marked on the respective dot rasters in i and ii with gray light and dark rectangles, along with PSTHs of those responses in the bottom plot of i and ii. PSTHS in iii and iv also shown in Fig. 2A. CSI(F) values are given in parentheses for the 6 neurons in B-G.

Figure S6. Same set of plots as in Fig. S5B (for L4 neurons of Fig. 2A), for the 3 representative SPN responses shown in Fig. 2B. CSI(F) values are given in parentheses for the 3 neurons in A-C.

Figure S7. A) Histograms of deviant selectivity (*N-f* case) measured with CSI values - CSI(F) in i, CSI in ii and CSI(P) in iii, for the entire population of neurons of L4 (top row in each plot i-

iii) and SP (bottom row) as a function of age (5 age groups considered). B) Same plot as in Fig. 1H-I, for CSI(P) for f_1-f_2 SD stimulus.

Figure S8. Ai) Shows the population CDFs of adaptation time constants (as -1/time constant) for L4 neurons (dark gray) and SP neurons (light gray) over different age groups (SP only for P12-15). Adaptation time constants, determined from exponential fits to mean responses to each successive token of Standards, increase with age. Aii) Shows population CDFs (for the same set of neurons and age groups as in the top row) of the number tokens in which there were significant responses in the first set of 7 (or 6) tokens before the deviant for the same population of neurons. B) Mean -1/Adaptation time constants for the data in Ai. C) Boxplots showing range with median, IQR and outliers for data in Aii.

Figure S9. A) Shows a sample image of the relevant part of a coronal section with MGB, in which single unit recordings from MGBv was performed (P14). B) Histograms of CSI(F) in the top row and CSI in the bottom row are shown for all single units recorded in MGBv from two age groups (left P14-15, right P24-26). C) Mean and standard errors of CSI(F) and CSI for the data in B, by age groups, are shown.

Figure S10. A) i) LFP in a single channel in SP, in response to noise obtained from 5 repetitions at P08. ii) Population average with SEM of the same in above. iii) Population average and SEM of rms values of LFP. B) i) Population average of LFP in SP and L4 to tones from 5 repetitions ii) Population average and SEM of rms values of LFP in SP and L4 to the same as above. iii) Representative, sample traces of LFP (average of 5 repetitions) obtained in P9 and P10 from SP and L4 (1 case each) showing responses to tones (each row, 6-48 kHz, ½ octave apart ~90 dB SPL, 50 ms tones). C) Dot rasters and PSTHs of spiking activity of 4 neurons (2 in L4 and 2 in SP, identified in each column) before ECO with pure tone presentations show unreliable spiking with 5 repetitions (thick black line – stimulus onset).

Figure S11 A) Left: Image of craniotomy in which wide field imaging was performed in a P7 mouse. Blue shaded regions showed positive maximum df/f post stimulus, with widefield imaging. Right: A sample trace shows the smoothed mean df/f across the frames of the region marked by the blue square on the craniotomy. Black horizontal bar represents the stimulus ('*' corresponds to minimum p-value among all frames, '.' represents the first significant window). B-C) Example traces of df/f of single neurons (arrows in 2-photon mean images of frame with cells expressing GCamp6f, bottom) in response to broadband noise (C) and tones (B) respectively at three different ages. The corresponding gray and black vertical lines represent stimulus onset. The error bars show the standards error of 40 repetitions. The red and black bars represent the earliest window over which the mentioned p-values were achieved.

Figure S12. Mean df/f traces of all the cells having more than 25% reliability in responses (significant response in >10 repetitions out of 40 repetitions) to tonal stimuli (frequencies in Hz mentioned) at the different ages. Respective p-values and degree of freedom for one-sided paired ttest is also shown. Imaging was performed with 40 repetitions of each frequency in P07-P11 (before ECO) and 5 repetitions in P12-13 after ECO. All imaged cells are included in traces for P12-13 irrespective of reliability.

Figure S13. A) i-ii) Similar plot as in Fig. 3B i-iii, for in-vivo 2-photon Ca^{2+} imaging based responses to broadband noise. . Bi-ii) Same as in Fig.3Ei-ii, for responses to broadband noise before ECO.

Figure S14. A) i-ii) Representative df/f traces of responding single neurons in L2/3 to the SD stimulus, obtained with 2-photon Ca^{2+} imaging (i: S=tone, D=noise, TN and ii: S=noise, D=tone, NT) at three different ages before ECO. The grey/black and black/grey vertical lines represent S onset and D respectively. Black (p<0.2) and red (p<0.05) bars (above traces) mark timing of significant responses (mean of 3 frames) to the standard and the deviant. iii-iv) Population mean df/f (311 neurons, n=3 (P7-P9)) in response to the two stimuli TN (iii) and NT (iv). v) Distribution of CSI values for the population of L2/3 single neurons.

Figure S15. A) i) Figure S15. A) i) the z-scores of responses in SD stimulus (20 reps, 4Hz) (left column) and Swap (right column) for 3 single units in L4 (top 3 rows) and 3 single units in SP (bottom 3 rows) are shown (same units as in Fig. 4B, first 3 columns). A) ii) Mean z-scores for the population of single units in L4 (top row) and that in SP (bottom row) are shown for the SD stimulus (left) and the corresponding Swap (right). B) i-ii) Same as Ai-ii, for responses to SD stimulus with 30 reps and at rate of 3.33 Hz.

Figure S16. Top and middle row show the mean CSI values of the population of L4 and SP neurons respectively for different choice of response latencies and response window sizes. Asterisks marks the response latency and response window size combination used in Fig. 4 CSI calculations. The three columns are for the 3 different CSIs used CSI, CSI(F) and CSI(P). Bottom row shows which combinations of response attribute have significantly higher CSI in SP than in L4 (brown, blue indicates NS).

Figure S17. A) 2 examples of cross-correlograms each for before ECO (top row) and after ECO (bottom wor) showing connections detected from SP to L4 (left) and L4 to SP (right). Blue and red colored lines indicate mean of cross-correlograms with errorbars and gray lines with errorbars show the same for shuffled data (see detailed methods). B) Bar plots summarize the data in Table S2 showing probability of connections from SP to L4 (left) and L4 to SP (right) at within 125 microns or greater distances at the 2 age groups before ECO and P12-13, after ECO).

Figure S18. A) Four example images of location (along cortical surface) of BFs on the cortical surface in the craniotomy of single units recorded in L4 at ages P28 and above (Fig. 5A single unit recording) identified in color (colorbar, bottom right) for four exposure groups EX2 and EX1 in the top row (SD exposure) and EX5 and EX6 in the bottom row (SS exposure). Broad tonotopy showing A1 and AAF are clear in the images. B) Bar plot shows % change in area of each of the preferred frequencies in A1 and AAF between control (EX0 group of mice) and exposed animals (EX5 group of mice).

Figure S19. Similar plots as in Fig. 5E, for the profile of population mean normalized rates to the relevant RF (color legend) for the 4 exposure groups (EX5 and EX6 left, EX2 and EX1 right) as a function of BF (re RF). Normalization was done by considering the maximum rate in each tuning curve (rate at BF) to be 100%. Gray profile shows the same for the maximum of 13 similar plots derived from the control data (C) considering each of the 13 frequencies used as the RF.

Figure S20. Bar plot summarizes population mean response to RF for neurons with BF at RF of all 6 EX cases (2 bars each, red and green for SD exposure cases and 1 blue for SS). Mean of the 13 control cases shown in gray bar in the centre.

Supplementary Figures

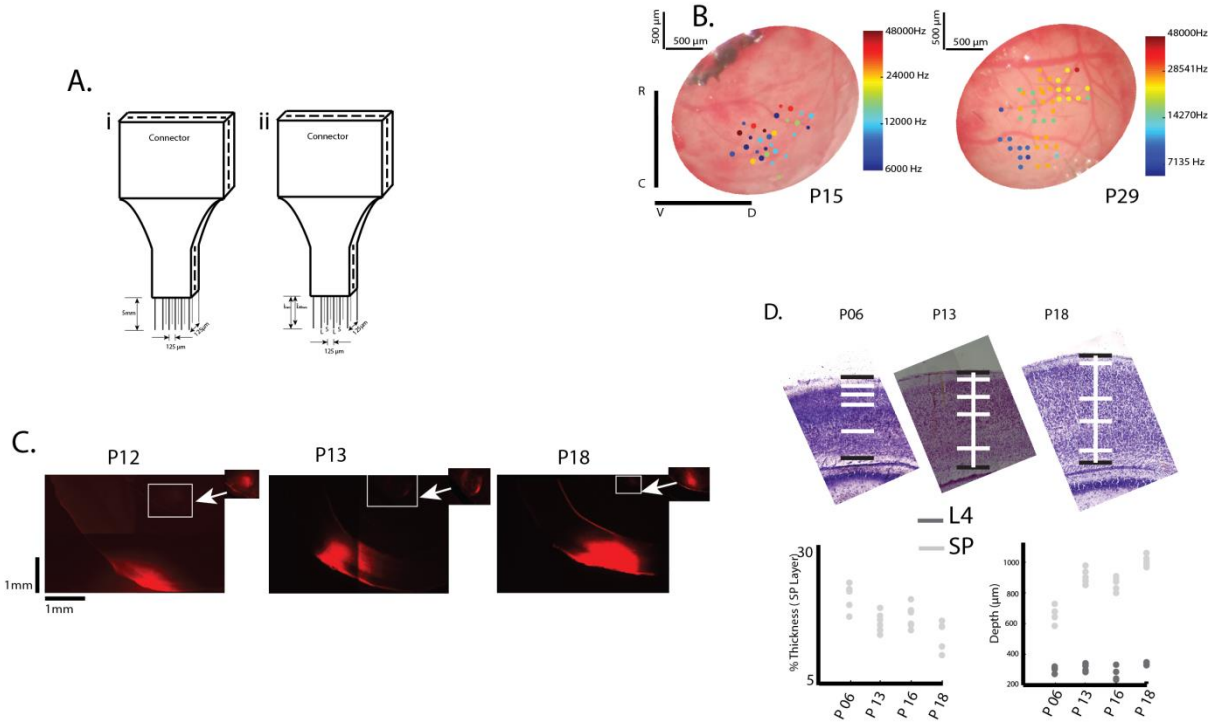

Figure S1. A) Schematic of types of 4x4 electrode arrays used – either all electrodes were of same lengths (i) or they had alternate short and long electrodes (ii) either 600 μm apart or 400 μm apart. B) Sample locations of recordings of single units mapped onto the cortical surface showing broad clearer tonotopy in P29 than in P15. C) Representative confirmation of recording in A1 in lower age groups P12, P13, P18 with DiI injections in the recording site with labelling in MGBv (inset). D) Thickness of SP as a percentage of cortical thickness and depth of L4 and SP over age determined from cell morphology with Nissl stains.

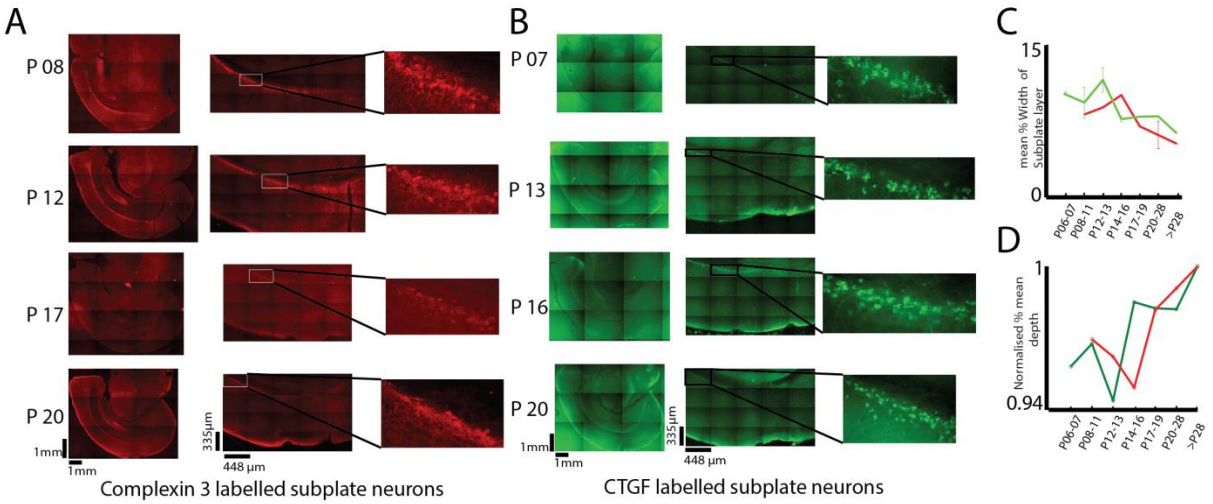

Figure S2. SP depth and thickness determined with immunohistochemistry (IHC) by labelling SPNs with antibodies of SPN markers Complexin-3 (A) and CTGF (B).

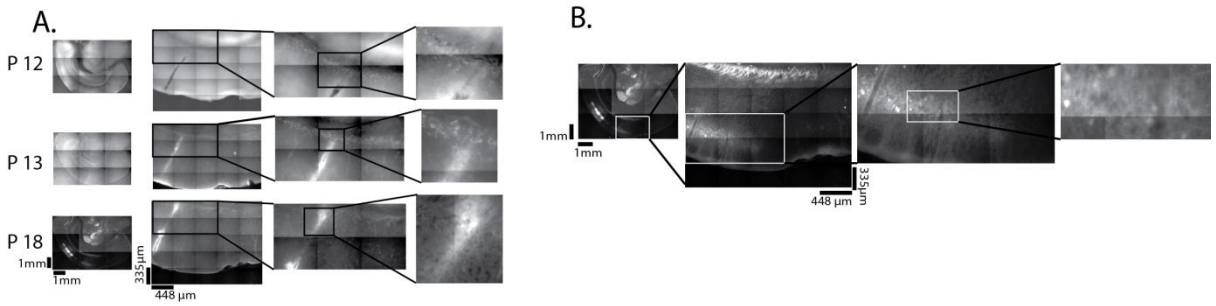

Figure S3. Slices were cut from brains (fixed) in which single unit recordings were performed in the ACX (representative examples at 3 ages, in A) and IHC was performed. Electrode tracks show recordings performed in SPN and in case of dual recordings (second electrode type, Fig. S1A) in SCNN1-td-tomato mouse show electrodes in L4 and SPN simultaneously (B).

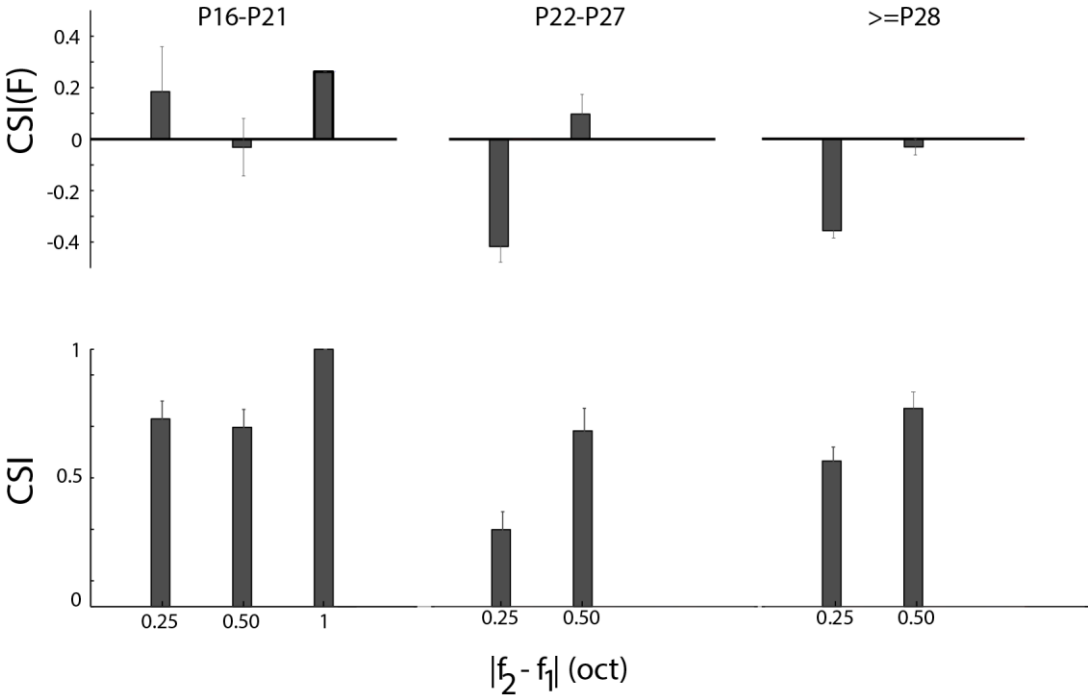

Figure S4. Top and bottom row show bar plots of mean CSI(F) and mean CSI for neurons in L4 at different f_1 and f_2 separations.

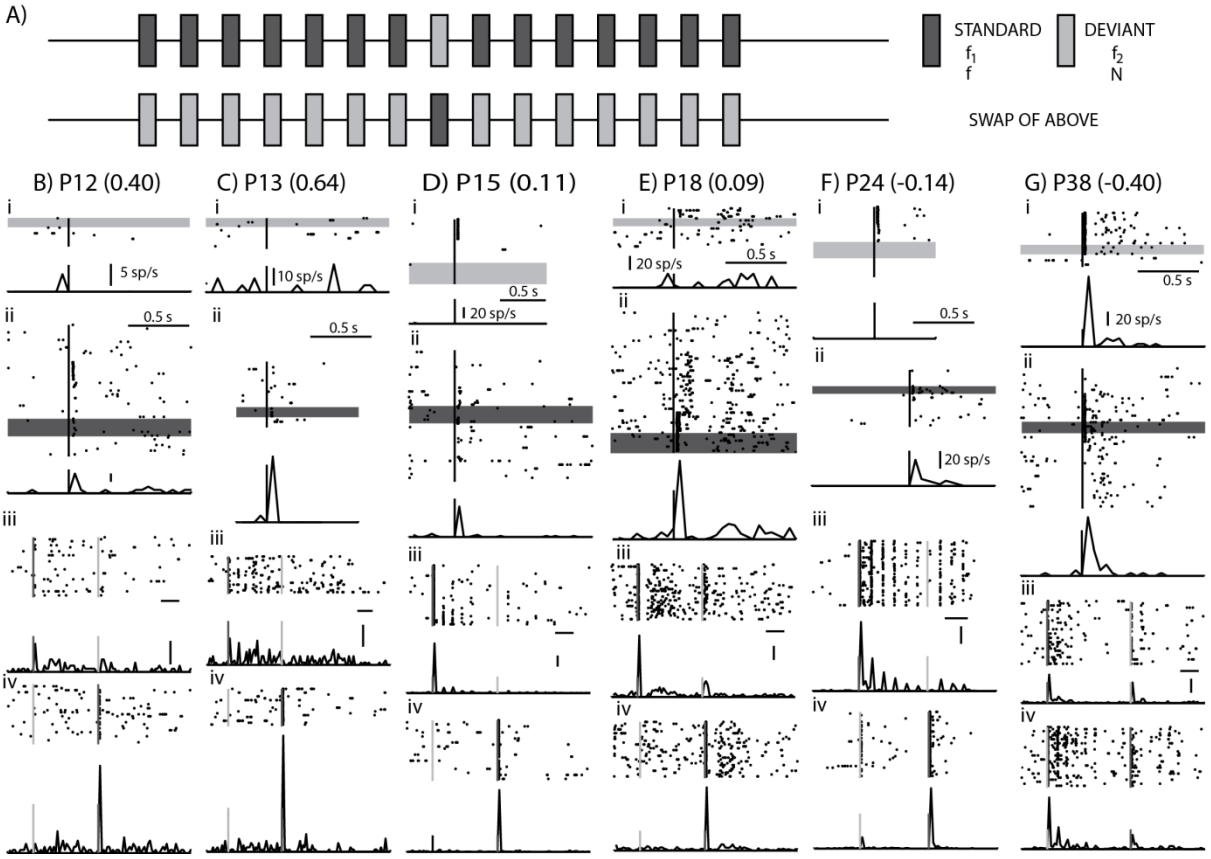

Figure S5. A) Schematic of SD tokens and its swap, which is the stimulus presentation protocol. B-G) Data from six representative L4 units at different ages (P12-P38, same as in Fig. 2), given in titles with respective CSI(F), are shown as dot rasters and PSTHs in response to the 4 stimulus sets (i-iv) – noise at multiple sound levels, pure tones at different frequencies, *f-N* SD stimulus and its swap. The chosen frequency and sound level of noise used in the SD stimuli are marked on the respective dot rasters in i and ii with gray light and dark rectangles, along with PSTHs of those responses in the bottom plot of i and ii. PSTHS in iii and iv also shown in Fig. 2A. CSI(F) values are given in parentheses for the 6 neurons in B-G.

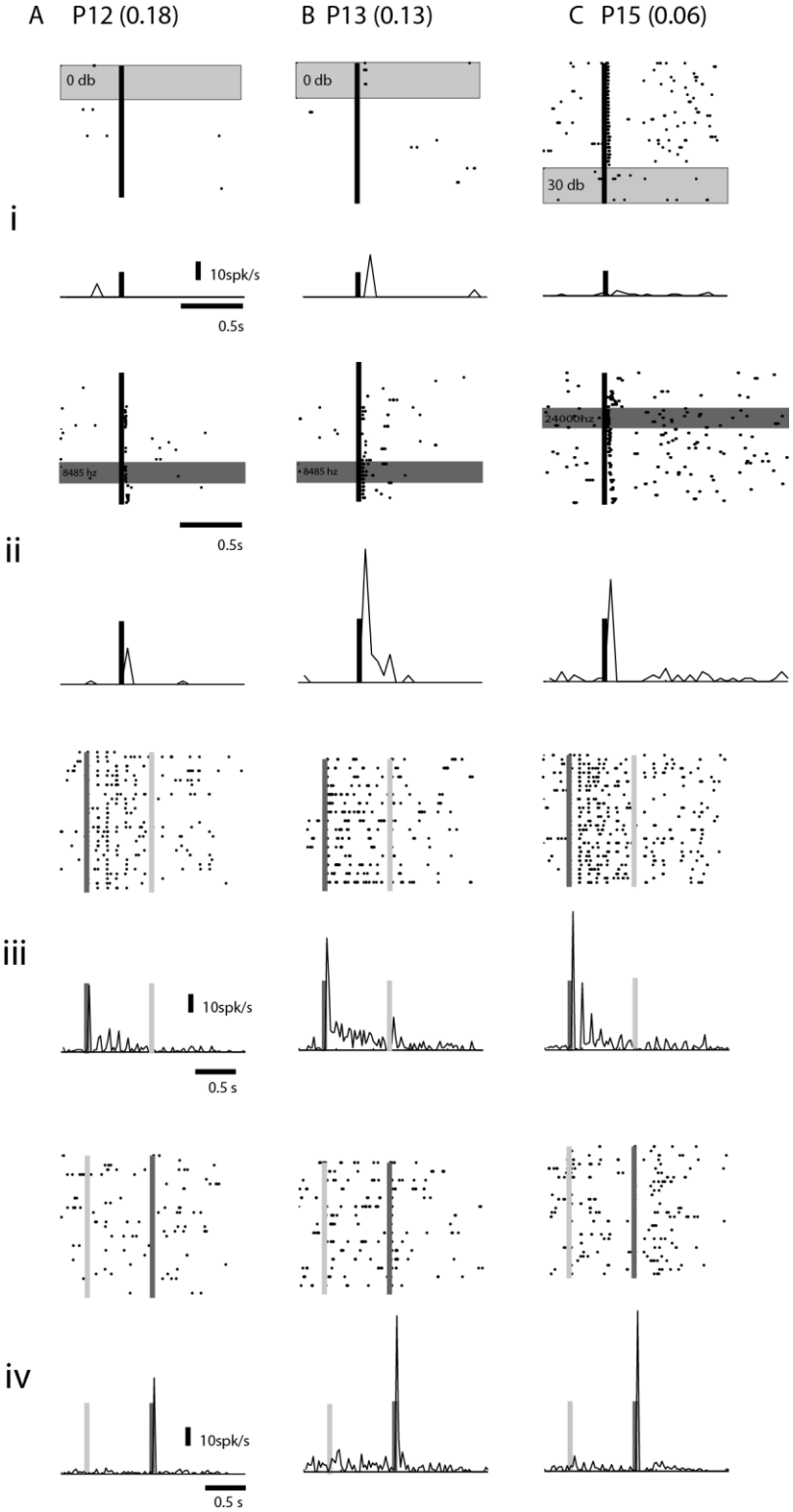

Figure S6. Same set of plots as in Fig. S5B (for L4 neurons of Fig. 2A), for the 3 representative SPN responses shown in Fig. 2B. CSI(F) values are given in parentheses for the 3 neurons in A-C.

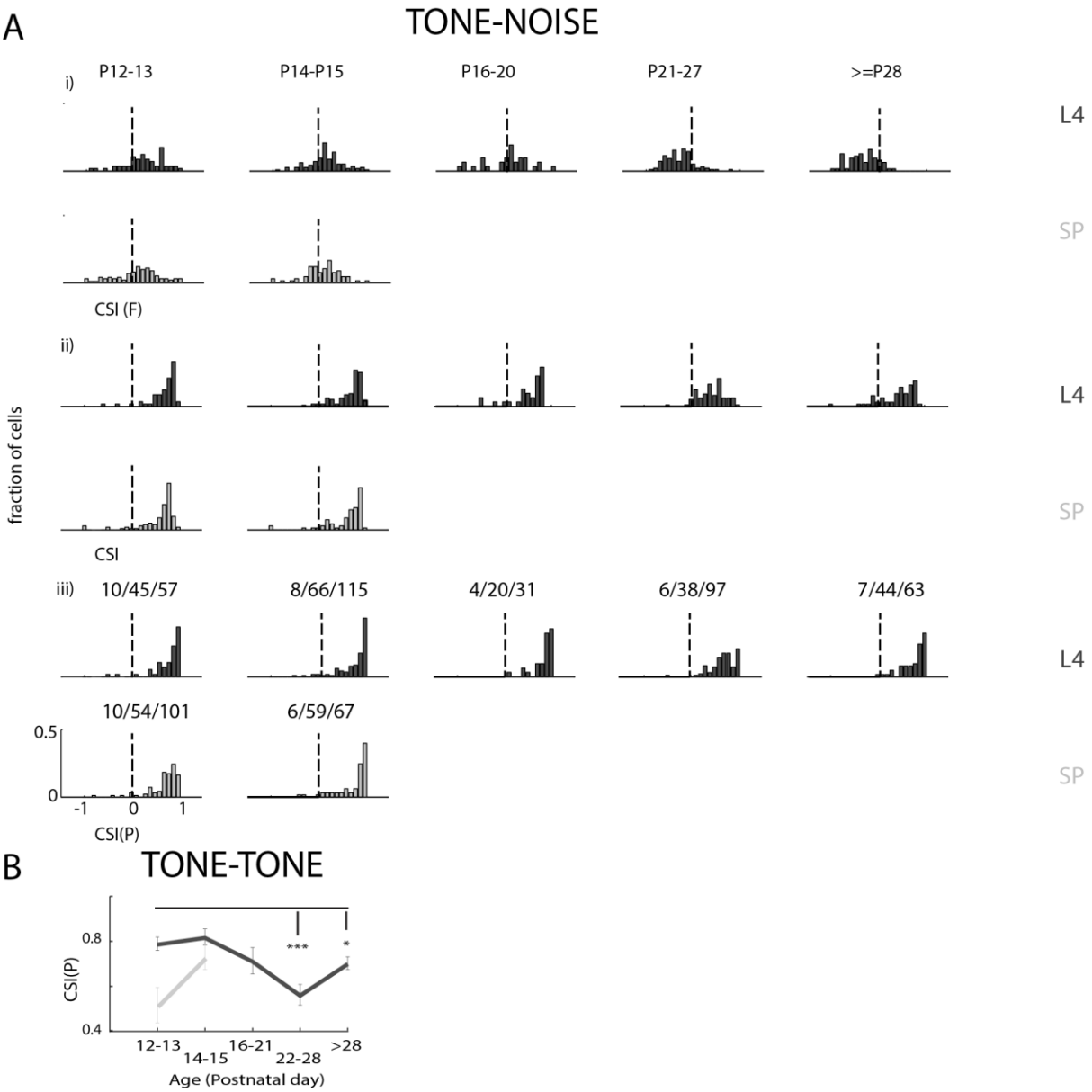

Figure S7. A) Histograms of deviant selectivity (*N-f* case) measured with CSI values - CSI(F) in i, CSI in ii and CSI(P) in iii, for the entire population of neurons of L4 (top row in each plot i-iii) and SP (bottom row) as a function of age (5 age groups considered). B) Same plot as in Fig. 1H-I, for CSI(P) for f_1-f_2 SD stimulus.

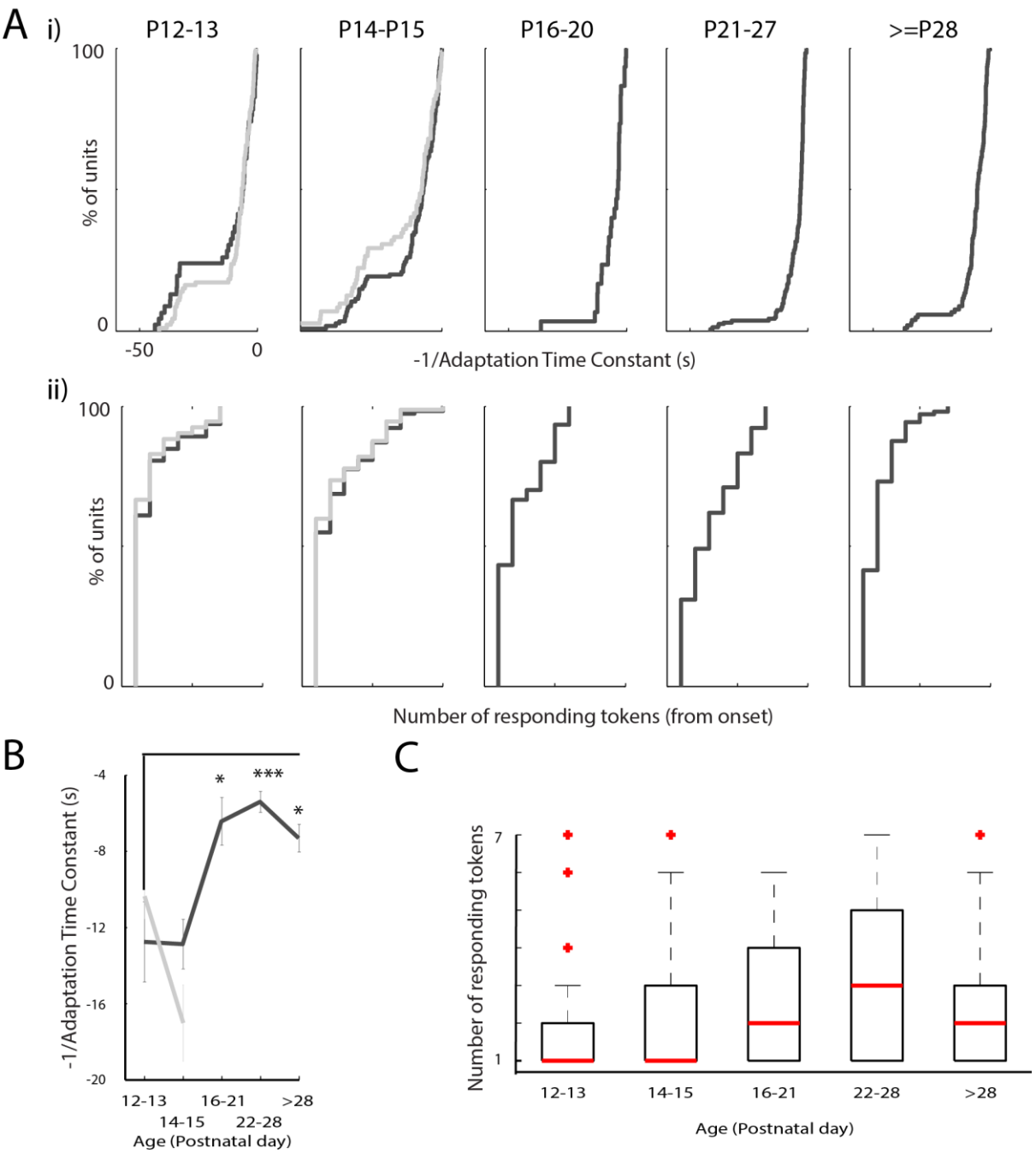

Figure S8. Ai) Shows the population CDFs of adaptation time constants (as -1/time constant) for L4 neurons (dark gray) and SP neurons (light gray) over different age groups (SP only for P12-15). Adaptation time constants, determined from exponential fits to mean responses to each successive token of Standards, increase with age. Aii) Shows population CDFs (for the same set of neurons and age groups as in the top row) of the number tokens in which there were significant responses in the first set of 7 (or 6) tokens before the deviant for the same population of neurons. B) Mean -1/Adaptation time constants for the data in Ai. C) Boxplots showing range with median, IQR and outliers for data in Aii.

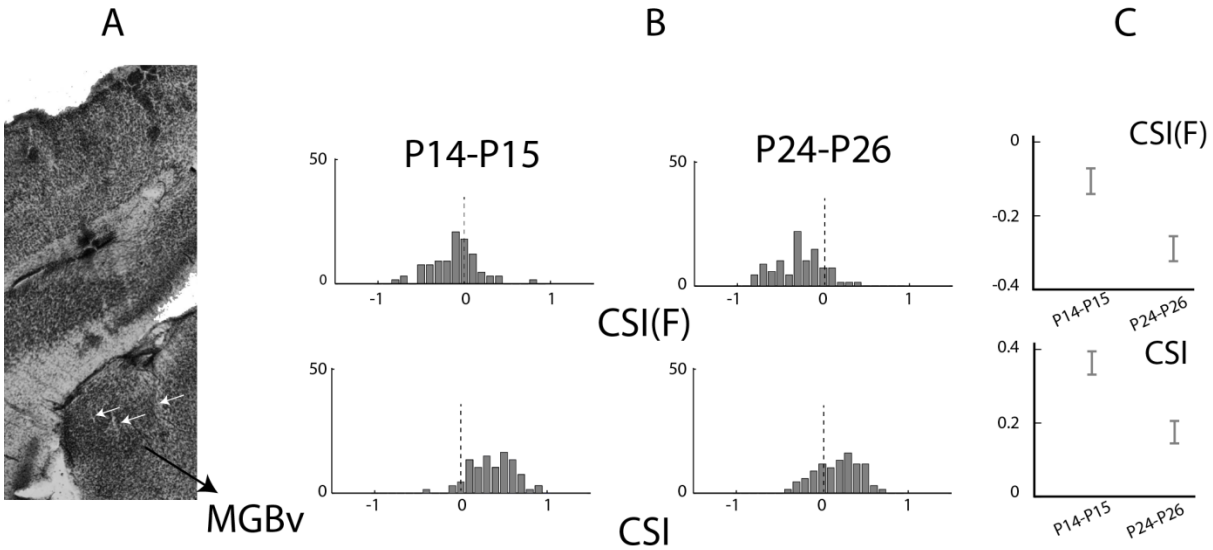

Figure S9. A) Shows a sample image of the relevant part of a coronal section with MGB, in which single unit recordings from MGBv was performed (P14). B) Histograms of CSI(F) in the top row and CSI in the bottom row are shown for all single units recorded in MGBv from two age groups (left P14-15, right P24-26). C) Mean and standard errors of CSI(F) and CSI for the data in B, by age groups, are shown.

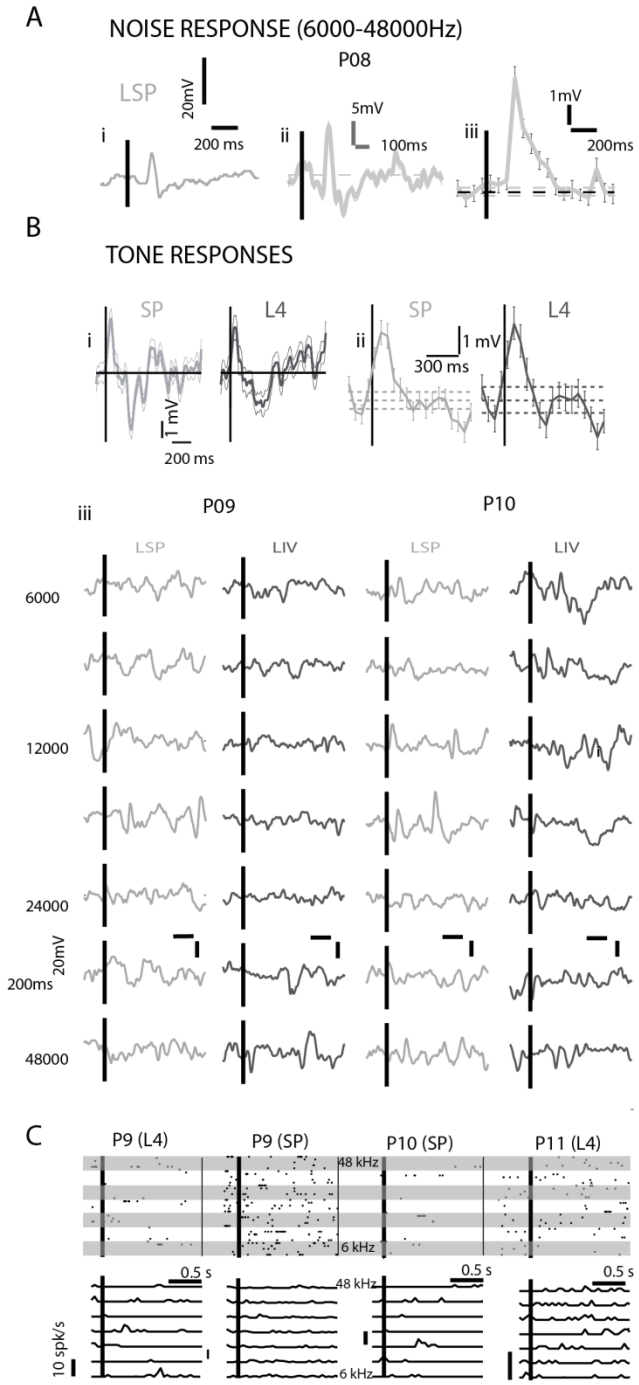

Figure S10. A) i) LFP in a single channel in SP, in response to noise obtained from 5 repetitions at P08. ii) Population average with SEM of the same in above. iii) Population average and SEM of rms values of LFP. B) i) Population average of LFP in SP and L4 to tones from 5 repetitions ii) Population average and SEM of rms values of LFP in SP and L4 to the same as above. iii) Representative, sample traces of LFP (average of 5 repetitions) obtained in P9 and P10 from SP and L4 (1 case each) showing responses to tones (each row, 6-48 kHz, ½ octave apart ~90 dB SPL, 50 ms tones). C) Dot rasters and PSTHs of spiking activity of 4 neurons (2 in L4 and 2 in SP, identified in each column) before ECO with pure tone presentations show unreliable spiking with 5 repetitions (thick black line – stimulus onset).

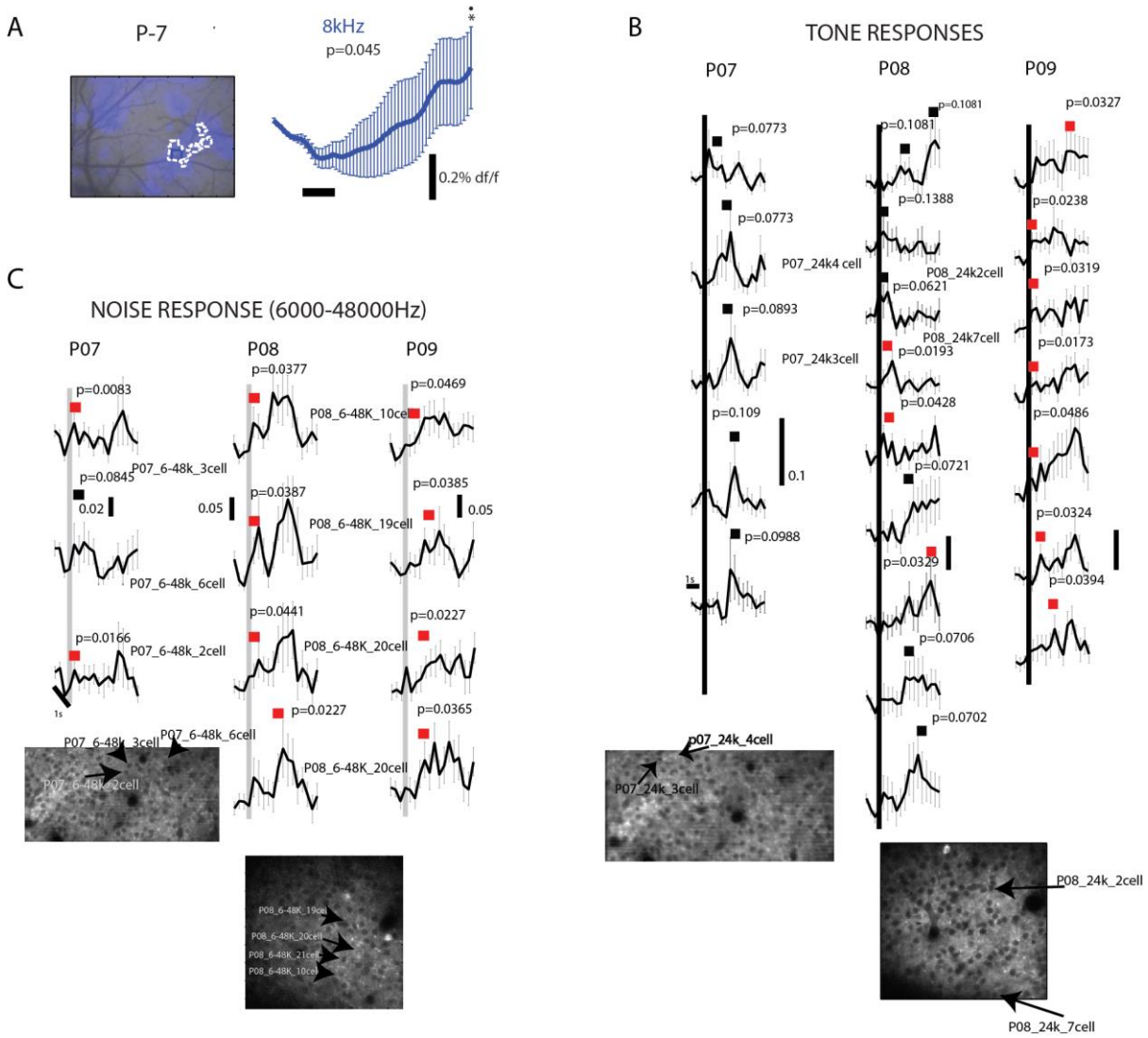

Figure S11 A) Left: Image of craniotomy in which wide field imaging was performed in a P7 mouse. Blue shaded regions showed positive maximum df/f post stimulus, with widefield imaging. Right: A sample trace shows the smoothed mean df/f across the frames of the region marked by the blue square on the craniotomy. Black horizontal bar represents the stimulus ('*' corresponds to minimum p-value among all frames, '.' represents the first significant window). B-C) Example traces of df/f of single neurons (arrows in 2-photon mean images of frame with cells expressing GCamp6f, bottom) in response to broadband noise (C) and tones (B) respectively at three different ages. The corresponding gray and black vertical lines represent stimulus onset. The error bars show the standards error of 40 repetitions. The red and black bars represent the earliest window over which the mentioned p-values were achieved.

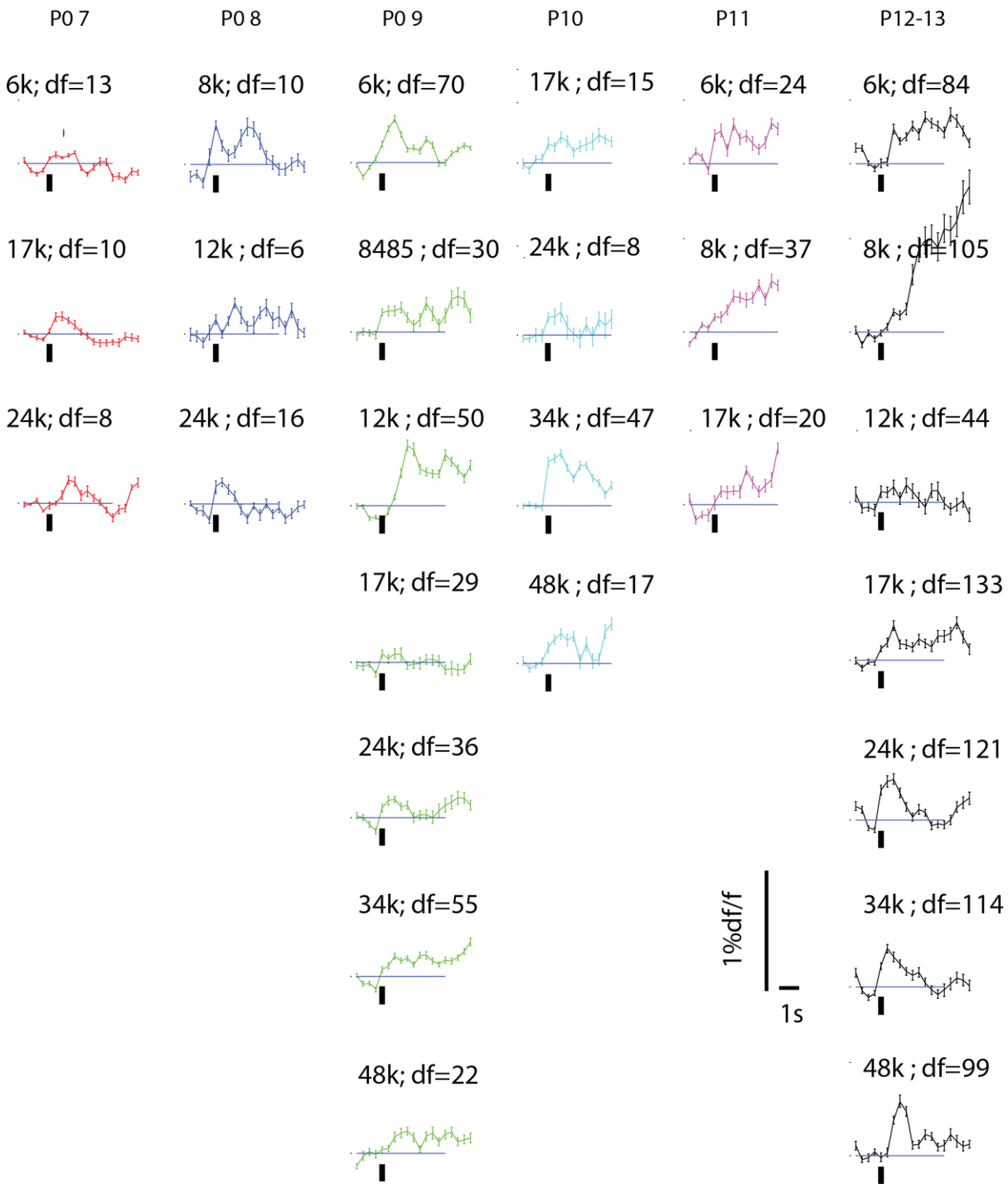

Figure S12. Mean df/f traces of all the cells having more than 25% reliability in responses (significant response in >10 repetitions out of 40 repetitions) to tonal stimuli (frequencies in Hz mentioned) at the different ages. Respective p-values and degree of freedom for one-sided paired ttest is also shown. Imaging was performed with 40 repetitions of each frequency in P07-P11 (before ECO) and 5 repetitions in P12-13 after ECO. All imaged cells are included in traces for P12-13 irrespective of reliability.

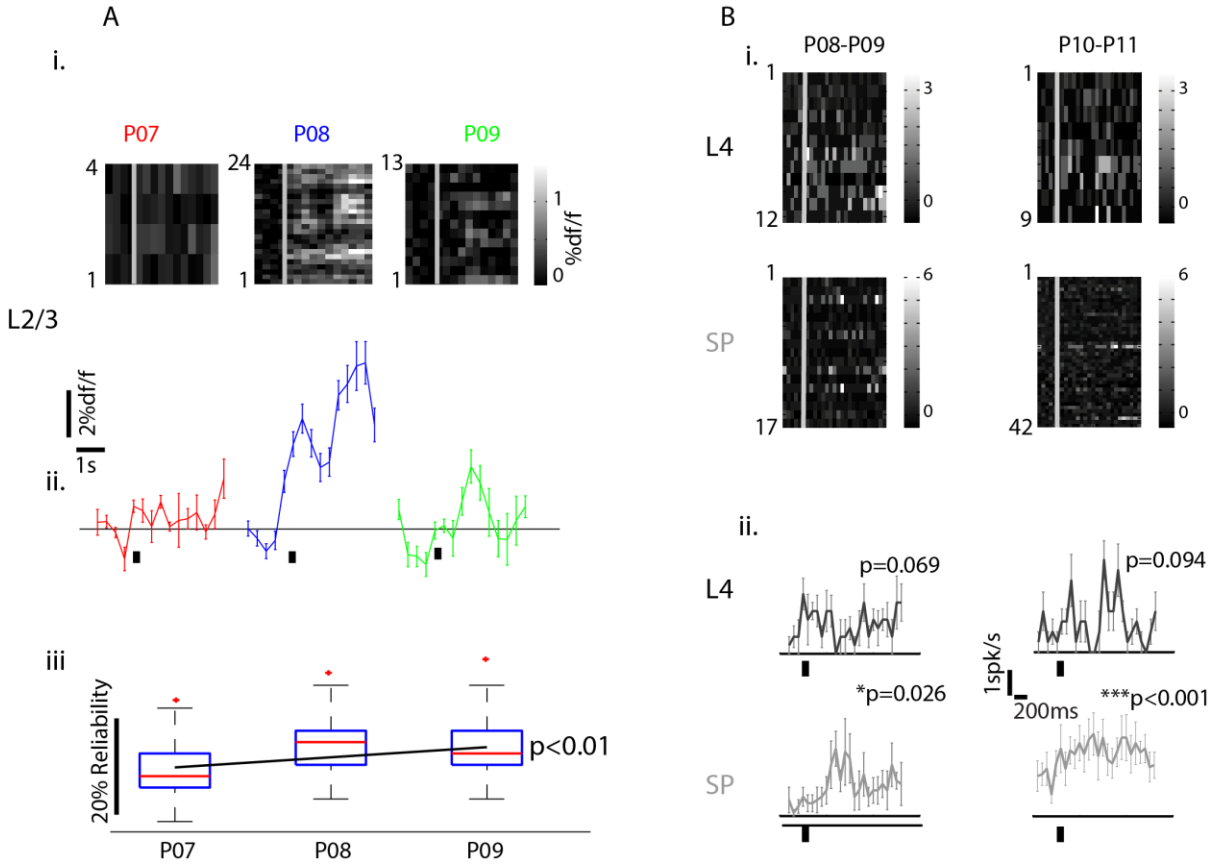

Figure S13. A) i-ii) Similar plot as in Fig. 3B i-iii, for in-vivo 2-photon Ca^{2+} imaging based responses to broadband noise. . Bi-ii) Same as in Fig.3Ei-ii, for responses to broadband noise before ECO.

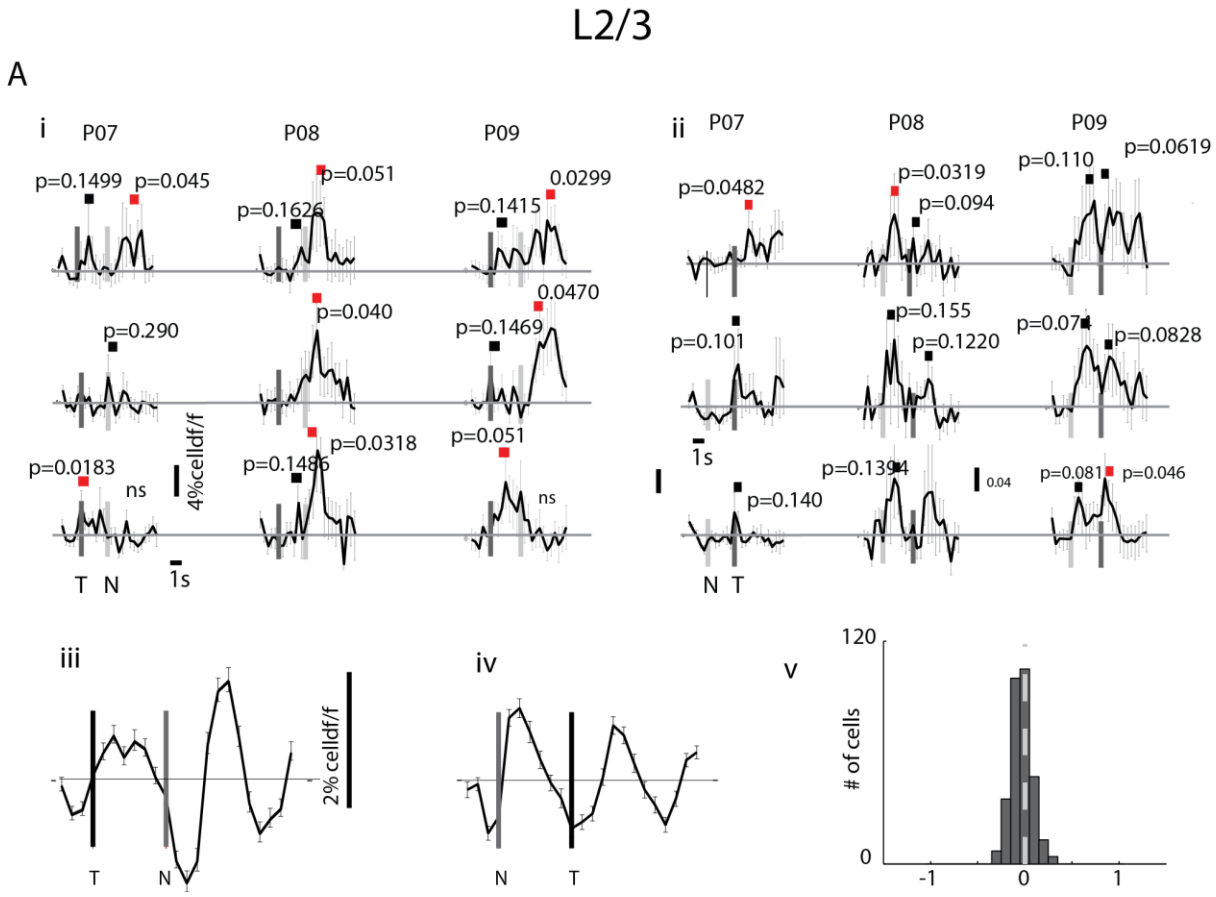

Figure S14. A) i-ii) Representative df/f traces of responding single neurons in L2/3 to the SD stimulus, obtained with 2-photon Ca^{2+} imaging (i: S=tone, D=noise, TN and ii: S=noise, D=tone, NT) at three different ages before ECO. The grey/black and black/grey vertical lines represent S onset and D respectively. Black (p<0.2) and red (p<0.05) bars (above traces) mark timing of significant responses (mean of 3 frames) to the standard and the deviant. iii-iv) Population mean df/f (311 neurons, n=3 (P7-P9)) in response to the two stimuli TN (iii) and NT (iv). v) Distribution of CSI values for the population of L2/3 single neurons.

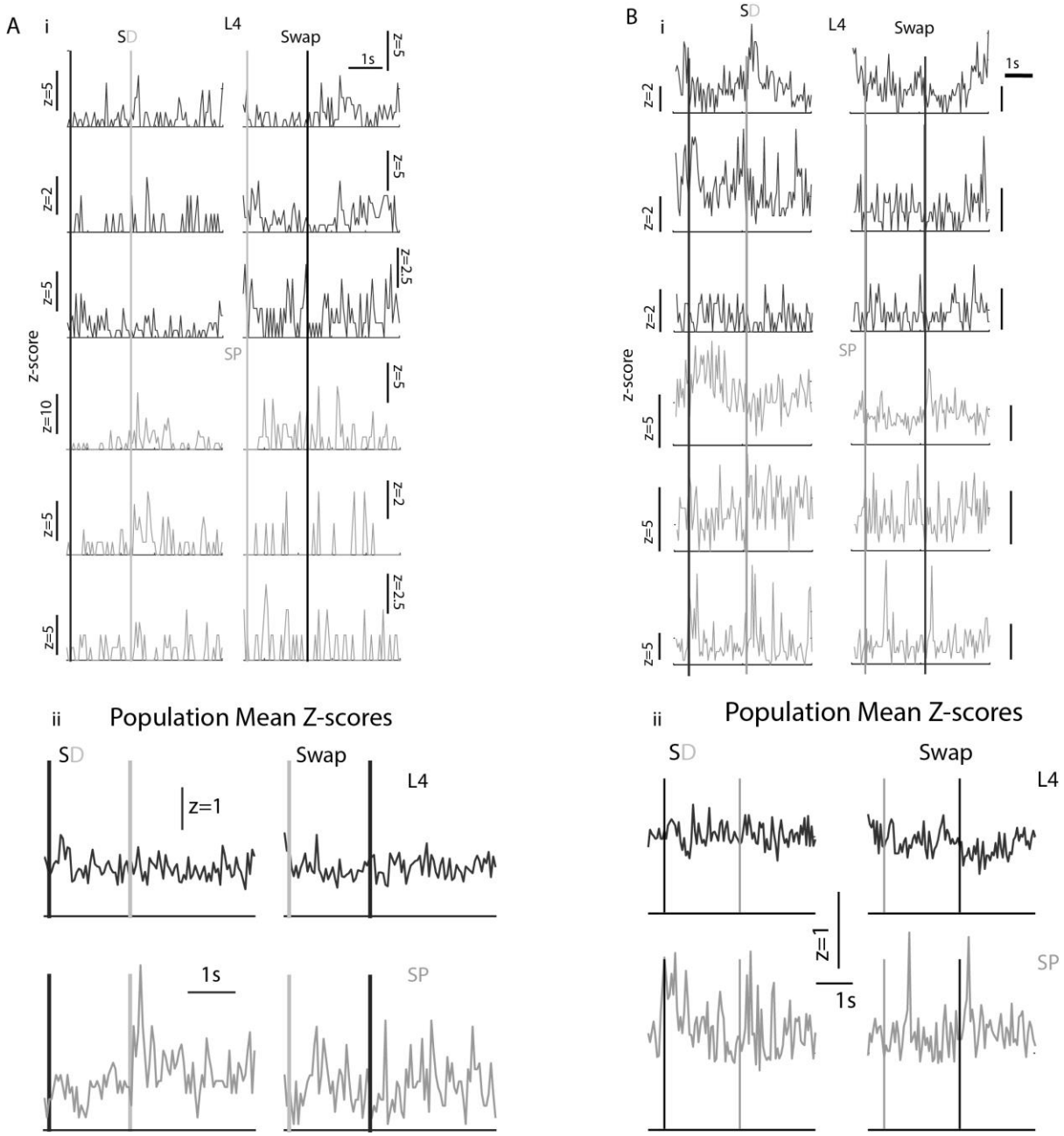

Figure S15. A) i) the z-scores of responses in SD stimulus (20 reps, 4Hz) (left column) and Swap (right column) for 3 single units in L4 (top 3 rows) and 3 single units in SP (bottom 3 rows) are shown (same units as in Fig. 4B, first 3 columns). A) ii) Mean z-scores for the population of single units in L4 (top row) and that in SP (bottom row) are shown for the SD stimulus (left) and the corresponding Swap (right). B) i-ii) Same as Ai-ii, for responses to SD stimulus with 30 reps and at rate of 3.33 Hz.

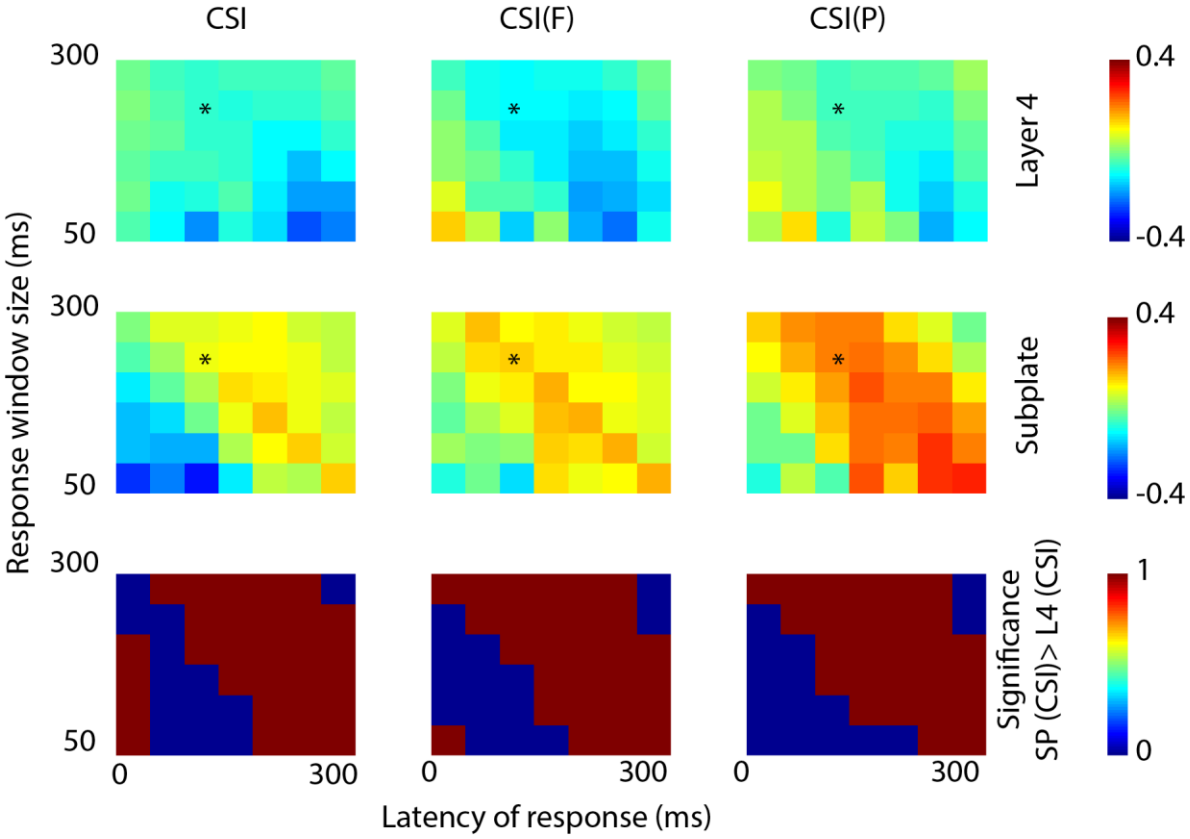

Figure S16. Top and middle row show the mean CSI values of the population of L4 and SP neurons respectively for different choice of response latencies and response window sizes. Asterisks marks the response latency and response window size combination used in Fig. 4 CSI calculations. The three columns are for the 3 different CSIs used CSI, CSI(F) and CSI(P). Bottom row shows which combinations of response attribute have significantly higher CSI in SP than in L4 (brown, blue indicates NS).

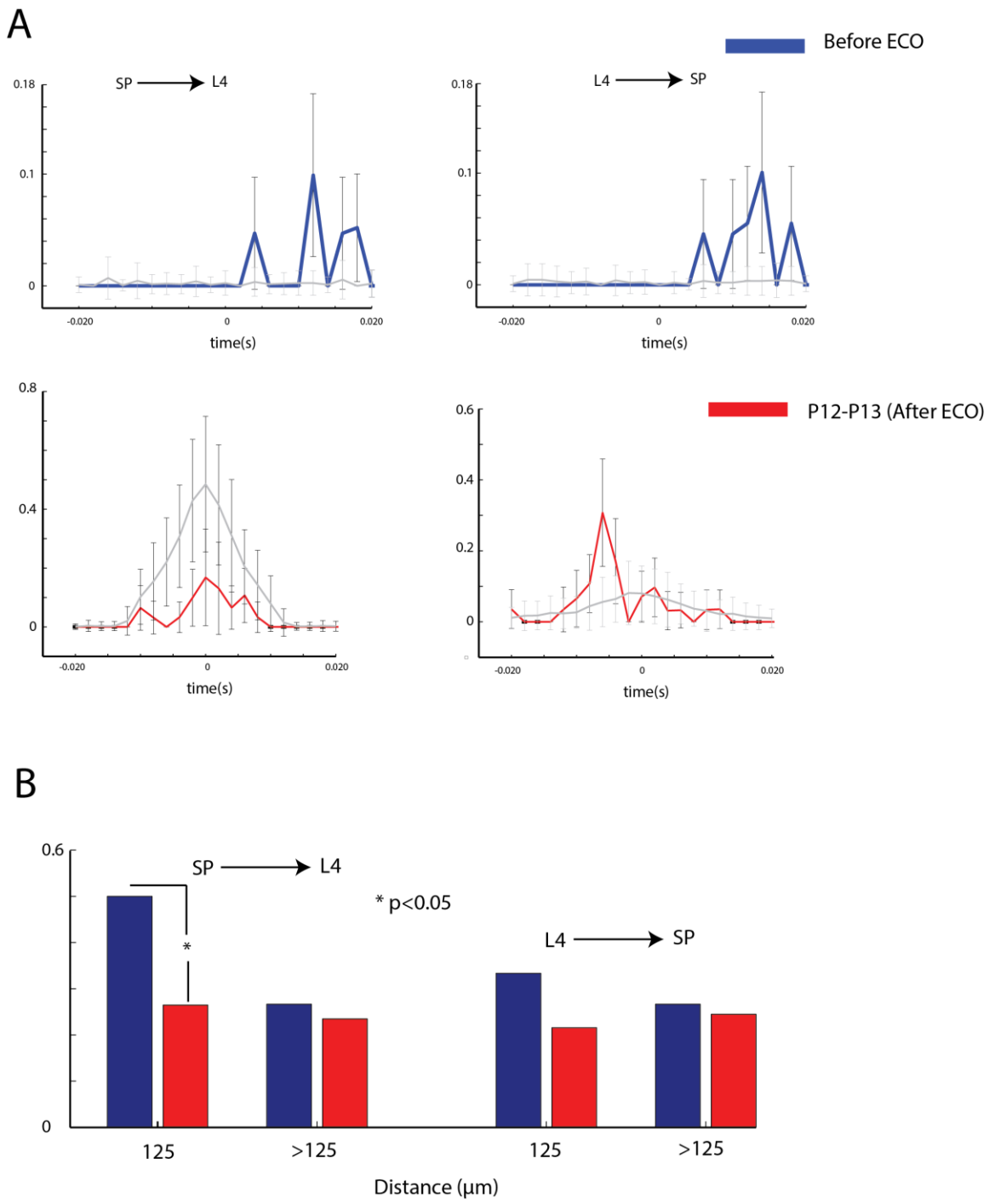

Figure S17. A) 2 examples of cross-correlograms each for before ECO (top row) and after ECO (bottom wor) showing connections detected from SP to L4 (left) and L4 to SP (right). Blue and red colored lines indicate mean of cross-correlograms with errorbars and gray lines with errorbars show the same for shuffled data (see detailed methods). B) Bar plots summarize the data in Table S2 showing probability of connections from SP to L4 (left) and L4 to SP (right) at within 125 microns or greater distances at the 2 age groups before ECO and P12-13, after ECO).

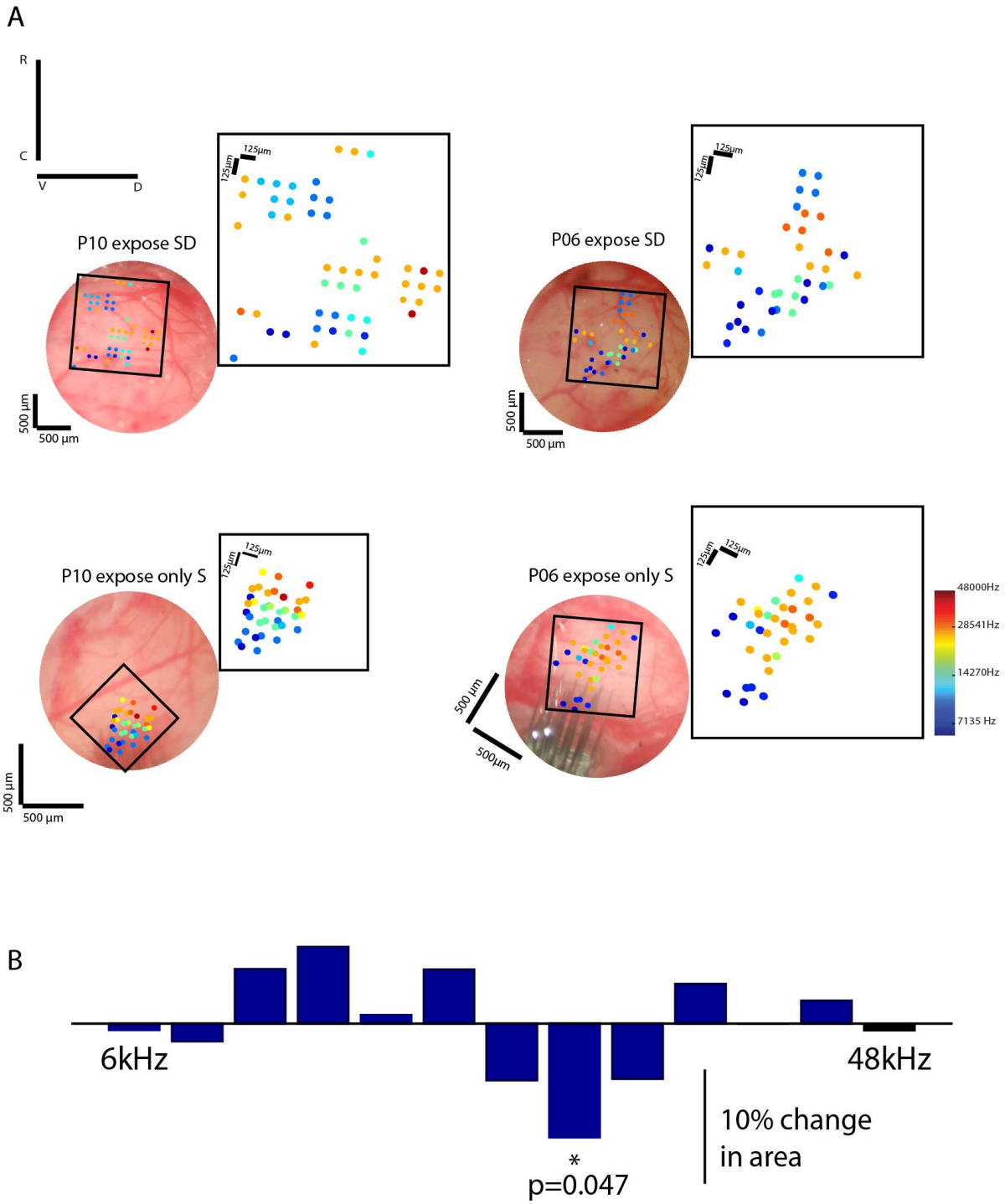

Figure S18. A) Four example images of location (along cortical surface) of BFs on the cortical surface in the craniotomy of single units recorded in L4 at ages P28 and above (Fig. 5A single unit recording) identified in color (colorbar, bottom right) for four exposure groups EX2 and EX1 in the top row (SD exposure) and EX5 and EX6 in the bottom row (SS exposure). Broad tonotopy showing A1 and AAF are clear in the images. B) Bar plot shows % change in area of each of the preferred frequencies in A1 and AAF between control (EX0 group of mice) and exposed animals (EX5 group of mice).

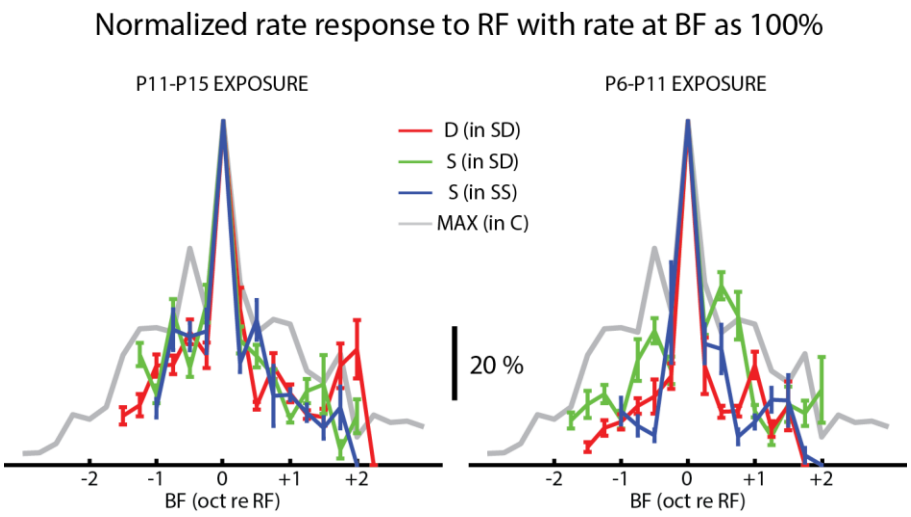

Figure S19. Similar plots as in Fig. 5E, for the profile of population mean normalized rates to the relevant RF (color legend) for the 4 exposure groups (EX5 and EX6 left, EX2 and EX1 right) as a function of BF (re RF). Normalization was done by considering the maximum rate in each tuning curve (rate at BF) to be 100%. Gray profile shows the same for the maximum of 13 similar plots derived from the control data (C) considering each of the 13 frequencies used as the RF.

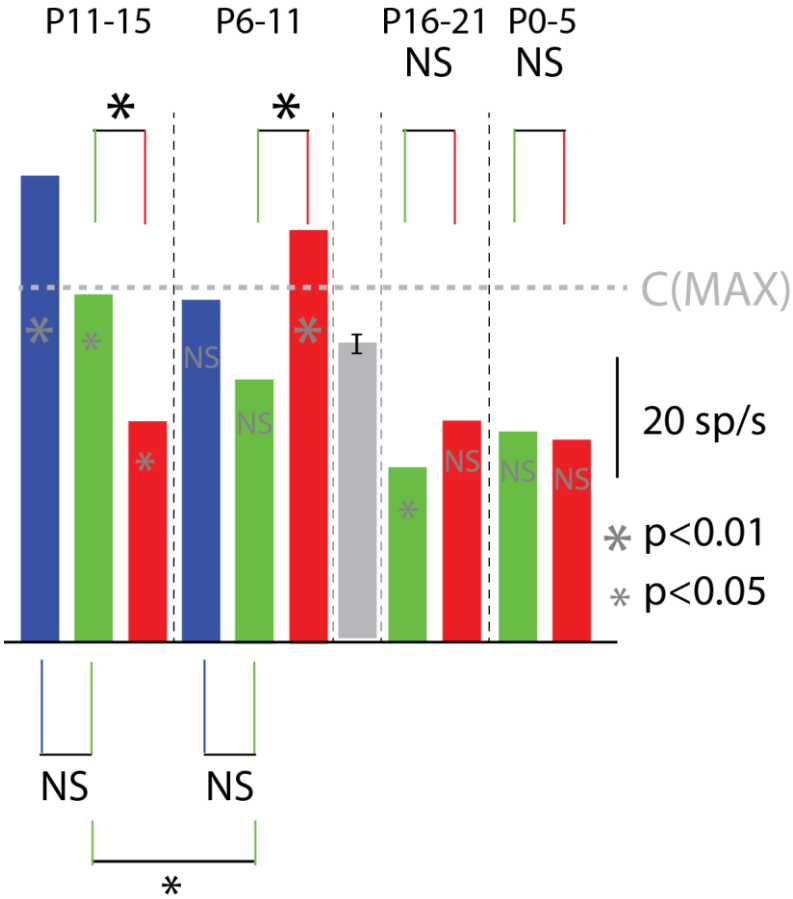

Figure S20. Bar plot summarizes population mean response to RF for neurons with BF at RF of all 6 EX cases (2 bars each, red and green for SD exposure cases and 1 blue for SS). Mean of the 13 control cases shown in gray bar in the centre.

References

1. Schreiner, C. E. & Polley, D. B. Auditory map plasticity: Diversity in causes and consequences. *Current Opinion in Neurobiology* vol. 24 143–156 (2014).
2. Hensch, T. K. Critical period plasticity in local cortical circuits. *Nature Reviews Neuroscience* (2005) doi:10.1038/nrn1787.
3. de Villers-Sidani, E., Chang, E. F., Bao, S. & Merzenich, M. M. Critical Period Window for Spectral Tuning Defined in the Primary Auditory Cortex (A1) in the Rat. *J. Neurosci.* (2007) doi:10.1523/JNEUROSCI.3227-06.2007.
4. Takesian, A. E., Bogart, L. J., Lichtman, J. W. & Hensch, T. K. Inhibitory circuit gating of auditory critical-period plasticity. *Nat. Neurosci.* (2018) doi:10.1038/s41593-017-0064-2.
5. Barkat, T. R., Polley, D. B. & Hensch, T. K. A critical period for auditory thalamocortical connectivity. *Nat. Neurosci.* (2011) doi:10.1038/nn.2882.
6. Zhou, X. & Merzenich, M. M. Enduring effects of early structured noise exposure on temporal modulation in the primary auditory cortex. *Proc. Natl. Acad. Sci. U. S. A.* (2008) doi:10.1073/pnas.0800009105.
7. Zhang, L. I., Bao, S. & Merzenich, M. M. Persistent and specific influences of early acoustic environments on primary auditory cortex. *Nat. Neurosci.* **4**, 1123–1130 (2001).
8. Luhmann, H. J., Kirischuk, S. & Kilb, W. The Superior Function of the Subplate in Early Neocortical Development. *Front. Neuroanat.* **12**, (2018).
9. Kanold, P. O. & Luhmann, H. J. The Subplate and Early Cortical Circuits. *Annu. Rev. Neurosci.* (2010) doi:10.1146/annurev-neuro-060909-153244.
10. Kanold, P. O., Kara, P., Reid, R. C. & Shatz, C. J. Role of subplate neurons in functional maturation of visual cortical columns. *Science (80-.).* (2003) doi:10.1126/science.1084152.
11. Kanold, P. O. & Shatz, C. J. Subplate Neurons Regulate Maturation of Cortical Inhibition and Outcome of Ocular Dominance Plasticity. *Neuron* (2006) doi:10.1016/j.neuron.2006.07.008.
12. Ghosh, A. & Shatz, C. J. Involvement of subplate neurons in the formation of ocular dominance columns. *Science (80-.).* (1992) doi:10.1126/science.1542795.
13. Ghosh, A., Antonini, A., McConnell, S. K. & Shatz, C. J. Requirement for subplate neurons in the formation of thalamocortical connections. *Nature* (1990) doi:10.1038/347179a0.
14. McConnell, S. K., Ghosh, A. & Shatz, C. J. Subplate neurons pioneer the first axon pathway from the cerebral cortex. *Science (80-.).* (1989) doi:10.1126/science.2475909.
15. Chang, E. F., Bao, S., Imaizumi, K., Schreiner, C. E. & Merzenich, M. M. Development of spectral and temporal response selectivity in the auditory cortex. *Proc. Natl. Acad. Sci. U. S. A.* (2005) doi:10.1073/pnas.0508239102.
16. Ulanovsky, N., Las, L. & Nelken, I. Processing of low-probability sounds by cortical neurons. *Nat. Neurosci.* (2003) doi:10.1038/nn1032.
17. Ghosh, A. & Shatz, C. J. A role for subplate neurons in the patterning of connections from thalamus to neocortex. *Development* (1993).
18. Zhao, C., Kao, J. P. Y. & Kanold, P. O. Functional Excitatory Microcircuits in Neonatal

Cortex Connect Thalamus and Layer 4. *J. Neurosci.* (2009) doi:10.1037/pha0000116.

19. Viswanathan, S., Bandyopadhyay, S., Kao, J. P. Y. & Kanold, P. O. Changing Microcircuits in the Subplate of the Developing Cortex. *J. Neurosci.* **32**, 1589–1601 (2012).
20. Wess, J. M., Isaiah, A., Watkins, P. V & Kanold, P. O. Subplate neurons are the first cortical neurons to respond to sensory stimuli. *Proc. Natl. Acad. Sci.* (2017) doi:10.1073/pnas.1710793114.
21. Pérez-González, D. & Malmierca, M. S. Adaptation in the auditory system: an overview. *Front. Integr. Neurosci.* (2014) doi:10.3389/fnint.2014.00019.
22. Nieto-Diego, J. & Malmierca, M. S. Topographic Distribution of Stimulus-Specific Adaptation across Auditory Cortical Fields in the Anesthetized Rat. *PLoS Biol.* (2016) doi:10.1371/journal.pbio.1002397.
23. Bandyopadhyay, S., Shamma, S. A. & Kanold, P. O. Dichotomy of functional organization in the mouse auditory cortex. *Nat. Neurosci.* (2010) doi:10.1038/nn.2490.
24. Issa, J. B. *et al.* Multiscale Optical Ca2+Imaging of Tonal Organization in Mouse Auditory Cortex. *Neuron* (2014) doi:10.1016/j.neuron.2014.07.009.
25. Sawatari, H. *et al.* Identification and characterization of an insular auditory field in mice. *Eur. J. Neurosci.* (2011) doi:10.1111/j.1460-9568.2011.07926.x.
26. Barbour, D. L. & Wang, X. Contrast tuning in auditory cortex. *Science (80-.).* (2003) doi:10.1126/science.1080425.
27. Mill, R., Coath, M., Wennekers, T. & Denham, S. L. Abstract stimulus-specific adaptation models. *Neural Computation* (2011) doi:10.1162/NECO_a_00077.
28. Clancy, B., Darlington, R. B. & Finlay, B. L. Translating developmental time across mammalian species. *Neuroscience* (2001) doi:10.1016/S0306-4522(01)00171-3.
29. Chang, A. *et al.* Specific Influences of Early Acoustic Environments on Cochlear Hair Cells in Postnatal Mice. *Neural Plast.* (2018) doi:10.1155/2018/5616930.
30. Babola, T. A. *et al.* Homeostatic Control of Spontaneous Activity in the Developing Auditory System. *Neuron* (2018) doi:10.1016/j.neuron.2018.07.004.
31. Anthwal, N. & Thompson, H. The development of the mammalian outer and middle ear. *J. Anat.* (2016) doi:10.1111/joa.12344.
32. Huangfu, M. & Saunders, J. C. Auditory development in the mouse: Structural maturation of the middle ear. *J. Morphol.* (1983) doi:10.1002/jmor.1051760302.
33. Kim, K. X. & Fettiplace, R. Developmental changes in the cochlear hair cell mechanotransducer channel and their regulation by transmembrane channel-like proteins. *J. Gen. Physiol.* (2013) doi:10.1085/jgp.201210913.
34. Lelli, A., Asai, Y., Forge, A., Holt, J. R. & Géléoc, G. S. G. Tonotopic gradient in the developmental acquisition of sensory transduction in outer hair cells of the mouse cochlea. *J. Neurophysiol.* (2009) doi:10.1152/jn.00136.2009.
35. Abe, T. *et al.* Developmental expression of the outer hair cell motor prestin in the mouse. *J. Membr. Biol.* (2007) doi:10.1007/s00232-007-9004-5.
36. Polley, D. B., Thompson, J. H. & Guo, W. Brief hearing loss disrupts binaural integration during two early critical periods of auditory cortex development. *Nat. Commun.* (2013) doi:10.1038/ncomms3547.
37. Ruebsamen, R. & Lippe, W. The development of cochlear function. in *Development of the auditory system* (eds. Rubel, E., Poppe, A. & Fay, R.) 193–270 (Springer, 1997).

38. Shnerson, A. & Pujol, A. Development: anatomy, electrophysiology, and behavior. in *The auditory psychobiology of the mouse* (ed. Willot, J.) 395–425 (Charles C. Thomas, 1983).
39. Pujol, R., Lavigne-Rebillard, M. & Lenoir, M. Development of sensory and neural structures in the mammalian cochlea. in *Development of the auditory system* (eds. Rubel, E., Popper, A. & Fay, R.) 146–192 (Spinger, 1997).
40. Tritsch, N. X. *et al.* Calcium action potentials in hair cells pattern auditory neuron activity before hearing onset. *Nat. Neurosci.* (2010) doi:10.1038/nn.2604.
41. Mill, R., Coath, M., Wennekers, T. & Denham, S. L. A neurocomputational model of stimulus-specific adaptation to oddball and markov sequences. *PLoS Comput. Biol.* (2011) doi:10.1371/journal.pcbi.1002117.
42. Yarden, T. S. & Nelken, I. Stimulus-specific adaptation in a recurrent network model of primary auditory cortex. *PLoS Comput. Biol.* (2017) doi:10.1371/journal.pcbi.1005437.
43. Hromádka, T., DeWeese, M. R. & Zador, A. M. Sparse representation of sounds in the unanesthetized auditory cortex. *PLoS Biol.* (2008) doi:10.1371/journal.pbio.0060016.
44. Lewicki, M. S. Efficient coding of natural sounds. *Nat. Neurosci.* (2002) doi:10.1038/nn831.
45. Smith, E. C. & Lewicki, M. S. Efficient auditory coding. *Nature* (2006) doi:10.1038/nature04485.
46. Sun, Y. J. *et al.* Fine-tuning of pre-balanced excitation and inhibition during auditory cortical development. *Nature* **465**, 927–931 (2010).
47. Blundon, J. A. *et al.* Restoring auditory cortex plasticity in adult mice by restricting thalamic adenosine signaling. *Science (80-.).* (2017) doi:10.1126/science.aaf4612.
48. Vickers, E. D. *et al.* Parvalbumin-Interneuron Output Synapses Show Spike-Timing-Dependent Plasticity that Contributes to Auditory Map Remodeling. *Neuron* (2018) doi:10.1016/j.neuron.2018.07.018.
49. Courtney E. Yaeger, Dario Ringach, J. T. T. Neuromodulatory control of localized dendritic spiking in critical period cortex. *Nature* **567**, 100–104 (2019).
50. Mehler, J. *et al.* A precursor of language acquisition in young infants. *Cognition* (1988) doi:10.1016/0010-0277(88)90035-2.
51. Voegtline, K. M., Costigan, K. A., Pater, H. A. & DiPietro, J. A. Near-term fetal response to maternal spoken voice. *Infant Behav. Dev.* (2013) doi:10.1016/j.infbeh.2013.05.002.
52. Portfors, C. V., Roberts, P. D. & Jonson, K. Over-representation of species-specific vocalizations in the awake mouse inferior colliculus. *Neuroscience* (2009) doi:10.1016/j.neuroscience.2009.04.056.
53. Wang, X. & Kadia, S. C. Differential Representation of Species-Specific Primate Vocalizations in the Auditory Cortices of Marmoset and Cat. *J. Neurophysiol.* (2001) doi:10.1152/jn.2001.86.5.2616.
54. Paxinos, G. & Franklin, K. B. J. *Paxinos and Franklin's the Mouse Brain in Stereotaxic Coordinates*. *São Paulo, Academic Press* (2012). doi:10.1364/OE.20.020998.
55. Torii, M. & Levitt, P. Dissociation of corticothalamic and thalamocortical axon targeting by an EphA7-mediated mechanism. *Neuron* (2005) doi:10.1016/j.neuron.2005.09.021.
56. Osheroff, H. & Hatten, M. E. Gene expression profiling of preplate neurons destined

for the subplate: Genes involved in transcription, axon extension, neurotransmitter regulation, steroid hormone signaling, and neuronal survival. *Cereb. Cortex* (2009) doi:10.1093/cercor/bhp034.

57. Hoerder-Suabedissen, A. *et al.* Novel markers reveal subpopulations of subplate neurons in the murine cerebral cortex. *Cereb. Cortex* (2009) doi:10.1093/cercor/bhn195.

58. Gee, J. M. *et al.* Imaging Activity in Neurons and Glia with a Polr2a-Based and Cre-Dependent GCaMP5G-IRES-tdTomato Reporter Mouse. *Neuron* (2014) doi:10.1016/j.neuron.2014.07.024.